UNIVERSITAT AUTÒNOMA DE BARCELONA

FACULTAT DE BIOCIÈNCIES
Departament de Genètica i Microbiologia

Effect of Environmental Changes and Metal Stress on Phototrophic Microorganisms in Extreme Environments

Development of New Methodologies in High-Resolution Microscopy Techniques

Laia Millach Carrobé

2017

Chapter 4 – General discussion

One of the most harmful effects of climate change is its influence on marine ecosystems (and especially on microbial mats) through rising temperatures causing these ecosystems to dry with the consequent increase in salinity. As a result of these environmental changes, microorganism populations, and especially microalgae and cyanobacteria, need to adapt to what are often very sudden changes and resist other more long-term changes. Such is the case with the microorganisms in the mats of the Ebro Delta, whereby the redistribution of the River Ebro means that an increasingly lower volume of water is flowing towards the river mouth (52.3 % less in the last 50 years)[1] and therefore less sediment is being transported, thus causing the delta to shrink and gradually allowing more seawater to enter the ecosystem and thereby raise salt levels. As well as considering the effects of environmental changes, the contribution of different pollutants, and especially metals, has also been analyzed in order to determine what strategies different phototrophic microorganisms develop.

The methodologies that have been used to date often fail to resolve the study of these variations at single-cell level mainly on a community or population of microorganisms, so there is a need to optimize and, in some cases, innovate new methods that can mainly enable determination of the physiological changes produced on individual cells in complex samples, both in the natural environment and in mixed laboratory cultures, due to the effect of environmental changes and/or the presence of different pollutants in the zone. CLSM has been shown to be the most useful technique in recent years for such studies, because it is especially appropriate for the study of phototrophic microorganisms with natural autofluorescence, using Chl *a* as a biomarker.

This section examines and discusses the role of this technology, and its many applications, in order to analyze physiological changes to different microorganisms in the same sample individually, including those that form aggregates or consortia, and

[1] Flow at the Ebro River mouth: from 18286 hm^3 $year^{-1}$ (1965) to 8832 hm^3 $year^{-1}$ (2015). Data obtained from *Confederación Hidrográfica del Ebro.*

omitting the problem of microorganisms that find it hard to grow 0n solid laboratory cultures or that cannot be obtained from axenic cultures. In all cases, very high resolution images are generated while minimizing the use of fluorochromes and image processing and analysis programs.

The first part of the discussion (**objectives 1 and 2**) presents the benefits of methods being optimized or applied for the first time in this PhD thesis and performed using CLSM and/or electron microscopy techniques, the latter being used both for the study of changes in cell morphology and ultrastructure and for analysis of the capacity of microorganisms to immobilize metals.

The second part discusses (**objective 3**) the impact of two environmental factors, light and salinity, as well as the effect of different metals both individually and in mixtures in two selected phototrophic microorganisms: the cyanobacterium *Geitlerinema* sp. DE2011 and the microalga *Scenedesmus* sp. DE2009, isolated from Ebro Delta microbial mats.

4.1. Methodological optimization

In this section, the author describes the improvements applied to the standard protocols defined in Chapter 2 (Materials and Methods) to obtain new and valuable results. In addition, the advantages and disadvantages of all the methodologies applied in this work compared to other techniques are discussed.

The main improvement was carried out with the CLSM. For determining the tolerance and resistance of phototrophic microorganisms in response to changing environmental parameters, the CLSM-*λscan* protocol described by Burnat et al., (2010) has been optimized. For the first time, it has been identified a Non-Photosynthetic Autofluorescence (NPAF) signal linked to dead cells. In this case, a 405 nm UV laser excitation was used to capture all the spectral visible range and distinguish this new autofluorescence signature. On the other hand, a new CLSM-DL method was developed to analyze *in vivo* the physiological state and cell viability of phototrophic microorganism at single-cell level and without the need of either staining or additional use of image treating software. This methodology can be applied in ecological researches as well as in ecotoxicological studies.

Concerning the preparation of samples for SEM, it is essential to prepare filters with the appropriate phototrophic biomass in order to avoid the obstruction of aggregates in the critical point drier device. Moreover, in order to obtain a good conductivity and contrast in the samples, metalizing is carried out with a noble metal. In this case, to avoid an excessive electron charge on the surface layer of the specimen, samples were coated on different inclined planes three times for 2 minutes. Doing that, the samples were evenly conductive and a better image quality was obtained.

For SEM-EDX experiments has been taken into account that the metal used for metalizing the samples has not the energy peak in the element spectrum overlapping the metal to be evaluated (chromium). For that, an alloy with gold (Au) and palladium (Pd) has been used.

Following, all the benefits of the methodologies used in this work have been summarized in tables 4.1 and 4.2. In some cases, preliminary works carried out by other members of our working group are also indicated.

Table 4.1. Methodologies based on pigment fluorescence.

CLSM Techniques			
Method	**Usefulness**	**Benefits**	**Reference**
CLSM-*λscan*	Determination of the sensitivity of phototrophic microorganisms to environmental changes and pollutants.	Provide data in short time consuming, *in vivo* and with minimal manipulating the samples. Easy to apply in mixed phototrophic populations at cell level.	*Maldonado et al., 2011;* *Millach et al., 2015; 2017* *(In this study)*
IC_{50} toxicity test	Toxicity test of pollutants. Parameters derived from the dose-response curves.	Useful to apply *in vivo* in phototrophic microorganism with difficulty to grow in solid media and tendency to form aggregates.	*Submitted to Aquatic Toxicology*
FLU-CLSM-IA	Estimation of changes in total biomass and cellular viability.	Use of specific fluorochromes and image treating software. Particularly useful for heterotrophic bacteria.	*Puyen et al.,2012a;* *Millach et al., 2015* *(In this study)*
CLSM-DL	Analysis of the physiological state and cell viability of phototrophic microorganisms.	Provide data in short time consuming, *in vivo* and with minimal manipulation of the samples. Easy to apply in mixed phototrophic populations at cell level.	*Millach et al., 2017* *(In this study)*
3D-CLSM projections	Characterization of the distribution of autofluorescence signals within the whole cell.	Easy to apply *in vivo* and at cell level in mixed phototrophic populations with difficulty to grow in solid media.	*Millach et al., 2017* *(In this study)*

Table 4.2. Methodologies based on electron microscopy techniques.

Electron Microscopy Techniques			
Method	**Usefulness**	**Benefits**	**Reference**
SEM	Topographical, morphological and compositional information	Powerful magnification and high image resolution (0.8 nm at 15 kV). Acceleration voltage: 0.2 – 30 kV. Detailed 3D-imaging and versatile information garnered from different detectors. Analysis of the changes in cell morphology.	*Burgos et al., 2012;* *Millach et al., 2017* *(In this study)*
TEM	Characterization of cellular ultrastructures	High contrast imaging and powerful magnification and resolution (0.4 nm at 120 kV). Acceleration voltage: 40 – 120 kV. Versatile information collected from different detectors. Useful to characterize the changes in ultrastructural inclusions and/or organelles.	*Burgos et al., 2012;* *Millach et al., 2017* *(In this study)*
SEM-EDX	External elemental microanalysis of the cells	Fast data collection. Semi-quantitative results. Metal biosorption studies.	*Burgos et al., 2012;* *Millach et al., 2015* *(In this study)*
TEM-EDX	Internal elemental microanalysis of the cells	Fast data collection. Semi-quantitative results. Research in metal bioaccumulation.	*Burgos et al., 2012;* *Millach et al., 2015* *(In this study)*
TXM	3D visualisation of the ultrastructural changes in a whole cell	High spatial resolution (30 – 50 nm). The data obtained is from entire and unstained cells, without need of sectioning the samples and preserving the ultrastructure of the cell.	*Sorrentino et al., 2015* *Otón et al., 2016*

The mentioned above methods avoid the problems described in Chapter 1 (Introduction) to study the phototrophic microorganisms of microbial mats. For this reason, other methodologies used in environmental studies are compared and discarded.

Firstly, the Minimum Inhibitory Concentration (MIC) technique is commonly used to determine the sensitivity of microorganisms to metals or antibiotics (Belapurkar et al., 2016), but this technique require that the microorganism tested to have growth capacity in solid medium. This means that these techniques are valid for the majority of

heterotrophic microorganisms and for some phototrophic microorganisms. However, this method cannot be applied in isolated phototrophic microorganisms from natural environments that show a slow and/or irregular growth, or directly do not grow in solid media.

On the other hand, most of fluorometric techniques are based on chl *a* fluorescence used as a biomarker. Chl *a* fluorescence is established as a rapid and non-intrusive parameter to monitor photosynthetic performance from phototrophic microorganisms, as well as to analyze their protective responses (Shing et al., 2012). Fluorometric methods are applied in ecophysiological and toxicological studies to examine the effect that environmental changes and pollutants may cause on photosynthetic capacity (Kumar et al., 2014). Among fluorometric techniques, Pulse-Amplitude-Modulation (PAM) fluorometry is one of the most common techniques used to study the induction and quenching of chlorophyll fluorescence in physiological studies (Schreiber, 1998). This methodology is non-invasive, and has frequently been used to estimate photosynthetic efficiency within oxygenic organisms (Genty et al., 1989; Perkins et al., 2002). Other technique, such as the pigment fluorescence analysis using the Plant Efficiency Analyzer (PEA), has also shown to be a sensitive method for the detection and quantification of changes induced in the photosynthetic apparatus (Mehta et al., 2010). Although all these techniques provide data in short time consuming, the information obtained is at population level and cannot be used for differentiating living cells from dead ones.

Most methods based on quantification of the chlorophyll content need a pigment extraction into an organic solvent and its subsequent determination by spectrophotometry, spectrofluorometry, or chromatography (Gregor and Maršálek, 2004; Wagenen et al. 2014). For instance, High-Performance Liquid Chromatography (HPLC) gives indirect biomass values from the pigments extracted of a photosynthetic

population (Chakrabortys et al., 2010). Nevertheless, this method does not allow a directly determination at cell level and requires long protocols and specific procedures.

Other alternative and common viability assays are using fluorochromes such as rodamin B, calcofluor white, fluorescein diacetate or DNA-specific SYTOX Green dye (Pouneva, 1997; Sato et al., 2004), as well as flow cytometry (Al-Rubeai et al., 1997; Veldhuis et al. 2001); but staining is required in both methodologies, and in the latter it is difficult to apply in filamentous cyanobacteria, and in microorganisms that tend to form aggregates.

On the other hand, SEM, TEM, SEM-EDX and TEM-EDX have been very useful in this work to determine changes in the morphology and ultrastructure of phototrophic cells, as well as, to evaluate the capacity of these microorganisms to sequester metals extra- and intracellularly; but the preparation of the samples requires long protocols. On the contrary, the advantages of use the TXM in comparison with the electron microscopy techniques described are: easy preparation of the samples, the cryo-preservation of the cell ultrastructure, 3D reconstructions without the need of sectioning the specimen and a spatial resolution better than 50 nm.

4.2. Effect of environmental changes and metal stress on phototrophic microorganisms

All the methodologies described in Chapter 2 (Material and Methods) have been applied to study the response of different phototrophic microorganisms to environmental changes and metal stress.

4.2.1. Assessment of the impact of changing environmental parameters

In recent years, environmental changes have become more extreme, harsh and drastic. These changes severely affect phototrophic populations, so it is important to know how phototrophic microorganisms respond to this environmental stress. In this dissertation, light intensity and salinity were selected as important natural parameters since: (i) light is one of the most important factors affecting the properties of the photosynthetic apparatus in phototrophic bacteria and (ii) ecosystems may undergo increased salinity levels because of global warming. Phototrophic microorganisms colonize most of the more extreme environments for supporting life, due to their capacity to use light as a source of energy. The way that the photosynthetic apparatus of these microorganisms adapts to changes in light intensity, both in their natural habitats and in laboratory cultures, has been known for many years.

Some of the first investigations carried out to analyze these adaptations were performed with anoxygenic phototrophic bacteria. In the case of red sulfur bacteria, a reduction in the number or diameter of intracytoplasmic vesicles at very high light intensities and, vice versa, an increase in the number or diameter of vesicles in highly limited light intensities was observed in *Chromatium* sp., *Rhodospirillum* sp. and *Rhodobacter* sp. (Esteve et al., 1990). Also, among green sulfur bacteria there were differences in the number of chlorosomes in similar experiments to those described above (Broch-Due et al., 1976). Meanwhile, in eukaryote microorganisms, such as

Scenedesmus sp. DE2009, these adaptations occur through changes in the distribution and location of the thylakoids inside the cytoplasm (unpublished results).

In lakes and small lagoons, such as those in the karstic system of Banyoles (Girona), this problem is more moderate because unlike oxygenic phototrophic bacteria, anoxygenic ones are located in much deeper layers where light still reaches, but where the conditions are anoxic. Nevertheless, some of these bacteria perform alternative metabolisms in light-limited conditions, such as endogen metabolism in the case of *Chromatium* sp., which oxidizes glycogen to poly-β-hydroxybutyrate (PHB), while reducing the accumulated sulfur to hydrogen sulfide (Sánchez et al., 1998; Overmann and van Gemerden, 2000); or the case of some strains of *Chlorobium* sp., which ferment products that have accumulated during the phase of exposure to light (Jeong and Kim, 1999).

At present and probably due to climate change, areas of partial or highly extreme drought are being produced in many places and are mainly affecting oxygenic phototrophic microorganisms, such as cyanobacteria and microalgae. These microorganisms are regularly exposed to high light intensities, especially in microbial mats, and they are located on the layers nearest to the surface. Many of these microorganisms are protected by siliceous structures like diatoms which in turn shade the microalgae and cyanobacteria located in deeper layers (Paerl et al., 2000). Another alternate strategy is the production of exopolysaccharides that form dense envelopes around the outside of the cell walls as a protective measure against strong irradiation (Rossi and De Philippis, 2015).

Furthermore, it is important to highlight that, the exposure of photosynthetic microorganisms to strong light intensities results in inhibition of the activity of photosystem II (PSII) and, in particular, damage to the D1 protein in the photochemical reaction center of PSII (Andersson and Aro, 2001; Nikolaou et al., 2015). This

phenomenon is known as photoinhibition. However, photosynthetic microorganisms are able to overcome the toxic effects of light via the rapid and efficient repair of PSII by replacement of damaged D1 protein with newly synthesized D1 (Aro et al., 1993; Murata et al., 2007).

As has been shown, there is an extensive knowledge of the different strategies used by phototrophic microorganisms to deal with major changes in light intensity. However, very little is known about the determination of the optimum light level for growth in laboratory cultures, where the limits are much tighter. In this work, the application of CLSM-*λscan* was very useful and much more precise for determining the optimum light intensity for *Scenedesmus* sp. DE2009 when it is grown in a narrow range of low light intensities (2 to 12 μE m^{-2} s^{-1}). At the same time, this technique, combined with the CLSM-DL has enabled evaluation of the percentage of living and dead cells, being the maximum viable cells coinciding totally with the light intensity that was found to be the optimum (6 to 8 μE m^{-2} s^{-1}). In the same way, our results in light experiments agree with those obtained in other microalgae studies at low light intensities. In this case, Ferreira et al., 2016 demonstrated an increase in chlorophyll content at 16.91 ± 0.45 μmol photons m^{-2} s^{-1} to capture light in a more efficient manner in *Scenedesmus dimorphus* (UTEX 1237); and Pal et al., 2013 indicated that 1000-1500 lux (6-9 μE m^{-2} s^{-1}) were the best light intensities in order to produce maximum yield in *Chaetoceros muelleri* (CS-178). Finally, by setting this essential parameter, and combining both techniques (CLSM-*λscan* and CLSM- DL) it was possible to study the effect of the changes in salinity on *Scenedesmus* sp.DE2009 cultures.

It has previously been mentioned that microorganisms have exceptional metabolic flexibility for adaptation to such stressful conditions, as high and low temperatures or drastic changes in pH, among others. However, the absence of water is still considered to be the most extreme factor, and hence deserts and zones that are being desertified, probably due to climate change, are considered extremely limiting for life. Despite this,

desiccation tolerance has been recorded for bacteria, yeast, fungi and lower and higher plants. (Crowe and Crowe, 1992; Hoekstra et al., 2001; Ratnakumar and Tunnacliffe, 2006; Chaibenjawong and Foster, 2011; Lebre et al., 2017).

The response by microorganisms to the absence of water has been analyzed since the early nineties, but these studies have mainly focused on osmolality when cells are immersed in solvent-solute mixtures. In 1994, Potts published the first and most comprehensive review of xerotolerant bacteria and archaea to date and details the role of water in the cell, desiccation damage, methods of water removal from cell and provides an overview of the main mechanisms of desiccation tolerance in the pre-genomic era. In this review, a very interesting result obtained by Hill et al., (1994) on a desiccated colony (dry for 12 years) of the filamentous cyanobacterium *Nostoc commune* was also described. Cross-sections of the desiccated cell showed an intact cell envelope surrounding the cyanobacterium cells, an electron-translucent layer, and a fibrous extracellular glycan. The authors highlight the important role of EPS in water retention.

In recent years, the study of cyanobacteria and also microalgae that live in arid zones, such as the Atacama Desert, has been of major interest. In the Yungay area, cocoidal cyanobacteria identified as *Chroococcidiopsis* sp. have been described as living in evaporyte rocks. These rocks are essentially composed of halite (96-99 %) with minor amounts of gypsum (1–3 %) and traces (<1 %) of sylvine (sodium) and quartz. It is important to note that there is practically no rain in this zone and that these microorganisms use the short time, when water vapor is produced in the atmosphere, to capture moisture, while using the light that passes through the translucent rocks as a source of energy (Wierzchos et al., 2006). Besides, these cyanobacteria, as occurs in *Nostoc commune,* are characterized by a remarkable ability to withstand the lethal effects of desiccation, thanks to a thick EPS envelope that surrounds the cell cytoplasm and acts

as a shield, slowing down desiccation and ameliorating the extreme external conditions (Tamaru et al., 2005; Knowles and Castenholz, 2008).

In this last sense, Roldán et al., (2014) investigated the fluorescent emission spectra recorded for endolithic microbial community found in Atacama Desert. The cyanobacteria isolated from halite pinnacles also presented two types of autofluorescences signals: PAF and NPAF. Under physiological point of view, PAF was considered as an indicator of integrity of the photosynthetic apparatus and cell viability (Billi et al., 2011), whereas green autofluorescence was considered by Tang and Dobbs (2007) a common feature in different organisms and that its presence was independent of the cells physiological status. However, we are totally disagree with this last hypothesis, because NPAF was detected only in a few cells in control cultures and a direct correlation was found between this type of nonspecific autofluorescence and non-viable cells, as demonstrated in this work in light and salinity experiments. Specifically, to validate the CLSM-DL method, microalga cells were exposed at high salt stress (as inductor of damage in the cells) to correlate whether NPAF corresponded to microalga dead cells. SEM images showed clear symptoms of cellular degradation such as invaginations of the cell wall, a reduction of cell volume and an irregular morphology. Additionally, ultrathin sections showed various pleomorphic cells and rupture of the cell wall and intracytoplasmic membrane. These results allowed us to conclude that NPAF may therefore be a useful indicator of senescence for any species of alga. In any case, NPAF may be attributable to fluorescence emitted by different molecules with different widely overlapping emission spectra, although the molecules responsible for NPAF have not yet been clearly identified.

On the other hand, *Scenedesmus* sp. DE2009 has been cultivated in an increasing salinity gradient that limits the availability of water and reproduces the changing conditions detected in flood and dry periods in the microbial mats of the Ebro Delta. The results indicated that, in short periods of time (7 days), the MIF peaks (Chl *a*)

decreased by mainly between 35 and 75 g NaCl L^{-1}; while for long periods (30 days), the MIF peaks were drastically reduced from 10 g NaCl L^{-1} and was not detected at 100 g NaCl L^{-1}. These results show that, at these high salt doses, there is a clear effect on photosynthetic pigments and this effect also increases with time.

Salt stress affects basic photosynthesis processes. One of the main factors responsible for the reduction in photosynthetic activity in algal cells is the decrease in PSII activity (Kirst, 1990). Several studies have demonstrated that thylakoid membrane proteins are affected by salt stress, stimulating the photoinhibition of PSII (Lu and Zhang, 1999; Liu and Shen, 2004; Sudhir and Murthy, 2004; Ohnishi and Murata, 2007; Zhang et al., 2010). Likewise, Allakhverdiev and Murata (2008) demonstrated that salt stress represses the repair of photo-damaged PSII by inhibiting the degradation and synthesis of D1 protein in *Synechococcus* cells.

Cellular viability under these conditions is still of major interest for studies in cells that can be considered dormant, but which can revert into viable cells under favorable conditions. According to our experiments, the changes in viability showed highly significant differences between the control and all of the salinities tested, which indicated a negative effect of salt on viability of the microalga cells. For 7 days of exposure to salinity, viable cells remained at high levels in low salinity concentrations (10 and 35 g NaCl L^{-1}); nevertheless, the trend was different for 30 days when viable cells decreased drastically from 10 to 100 g NaCl L^{-1} (corresponding to a reduction of 70.9 %), being the exposure a very important variable to consider. These results agree with Ferjani et al., (2003), who demonstrated that over a longer period of several days, salt stress inhibits cell division.

It is important to highlight that salinity has a major influence on the percentages of living and dead *Scenedesmus* sp. DE2009 cells, since a small proportion of these cells (8.27 %) was still active in high salt concentrations. In this regard, Aanderud et al.,

(2016) estimated bacterial dormancy in different hypersaline and freshwater lakes and found that the proportion of the community exhibiting dormancy was 16 % lower in the former than the latter. An explanation for this result is that halophiles are highly adapted to hypersalinity in stable ecosystems, while salinity is variable in freshwater lakes (Madigan and Marrs, 1997; Harrison et al., 2013).

4.2.2. Evaluation of the effect and immobilization of metals

For this goal, it has been evaluated the *in vivo* toxic effect and cell viability of Pb^{2+}, Cu^{2+} and Cr^{3+} on two phototrophic microorganisms isolated from natural environment (CLSM); and the ability of these microorganisms to uptake Cr^{3+} extra- and/or intracellularly (SEM-EDX and TEM-EDX) as described in Sections 3.2 and 3.3.

The results demonstrated that *Scenedesmus* sp. DE2009 show greater tolerance to Cr^{3+} (0.75 μM Cr^{3+}) than *Geitlerinema* sp. DE2011 (0.25 μM Cr^{3+}), being the Minimum Metal Concentration (MMC) values lower than the level permitted in continental surface waters (50 μg L^{-1} Cr) in accordance with the Spanish law: Real Decreto 817/2015, Annex IV and V. For that reason, both microorganisms could be considered as good indicators of Cr-toxicity in contaminated natural ecosystems, since they detect chromium at low concentrations.

In addition, when *Scenedesmus* sp. DE2009 is polluted with multiple metals (separately and in combination), the MMC values obtained in single metal tests corresponded to the highest Maximum Intensity Fluorescences (MIFs) and, these decreased slightly as compared to the control cells following the order: Pb^{2+} > Cr^{3+} > Cu^{2+}. On the contrary, a decrease in the MIF peaks in response to varying metals mixtures were observed, being the most toxic the combinations with Cu^{2+}. Similar results was obtained in the viability experiments, since *Scenedesmus* sp. DE2009 was more resistant to Pb^{2+} followed by Cr^{3+} and Cu^{2+} in cultures contaminated with a single

metal. Besides, the percentage of living cells decreased in multimetal combinations with Cu^{2+}, whereas the presence of Pb^{2+} and Cr^{3+} in binary and ternary mixtures did not have such a considerable effect.

Despite being a metal considered essential nutrient in cell metabolism for phototrophic microorganisms, copper can be toxic at concentrations as low as 1 μg L^{-1} (Stauber and Davies, 2000); and our results allow to conclude that Cu^{2+} is much more toxic than Pb^{2+} and Cr^{3+} and suggest that, even at low concentration of 0.1 μM Cu^{2+}, the effect of copper is very harmful for living phototrophic microorganisms. Copper has the potential to disturb the photosynthetic electron transport by blocking the enzymes of the PSII (Mohanty et al., 1989; Leunert, et al., 2013).

In aquatic ecological systems, microalgae and cyanobacteria are sensitive indicators of environmental changes and are therefore important test species for the regulatory assessment of metals (Levy et al., 2007). For that reason, it is important to ascertain the IC_{50} parameter as an indicator of metal pollution. In general, the analysis of the IC_{50} is at population level and following standard protocols. Nevertheless, for the first time, the IC_{50} values were determined by CLSM-*λscan* for *Scenedesmus* sp. DE2009 at cell level from the dose-response curves for Pb^{2+}, Cr^{3+} and Cu^{2+} ions and its tri-metallic mixture as an alternative for phototrophic microorganisms that either form aggregates or consortia, or do not grow in solid medium.

In this cases, it was again confirmed that Cu^{2+} was the most toxic metal followed by Cr^{3+} and Pb^{2+} (IC_{50} = 0.328 ± 0.016 mM Cu^{2+}, 2.343 ± 0.162 mM Cr^{3+} and 6.427 ± 0.529 mM Pb^{2+}). Comparing the results obtained by other authors, *Scenedesmus* sp. DE2009 was slightly more sensitive to copper than others microalgae such as *Euglena gracilis* (0.54 ± 0.26 mM Cu^{2+}) (Willeman, 2002) or *Tetraselmis suecica* (0.63 ± 0.06 mM Cu^{2+}) (Millán de Kuhn et al., 2006), respectively. The interactive effect between single metal exposure and tri-metallic solution (IC_{50} ratio) was also found to be synergistic,

thus highlighting the fact that single Pb^{2+} ion was 36.52 times less toxic than in tri-metallic combination with Cr^{3+} and Cu^{2+}. Although the toxicity of Pb^{2+} on cyanobacteria and algae is less harmful than other metals, the binding of the metal onto thylakoid or mitochondria membranes lead to membrane damage and impedes photosynthetic activities (Heng et al., 2004). In general, the presence of heavy metals is reported to inhibit the photosynthesis by the binding to the oxidation sites and the reduction of PSII (Clijsters and Assche, 1985; Shing et al., 2012).

Finally, it is important to worthlight that, the CLSM-*λscan* and CLSM-DL techniques are very sensitive because allows us to detect changes in fluorescence intensity at metal concentrations up to 100 nM.

SEM micrographs show how *Scenedesmus* sp. DE2009 and *Geitlerinema* sp. DE2011 have dense EPS envelopes that can be present in the form of sheaths or slimes. The EPS is one of the strategies used by phototrophic and heterotrophic microorganisms to mitigate the effect of metals. The cell surface consists of polysaccharides, proteins, and lipids that may act as a basic binding site of heavy metals. Various authors have suggested that the overall negative charge of EPS may be essential for sequestering metal cations that are necessary for cell growth and/or preventing the direct contact between the cells and toxic heavy metals dispersed in the environment at low concentrations (Pereira et al., 2011; Mota et al., 2013). Although the functions of EPS in metal uptake are known, studies on exopolysaccharides from algae and cyanobacteria have dealt largely with chemical composition and their protective role, such as protection against dehydration or UV radiation, phagocytosis, and adhesion capacity to the surrounding substrate (Panof et al., 1988; De Philippis and Vincenzini, 2003).

Concerning in the analysis by SEM-EDX, in this study has been demonstrated that *Scenedesmus* sp. DE2009 had the capacity to immobilize Cr^{3+} in the EPS, while

Geitlerinema sp. DE2011 gave a negative result for Cr^{3+} uptake. Nevertheless, in previous studies, it was showed that this cyanobacterium was able to capture Pb^{2+} and Cu^{2+} extracellularly (Burgos et al., 2013). These differences in metal immobilization were probably due to the fact that the same microorganisms can capture distinct metals using different functional groups in the EPS. Priester et al., (2006) detected differences in the monosaccharide composition of EPS in Cr^{6+}-exposed *Pseudomonas putida.*

Moreover, a tendency to increase the thickness of the EPS in a directly proportional way to the concentration of the metal tested has been observed through the images obtained by SEM. In this sense, Decho (1994) observed an increase in EPS production in different microorganisms when they grow in the presence of toxic compounds. A similar correlation was detected by Fang et al., (2002) in a sulphate-reducing bacterial biofilms, an increase of EPS in a nearly 82 % was observed after an exposure of Cr^{3+}. Ozturk and Aslim (2008) also demonstrated that Cr^{6+} was an important stress factor that increase EPS concentration in some cyanobacterial isolates. It can be concluded that differences in composition and values of EPS may promote metal resistance in a microorganism.

TEM micrographs of the ultrathin sections of *Scenedesmus* sp. DE2009 and *Geitlerinema* sp. DE2011 growing with Cr^{3+} showed abundant high electron dense intracytoplasmic inclusions of different sizes in their cytoplasm identified as polyphosphate inclusions (PP). It has been shown using the EDX spectra that, these inclusions are PP because they contain phosphorus (P) and also cations of calcium (Ca) and/or potassium (K). The ability of these inclusions to capture heavy metals were described for the first time by Jensen and Sicko (1974) and Stevens et al., (1985). Their investigations demonstrated that these inclusions have been found when cells are grown in adverse culture conditions, for example, restricted access to nutrients like nitrogen. Recently, different authors described that this kind of inclusions are able to uptake metals and that is why, the microorganisms which accumulate these PP inclusions could

play an important role to detoxify environments polluted by metals (Maldonado et al., 2011; Acharya and Apte, 2013; Burgos et al., 2013; Millach et al., 2015; Rugnini et al., 2017).

The results obtained through EDX analysis of these inclusions demonstrated that *Scenedesmus* sp. DE2009 was able to immobilize Cr^{3+} internally in PP inclusions. By contrast, despite showing PP inclusions, *Geitlerinema* sp. DE2011 did not have the capacity to accumulate Cr^{3+}, giving a negative result for metal uptake as in SEM-EDX analysis. According to the investigations carried out by Zhou et al., (2012) and Kováĉik et al., (2015), microalgae seem to be more effective than cyanobacteria in capturing metals in laboratory cultures, as has been shown in this work. However, in studies made in the natural habitat, in which cyanobacteria are dominant, most of them can sequester metals (Esteve et al., 2013).

Finally, the results obtained in the last eight years by the Microbial Ecology Lab group members considering the effect, biomass and viability of various phototrophic and heterotrophic microorganisms in front of Pb^{2+}, Cu^{2+} and Cr^{3+} are summarized in tables 4.3, 4.4 and 4.5.

Table 4.3. Methodologies used to determine the toxic effect, biomass, viability and sequestration of Pb^{2+} by different microorganisms.

Lead (Pb^{2+})								
Microorganism		**Minimum Inhibitory Concentration**	**CLSM-λscan**	**FLU-CLSM-IA**		**SEM-EDX**	**TEM-EDX**	**Reference**
				Total Biomass (mgC/cm^3)	**Viability** (%)			
Heterotrophic Bacteria	*Micrococcus luteus* sp. DE2008	3 mM	*NA*	96,25 (C) to 77,88 (1,5 mM)	87,52 (C) to 62,5 (1,5 mM)	+ (25 mM)*	-	Maldonado et al., 2010a; Puyen et al., 2012b
	Paracoccus sp. DE2007	*ND*	*NA*	*ND*	*ND*	+ (5 mM)*	-	Baratelli et al., 2011
	Ochrobactrum sp. DE2010	*ND*	*NA*	*ND*	*ND*	+ (10 mM)*	*ND*	Jordi Creus (Master's thesis 2011)
Culture Collection	*Oscillatoria* sp. PCC 7517	*NA*	0,1 mM	*ND*	*ND*	+ (10 mM)*	+ (10 mM)*	Maldonado et al., 2011
	Chroococcus sp. PCC 9106	*NA*	0,5 mM	*ND*	*ND*	+ (10 mM)*	+ (10 mM)*	Maldonado et al., 2011
	Spirulina sp. PCC 6313	*NA*	0,1 mM	*ND*	*ND*	+ (10 mM)*	+ (10 mM)*	Maldonado et al., 2011
Isolated Ebro Delta	*Microcoleus* sp. DE2006	*NA*	0,25 mM	8,326 (C) to 0,507 (25 mM)	*ND*	+ (25 mM)*	+ (25 mM)*	Burnat et al., 2009; 2010
	Scenedesmus sp. DE2009	*NA*	0,1 μM	27,01 (C) to 3,82 (10 mM)	89,61 (C) to 48,83 (10 mM)	+ (10 mM)*	+ (10 mM)*	Maldonado et al., 2010b; Submitted to Aquat. Tox.
In consortia	*Geitlerinema* sp. DE2011	*NA*	0,75 mM	*ND*	*ND*	+ (0,75 mM)**	+ (0,75 mM)**	Burgos et al., 2013
	Scenedesmus sp. DE2009	*NA*	0,1 mM	*ND*	*ND*	+ (0,75 mM)**	+ (0,75 mM)**	Burgos et al., 2013
	Spirulina sp. PCC 6313	*NA*	0,1 mM	*ND*	*ND*	+ (1 mM)**	+ (1 mM)**	Burgos et al., 2013
	Chroococcus sp. PCC 9106	*NA*	0,1 mM	*ND*	*ND*	+ (1 mM)**	+ (1 mM)**	Burgos et al., 2013

* Results obtained from one concentration assayed
** Results obtained from several concentrations assayed
(C): Control experiment
ND: Not Determined
NA: Not Applicable

Table 4.4. Methodologies used to determine the toxic effect, biomass, viability and sequestration of Cu^{2+} by different microorganisms.

Copper (Cu^{2+})								
Microorganism		**Minimum Inhibitory Concentration**	**CLSM-λscan**	**FLU-CLSM-IA**		**SEM-EDX**	**TEM-EDX**	**Reference**
				Total Biomass (mgC/cm^3)	**Viability** (%)			
Heterotrophic Bacteria	*Micrococcus luteus* sp. DE2008	1,5 mM	*NA*	96,25 (C) to 42,11 (1,5 mM)	87,52 (C) to 67 (1,5 mM)	+ (25 mM)*	*NC*	Maldonado et al., 2010a; Puyen et al., 2012b
	Ochrobactrum sp. DE2010	*ND*	*NA*	*ND*	*ND*	-	*ND*	Jordi Creus (Master's thesis 2011)
Culture Collection	*Chroococcus* sp. PCC 9106	*NA*	0,1 μM	*ND*	*ND*	+ (5 nM)**	*NC*	Burgos et al., 2012; Seder-Colomina et al., 2013
	Spirulina sp. PCC 6313	*NA*	0,1 μM	*ND*	*ND*	+ (2 mM)**	*NC*	Burgos et al., 2012; Seder-Colomina et al., 2013
Isolated Ebro Delta	*Microcoleus* sp. DE2006	*NA*	0,25 mM	3,622 (C) to 0,199 (10 mM)	*ND*	+ (10 nM)**	*NC*	Burnat et al., 2009; 2010; Burgos et al., 2012
	Scenedesmus sp. DE2009	*NA*	0,1 μM	*ND*	*ND*	+ (5 μM)**	*NC*	Burgos et al., 2012; Submitted to Aquat. Tox.
	Geitlerinema sp. DE2011	*NA*	0,3 μM	*ND*	*ND*	*ND*	*ND*	Seder-Colomina et al., 2013
I In consortia	*Geitlerinema* sp. DE2011	*NA*	0,1 μM	*ND*	*ND*	+ (5 μM)**	*NC*	Burgos et al., 2013
	Scenedesmus sp. DE2009	*NA*	0,1 μM	*ND*	*ND*	+ (5 μM)**	*NC*	Burgos et al., 2013
	Spirulina sp. PCC 6313	*NA*	1 nM	*ND*	*ND*	+ (10 nM)**	*NC*	Burgos et al., 2013
	Chroococcus sp. PCC 9106	*NA*	1 nM	*ND*	*ND*	+ (10 nM)**	*NC*	Burgos et al., 2013

* Results obtained from one concentration assayed
** Results obtained from several concentrations assayed
(C): Control experiment
ND: Not Determined
NA: Not Applicable
NC: Not Conclusive

Table 4.5. Methodologies used to determine the toxic effect, biomass, viability and sequestration of Cr^{3+} by different microorganisms.

Chromium (Cr^{3+})								
Microorganism		**Minimum Inhibitory Concentration**	**CLSM-λscan**	**FLU-CLSM-IA**		**SEM-EDX**	**TEM-EDX**	**Reference**
				Total Biomass (mgC/cm^3)	**Viability** (%)			
Heterotrophic Bacteria	*Micrococcus luteus* sp. DE2008	3 mM	*NA*	96,25 (C) to 77,88 (1,5 mM)	87,52 (C) to 62,5 (1,5 mM)	+ (0,5 mM)**	*ND*	Natalia Garcia (Master's thesis 2014)
	Paracoccus sp. DE2007	*ND*	*NA*	*ND*	*ND*	+ (2 mM)**	*ND*	Natalia Garcia (Master's thesis 2014)
	Ochrobactrum sp. DE2010	*ND*	*NA*	*ND*	*ND*	+ (2 mM)**	+ (5 mM)**	Aleix Obiol (Master's thesis 2015)
Culture Collection	*Chroococcus* sp. PCC 9106	*ND*	0,26 mM	44,57 (C) to 32,5 (1 mM)	90,08 (C) to 70,28 (1 mM)	+ (1,5 mM)**	+ (1,5 mM)**	Puyen et al., 2017
Isolated Ebro Delta	*Geitlerinema* sp. DE2011	*ND*	0,25 μM	*ND*	*ND*	-	-	Millach et al., 2015
	Scenedesmus sp. DE2009	*ND*	0,75 μM	47,92 (C) to 42,39 (500 μM)	87,2 (C) to 81,6 (500 μM)	+ (200 μM)**	+ (200 μM)**	Millach et al., 2015

* Results obtained from one concentration assayed
** Results obtained from several concentrations assayed
(C): Control experiment
ND: Not Determined
NA: Not Applicable

Chapter 5 – Conclusions and Future prospects

The conclusions set out below describe, on the one hand, the benefits of the methodologies used, and on the other, their application in assessing the effect of changing environmental parameters and metal pollution on *Scenedesmus* sp. DE2009 and *Geitlerinema* sp. DE2011 selected in this work.

Conclusions obtained based on methodological optimization

1. All the CLSM methodologies presented in this work that use the Chl *a* fluorescence as a biomarker are: *in vivo*, at single-cell level, non-invasive, highly sensitive, versatile, accurate, and provide reliable results in a short time.

2. Pigment analysis by CLSM-*λscan* function is an accurate and suitable technique, which has been applied to evaluate the tolerance and resistance of *Scenedesmus* sp. DE2009 and *Geitlerinema* sp. DE2011 against metal pollution, as well as analyze the impact of environmental changes on *Scenedesmus* sp. DE2009 at pigment level.

3. The estimation of the IC_{50} parameter, from the dose-response curves obtained by CLSM-*λscan*, is a good alternative for the *in vivo* determination of the toxicity of metals on *Scenedesmus* sp. DE2009, which forms consortium with heterotrophic bacteria and grow with difficulty on solid medium.

4. The application of the 405 nm UV laser excitation to capture the whole spectral visible range in CLSM-*λscan* experiments, make it possible to distinguish and identify a new autofluorescence signature: the Non-Photosynthetic Autofluorescence (NPAF) signal linked to dead cells.

5. The newly developed CLSM-DL method, that do not require staining or additional use of image processing software, can be useful to (i) distinguish viable and non-viable cells of *Scenedesmus* sp. DE2009 consortium, because it rules out any interference with heterotrophic microorganisms; and (ii) characterize the physiological state of individual cells within microbial communities in extreme environments, in which dead and living cells coexist.

6. The CLSM-DL method combined with the CLSM-*λscan* function confirms that there is a strong and good correlation between the performance of photosynthetic pigments and the percentages of living and dead individual cells. The simultaneous application of various CLSM techniques allows a swift diagnosis of different stressing factors as it is demonstrate in *Scenedesmus* sp. DE2009 growing at different salt concentrations.

7. Samples preparation for SEM is optimized to obtain filters with the appropriate phototrophic biomass, in order to avoid the obstruction of aggregates in the critical point drier device. For SEM-EDX samples, the metallization is carried out with Au-Pd because these metals do not cause any interference with the Cr peak in EDX microanalysis; and several times to avoid an excessive electron charge on the surface layer of the specimen.

8. The observation of the samples by the electronic microscopy allows evaluating the changes in cell morphology (SEM) and cellular ultrastructure (TEM) of *Scenedesmus* sp. DE2009 and *Geitlerinema* sp. DE2011. Furthermore, SEM-EDX and TEM-EDX are very useful techniques to check the capacity of these microorganisms to immobilize a metal extracellularly in the EPS and/or intracellularly in the PP inclusions.

Conclusions from the results obtained

9. The optimal light condition for the growth of *Scenedesmus* sp. DE2009 determined in laboratory cultures is in the range of 6 – 8 μE m^{-2} s^{-1}. This parameter has been fixed in order to perform the subsequent salinity experiments. This light intensity is recommended for any other type of study related with this microorganism.

10. The assessment of the salinity effect on *Scenedesmus* sp. DE2009 demonstrates that the impact on photosynthetic pigments and percentage of living cells is harmful from 35 g L^{-1} over a short period and drastic from 10 g L^{-1} over a long period of time. However, a small proportion of the microalga cells (8.27 %) is still active after 30 days of exposure at the highest salt dose.

11. *Scenedesmus* sp. DE2009 and *Geitlerinema* sp. DE2011 could be considered as good bioindicators of metal toxicity in natural contaminated environments, since significant changes in the biomarker (Chl *a*) are observed even at very low concentrations (0.1 μM Pb^{2+}, 0.1 μM Cu^{2+} and 0.75 μM Cr^{3+}).

12. SEM-EDX and TEM-EDX analysis of *Scenedesmus* sp. DE2009 and *Geitlerinema* sp. DE2011 demonstrate that, at wide range of Cr-concentrations assayed, only *Scenedesmus* sp. DE2009 is able to capture Cr^{3+} extracellularly in EPS and intracellularly in PP inclusion from 200 μM Cr^{3+}. In addition, the microalga biomass slightly decrease from 47.92 ± 2.73 mgC cm^{-3} (control culture) to 42.39 ± 1.96 mgC cm^{-3} (500 μM Cr^{3+}) and it also maintains an elevated cellular viability (81.61 % at 500 μM Cr^{3+}).

13. In cultures contaminated with a single metal, *Scenedesmus* sp. DE2009 is more resistant to Pb^{2+} followed by Cr^{3+} and Cu^{2+}. On the contrary, the pigment fluorescence and the percentage of living microalga cells decrease in multi-metal combinations, especially with Cu^{2+}. Therefore, copper has a greater toxicity than chromium and lead (Cu >> Cr > Pb).

14. The interactive effect between single metal exposure versus the tri-metallic solution (IC_{50} ratio) is synergistic; thus highlighting the fact that single Pb^{2+} is 36.52 times less toxic than in tri-metallic combination. This is probably due to the presence of copper that, even at a low concentration of 100 nm Cu^{2+}, is very harmful for *Scenedesmus* sp. DE2009 cells.

Future prospects

The study presented opens up new short- and long-term prospects for research. In the short-term, and in accordance with the results obtained, the work started during my stay in the NASA Ames Research Center, California, USA, should be completed. The aim of that work was to evaluate the photosynthetic activity in *Scenedesmus* sp. DE2009 using the PAM fluorometric technique, obtaining several photo-physiological results, such as photosynthetic efficiency, or irradiance curves versus photosynthesis. Experiments were also started to determine whether the *Scenedesmus* sp. DE2009 consortium was more resistant to environmental changes than the axenic culture of this microorganism.

In the longer term, the results obtained in this work provide many possibilities to study the different extreme environments in which phototropic microorganisms dominate. In this work, it is shown that the combination of all the methodologies described, and the use of CLSM, when applied simultaneously, can evaluate at the same time and in the same sample: the diversity, the physiological state of photosynthetic pigments, the biomass and the viability of a phototropic microorganism against any stress factor, preventing the heterotrophic community that forms the consortium, since they do have autofluorescence.

Samples from the Namibia Desert are currently being analyzed using some of the methodologies described in this work, and it is expected to perform analogous studies in samples from Antarctica. The samples come from a project, in which the Microbial Ecological Lab (UAB) collaborates, and for which Dr. Asunción de los Ríos is the investigator.

Finally, the identification of the NPAF signal linked to dead cells opens new possibilities to study the origin of this green autofluorescence signal and to what it could be due, thus requiring further studies to be carried out.

References

Aanderud, Z.T., Vert, J.C., Lennon, J.T., Magnusson, T.W., Breakwell, D.P., Harker, A.R. **(2016)** Bacterial dormancy is more prevalent in freshwater than hypersaline lakes. *Front. Microbiol.* 7, 853.

Acharya, C., Apte, S.K. **(2013)** Novel surface associated polyphosphate bodies sequester uranium in the filamentous, marine cyanobacterium, *Anabaena torulosa. Metallomics.* 5, 1595-1598.

Allakhverdiev, S.I., Murata, N. **(2008)** Salt stress inhibits photosystems II and I in cyanobacteria. *Photosynth. Res.* 98, 529-539.

Al-Rubeai, M., Welzenbach, K., Lloyd, D.R., Emery, A.N. **(1997)** A rapid method for evaluation of cell number and viability by flow cytometry. *Cytotechnology.* 24, 161.

Andersson, B., Aro, E.M. **(2001)** Photodamage and D1 protein turnover in photosystem II, in: Aro, E.M., Anderson, B. (Eds.) *Regulation of Photosynthesis.* Kluwer Academic, Dordrecht, the Netherlands, pp. 377-393.

Antibus, D.E., Leff, L.G., Hall, B.L., Baeseman, J.L., Blackwood, C.B. **(2012)** Cultivable bacteria from ancient algal mats from the McMurdo Dry Valleys, Antarctica. *Extremophiles.* 16, 105-114.

Aro, E.M., Virgin, I., Andersson, B. **(1993)** Photoinhibition of photosystem II: inactivation, protein damage and turnover. *Biochim. Biophys. Acta.* 1143, 113-134.

Azua-Bustos, A., Urrejol, C., Vicuña, R. **(2012)** Life at the dry edge: Microorganisms of the Atacama Desert. *FEBS Letters.* 586, 2939-2945.

Balasch, E., Ruiz, Y. **(1998)** El Parque Natural del Delta del Ebro, Geoplaneta. Barcelona, Planeta.

Belapurkar, P., Goyal, P., Kar, A. **(2016)** In vitro evaluation of bioremediation capacity of a commercial probiotic, Bacillus coagulans, for chromium (VI) and lead (II) toxicity. *J. Pharm. Bioallied Sci.* 8(4), 272-276.

Billi, D., Viaggiu, E., Cockell, C.S., Rabbow, E., Horneck, G., Onofri, S. **(2011)** Damage escape and repair in dried *Chroococcidiopsis* spp. from hot and cold deserts exposed to simulate space and Martian conditions. *Astrobiology.* 11, 65-73.

Broch-Due, M., Ormerod, J.G., Strand, F. **(1976)** Effect of light intensity on vesicle formation in *Chlorobium. Arch. Microbiol.* 116(3), 269-274.

Büchel, C., Wilhelm, C. **(1993)** In vivo analysis of slow chlorophyll fluorescence induction kinetics in algae: progress, problems and perspectives. *Photochem. Photobiol.* 58, 137-148.

Buck, J.D. **(1979)** The plate count in aquatic microbiology, in: Costerton, J.W., Colwell, R.R. (Eds.), Native aquatic bacteria: enumeration, activity, and ecology. *ASTM STP 695*, Baltimore, pp. 19-28.

Burgos, A., Seder-Colomina, M., Maldonado, J., Solé, A., Esteve, I. **(2012)** Scanning Electron Microscopy coupled to an Energy Dispersive X-ray detector to study copper removal on different phototrophic microorganisms, in: Méndez-Vilas, A. (Ed.), *Current Microscopy Contributions to Advances in Sceince and Technology*. Microscopy Book Series, Formatex Research Center. Number 5, Vol. 1, pp. 222-229.

Burgos, A., Maldonado, J., de los Ríos, A., Solé, A., Esteve, I. **(2013)** Effect of copper and lead on two consortia of phototrophic microorganisms and their capacity to sequester metals. *Aquat. Toxicol.* 140-141, 324-336.

Burnat, M., Diestra, E., Esteve, I., Solé, A. **(2009)** *In situ* determination of the effects of lead and copper on cyanobacterial populations in microcosms. *PLoS One.* 4, e6204.

Burnat, M., Diestra, E., Esteve, I., Solé, A. **(2010)** Confocal laser scanning microscopy coupled to a spectrofluorometric detector as a rapid tool for determining the *in vivo* effect of metals on phototrophic bacteria. *Bull. Environ. Contam. Toxicol.* 84, 55-60.

Campidelli, S., Abou Khachfe, R., Jaouen, K., Monteiller, J., Amra, C., Zerrad, M., Cornut, R., Derycke, V., Ausserré, D. **(2017)** Backside absorbing layer microscopy: Watching graphene chemistry. *Sci. Adv.* 3(5):e1601724.

Chaibenjawong, P., Foster, S.J. **(2011)** Desiccation tolerance in *Staphylococcus aureus. Arch. Microbiol.* 193, 125-135.

Chakraborty P., Raghunadh Babu P.V., Acharyya T., Bandyopadhyay D. **(2010)** Stress and toxicity of biologically important transition metals (Co, Ni, Cu and Zn) on phytoplankton in a tropical freshwater system: An investigation with pigment analysis by HPLC. *Chemosphere.* 80(5), 548–553.

Chang, F.C., Ko, C.H., Tsai, M.J., Wang, Y.N., Chung, C.Y. **(2014)** Phytoremediation of heavy metals contaminated soil by *Jatropha curcas. Ecotoxicology.* 23, 1969-1978.

Cheng, Y., Yan, F., Huang, F., Chu, W., Pan, D., Chen, Z., Zheng, J., Yu, M., Lin, Z., Wu, Z. **(2010)** Bioremediation of Cr(IV) and immobilization as Cr(III) by *Ochrobactrum anthropi. Environ. Sci. Technol.* 44, 6357-6363.

Clijsters, H., Assche, V.V. **(1985)** Inhibition of photosynthesis by heavy metals. *Photosyn. Res.* 7, 31-40.

Cole, J.K., Hutchison, J.R., Renslow, R.S., Kim, Y.M., Chrisler, W.B., Engelmann, H.E., Dohnalkova, A.C., Hu, D., Metz, T.O., Fredrickson, J.K., Lindemann, S.R. **(2014)** Phototrophic biofilm assembly in microbial-mat-derived unicyanobacterial consortia: model systems for the study of autotroph-heterotroph interactions. *Front. Microbiol.* 5, 109.

Coreño-Alonso, A., Solé, A., Diestra, E., Esteve, I., Gutiérrez-Corona, J.F., Reyna López, G.E., Fernández, F.J., Tomasini, A. **(2014)** Mechanisms of interaction of chromium with *Aspergillus niger* var *tubingensis* strain Ed8. *Bioresour. Technol.* 158, 188-192.

Crowe, L.M., Crowe, J.H. **(1992)** Anhydrobiosis: a strategy for survival. *Adv. Space Res.* 12, 239-247.

Csotonyi, J.T., Swiderski, J., Stackebrandt, E., Yurkov, V. **(2010)** A new extreme environment for aerobic anoxygenic phototrophs: biological soil crusts. *Adv. Exp. Med. Biol.* 675, 3-15.

Cuadrado, D.G., Pan, J., Gómez, E.A., Maisano, L. **(2015)** Deformed microbial mat structures in a semiarid temperate coastal setting. *Sediment. Geol.* 325, 106-118.

Çelekli, A., Kapı, M., Bozkurt, H. **(2013)** Effect of cadmium on biomass, pigmentation, malondialdehyde, and proline of *Scenedesmus quadricauda* var. *longispina. Bull. Environ. Contam. Toxicol.* 91, 571-576.

de los Ríos, A., Wierzchos, J., Sancho, L.G., Ascaso, C. **(2004)** Exploring the physiological state of continental Antarctic endolithic microorganisms by microscopy. *FEMS Microbiol. Ecol.* 50, 143–152.

de los Ríos, A., Wierzchos, J., Ascaco, C. **(2014)** The lithic microbial ecosystems of Antarctica's McMurdo Dry Valleys. *Antarct. Sci.* 26(05), 459-477.

de los Ríos, A., Ascaso, C., Wierzchos, J., Vincent, W.F., Quesada, A. **(2015)** Microstructure and cyanobacterial composition of microbial mats from the High Artic. *Biodivers. Conserv.* 24(4), 841-863.

de la Torre, J.R., Goebel, B.M., Friedmann, E.I., Pace, N.R. **(2003)** Microbial Diversity of Cryptoendolithic Communities from the McMurdo Dry Valleys, Antarctica. *Appl. Environ. Microbiol.* 69(7), 3858-3867.

De Philippis, R., Vincenzini, M. **(2003)** Outermost polysaccharidic investments of cyanobacteria: nature, significance and possible applications. *Recent. Res. Dev. Microbiology.* 7, 13-22.

Decho, A.W. **(1994)** Exopolymers in microbial mats: assessing their adaptative roles, in: Stal L.J., Caumette P. (Eds.), *Microbial Mats. Structure, development and environment significance.* Springer-Verlag, Berlin, Heidelberg, pp. 215-219.

Deutzmann, J.S., Stief, P., Brandes, J., Schink, B. **(2014)** Anaerobic methane oxidation coupled to denitrification is the dominant methane sink in a deep lake. *Proc. Natl. Acad. Sci.* 111(51), 18273-18278.

Diestra, E., Solé, A., Martí, M., García de Oteyza, T., Grimalt, J.O., Esteve, I. **(2005)** Characterization of an oil-degrading *Microcoleus* consortium by means of confocal scanning microscopy, scanning electron microscopy and transmission electron microscopy. *Scanning.* 27, 176-180.

Diestra, E., Esteve, I., Burnat, M., Maldonado, J. Solé, A. **(2007)** Isolation and characterization of a heterotrophic bacterium able to grow in different enviormental stress, including crude oil and heavy metals, in: Méndez-Vilas, A. (Ed.), *Communicating Current Research and Educational Topics and Trends in Applied Microbiology: an Overview.* Microbiology Book Series, Formatex Research Center. Number 1, Vol. 1, pp. 90-99.

Dorsey, J., Yentsch, C.M., Mayo, S., McKenna, C. **(1989)** Rapid analytical technique for the assessment of cell metabolic activity in marine microalgae. *Cytometry.* 10, 622-628.

Dworkin, J., Shah, I.M. **(2010)** Exit from dormancy in microbial organisms. *Nat. Rev. Microbiol.* 8, 890-896.

Edwardson, C.F., Planer-Friedrich, B., Hollibaugh, J.T. **(2014)** Transformation of monothioarsenate by haloalkaliphilic, anoxygenic photosynthetic purple sulfur bacteria. *FEMS Microbiol. Ecol.* 90, 858–868.

Esteve, I., Montesinos, E., Mitchell, J.G., Guerrero, R. **(1990)** A quantitative ultrastructural study of *Chromatium minus* in the bacterial layer of Lake Cisó (Spain). *Arch. Microbiol.* 153, 316-323.

Esteve, I., Martínez-Alonso, M., Mir, J. **(1992)** Distribution, typology and structure of microbial mat communities in Spain. Preliminary studies. *Limnetica.* 8, 185-195.

Esteve, I., Ceballos, D., Martínez-Alonso, M., Gaju, N., Guerrero, R. **(1994)** Development of versicolored microbial mats: succession of microbial communites, in: Stal L.J. and Caumette P. (Eds.), *Microbial mats: structure, development and environmental significance.* NATO ASI Series G: Ecological Sciences, Springer-Verlag, Berlin, Heidelberg, pp. 4165–4420.

Esteve, I., Maldonado, J., Burgos, A., Diestra, E., Burnat, M., Solé, A. **(2013)** Confocal laser scanning and electron microscopic techniques as powerful tools for determining the in vivo effect and sequestration capacity of lead in cyanobacteria, in: da Silva Ferrão Filho, A. (Eds.), Cyanobacteria: Toxicity, Ecology and Management. *ISBN Nova Science Publishers.*

Faisal, M., Hasnain, S. **(2004)** Comparative study of Cr(VI) uptake and reduction in industrial effluent by *Ochrobactrum intermedium* and *Brevibacterium* sp. *Biotechnol. Lett.* 26, 1623-1628.

Fang, H.H.P., Xu, L.C., Chan, K.Y. **(2002)** Effects of toxic metals and chemicals on biofilm and biocorrosion. *Water Res.* 36, 4709-4716.

Ferjani, A., Mustardy, I., Sulpice, R., Marin, K., Suzuki, I., Hagemann, M., Murata, N. **(2003)** Glucosylglycerol, a compatible solute, sustains cell division under salt stress. *Plant Physiol.* 131, 1628-1637.

Fernández-Martínez, M.A., Pointing, S.B., Pérez-Ortega, S., Arróniz-Crespo, M., Green, T.G.A., Rozzi, R., Sancho, L.G., de los Ríos, A. **(2016)** Functional ecology of soil microbial communities along a glacier forefield in Tierra del Fuego (Chile). *Int. Microbiol.* 19(3), 161-173.

Ferreira, V.S., Pinto, R.F., Sant'Anna, C. **(2016)** Low light intensity and nitrogen starvation modulate the chlorophyll content of *Scenedesmus dimorphus. J. Appl. Microbiol.* 120 (3), 661-70.

Franklin, N.M., Stauber, J.L., Lim, R.P., Petocz, P. **(2002)** Toxicity of metal mixtures to a tropical freshwater alga (*Chlorella* sp.): the effect of interactions between copper, cadmium, and zinc on metal cell binding and uptake. *Environ. Toxicol. Chem.* 21(11), 2412-2422.

Fry, J.C. **(1990)** Direct methods and biomass estimation. *Method Microbiol.* 22, 41-85.

García-Moyano, A., González-Toril, E., Aguilera,A., Amils, R. **(2012)** Comparative microbial ecology study of the sediments and the water column of the Río Tinto, an extreme acidic environment. *FEMS Microbial. Ecol.* 81(2), 303-314.

Garcia-Pichel, F., López-Cortés, A., Nübel, U. **(2001)** Phylogenetic and Morphological Diversity of Cyanobacteria in Soil Desert Crust from the Colorado Plateau. *Appl. Environ. Microbiol.* 67(4), 1902-1910.

Genty, B., Briantais, J.M., Baker, N.R. **(1989)** The relationship between the quantum yield of photosynthetic electron transport and quenching of chlorophyll fluorescence. *Biochim. Biophys. Acta.* 990, 87–92.

Gilbert, E.S., Khlebnikov, A., Meyer-Ilse, W., Keasling, J.D. **(1999)** Use of soft X-ray microscopy for analysis of early-stage biofilm formation. *Water Sci. Technol.* 39(7), 269-272.

Glaring, M.A., Vester, J.K., Lylloff, J.E., Abu Al-Soud, W., Sørensen, S.J., Stougaard, P. **(2015)** Microbial Diversity in a Permanently Cold and Alkaline Environment in Greenland. *PLoS One.* 10(4): e0124863.

Goldberg, J., González, H., Jensen, T.E., Corpe, W.A. **(2001)** Quantitative analysis of the elemental composition and the mass of bacterial polyphosphate bodies using STEM EDX. *Microbios.* 106, 177-188.

Gómez, V., Callao, M.P. **(2006)** Chromium determination and speciation since 2000. *Trends Analyt. Chem.* 25, 1006-1015.

González-Ramírez, A.I., Ramírez-Granillo, A., Medina-Canales, M.G., Rodríguez-Tovar, A.V., Martínez-Rivera, M.A. **(2016)** Analysis and description of the stages of Aspergillus fumigatus biofilm formation using scanning electron microscopy. *BCM Microbiol.* 18(1), 243.

Gordon, R., Bender, R., Herman, G.T. **(1970)** Algebraic reconstruction techniques (ART) for three-dimensional electron microscopy and x-ray photography. *J. Theor. Biol.* 29(3), 471-481.

Green, S.J., Blackford, C., Bucki, P., Jahnke, L.L., Prufert-Bebbout, L. **(2008)** A salinity and sulfate manipulation of hypersaline microbial mats reveals stasis in the cyanobacterial community structure. *ISME J.* 2, 457-470.

Gregor, J., Maršálek, B. **(2004)** Freshwater phytoplankton quantification by chlorophyll a: a comparative study of in vitro, in vivo and in situ methods. *Water Res.* 38, 517-522.

Guerrero, R., Piqueras, M., Berlanga, M. **(2002)** Microbial mats and the search for minimal ecosystems. *Int. Microbiol.* 5, 177-188.

Hanikenne, M., Krämer, U., Demoulin V., Baurain, D. **(2005)** A comparative inventory of metal transporters in the green alga *Chlamydomonas reinhardtii* and the red alga *Cyanidioschizon merolae*. *Plant Physiol.* 137, 428-446.

Harrison, J.P., Gheeraert, N., Tsigelnitskiy, D., Cockell, C.S. **(2013)** The limits for life under multiple extremes. *Trends Microbiol.* 21, 204-212.

Hayashida, G., Schneider, C., Espíndola, L., Arias, D., Riquelme, C., Wulff-Zottele, C., Díaz-Palma, P., Rivas, M. **(2017)** Characterization of a Chlorophyta microalga isolated from a microbial mat in Salar de Atacama (northern Chile) as a potential source of compounds for biotechnological applications. *Phycological Res.* doi: 10.1111/pre.12176.

Heng, L.Y., Jusoh, K., Mui Ling, C.H., Idris, M. **(2004)** Toxicity of single and combinations of lead and cadmium to the cyanobacteria *Anabaena flos-aquae*. *Bull. Environ. Contam. Toxicol.* 72, 373-379

Hill, D.R., Peat, A., Potts, M. **(1994)** Biochemistry and structure of the glycan secreted by desiccation-tolerant *Nostoc commune* (Cyanobacteria). *Protoplasma.* 182(3), 126-148.

Hoehler, T.M., Bebout, B.M., Des Marais, D.J. **(2001)** The role of microbial mats in the production of reduced gases on the early Earth. *Nature* 412, 324–327.

Hoekstra, F.A., Golovina, E.A., Buitink, N.J. **(2001)** Mechanisms of plant desiccation tolerance. *Trends Plant Sci.* 6(9), 431- 438.

Hoffmann, D., Maldonado, J., Wojciechowski, M.F., Garcia-Pichel, F. **(2015)** Hydrogen export from intertidal cyanobacterial mats: sources, fluxes and the influence of community composition. *Environ. Microbiol.* 17(10), 3738-53.

Horikoshi, K., Grant, W.D. **(1998)** Extremophiles: Microbial Life in Extreme Environments, Wiley-Liss.

Hou, W., Chen, X., Song, G., Wang, Q., Chang, C.C. **(2007)** Effects of copper and cadmium on heavy metal polluted waterbody restoration by duckweed (*Lemna minor). Plant Physiol. Biochem.* 45, 62-69.

Huot, Y., Babin, M. **(2011)** Overview of fluorescence protocols: theory, basic concepts and practice, in: Suggett, D.J., Prášil, O., Borowizka, M.A. (Eds.), *Chlorophyll a fluorescence in aquatic sciences: methods and applications.* Springer, Dordrecht, pp. 31-74.

Jensen, T.E., Sicko, L.M. **(1974)** Phosphate metabolism in blue-green algae. I. Fine structure of the "polyphosphate overplus" phenomenon in *Plectonema boryanum. Can. J. Microbiol.* 20, 1235-1239.

Jeong, G.S., Kim, B.W. **(1999)** The influence of light/dark cycle at low light frequency on the desulfurization by a photosynthetic microorganism. *J. Biosci. Bioeng.* 87(4), 481-488.

Jungblut, A.D., Neilan, B.A. **(2010)** NifH-gene diversity and expression in a microbial mat community on the McMurdo Ice Shelf, Antarctica. *Antarc. Sci.* 22, 117-122.

Kalita, D., Shome, D., Jain, V.G., Chadha, K., Bellare, J.R. **(2014)** In Vivo Intraocular Distribution and Safety of Periocular Nanoparticle Carboplatin for Treatment of Advanced Retinoblastoma in Humans. *Am. J. Ophtal.* 157(5), 1109-1115.

Kamala-Kannan, S., Dass Batvari, B.P., Lee, K.J., Kanna, N., Krishnamoorthy, R., Shanti, K., Jayaprakash, M. **(2008)** Assessment of heavy metals (Cd, Cr and Pb) in water, sediment and seaweed (*Ulva lactuca*) in the Pulicat Lake, South East India. *Chemosphere.* 71, 1233-1240.

Kato, S., Kobayashi, C., Kakegawa, T., Yamagishi, A. **(2009)** Microbial communities in iron-silica-rich microbial mats at deep-sea hydrothermal fields of the Southern Mariana Trough. *Environ. Microbiol.* 11, 2094-2111.

Kirst, G.O. **(1990)** Salinity tolerance of eukaryotic marine algae. *Annu. Rev. Plant Physiol. Plant Mol. Biol.* 41, 21-53.

Knowles, E.J., Castenholz, R.W. **(2008)** Effect of exogenous extracellular polysaccharides on the desiccation and freezing tolerance of rock-inhabiting phototrophic microorganisms. *FEMS Microbiol. Ecol.* 66(2), 261-270.

Kováčik, J., Babula, P., Hedbavny, J., Kryštofová, O., Provaznik, I. **(2015)** Physiology and methodology of chromium toxicity using alga *Scenedesmus quadricauda* as model object. *Chemosphere.* 120, 23-30.

Kremer, J.R., Mastronarde, D.N., McIntosh, J.R. **(1996)** Computer visualitzation of three-dimensional image data using IMOD. *J. Struct. Biol.* 116, 71-76.

Kroemer, G., Petit, P., Zamzami, N., Vayssière, J.L., Mignotte, B. **(1995)** The biochemistry of programmed cell death. *FASEB J.* 9, 1277-1287.

Kumar, K.S., Dahms, H.U., Lee, J.S., Kim, H.C., Lee, W.C., Shin, K.H. **(2014)** Algal photosynthetic responses to toxic metals and herbicides assessed by chlorophyll *a* fluorescence. *Ecotoxicol. Environ. Saf.* 104, 51-71.

Lan, S., Wu, L., Zhang, D., Hu, C. **(2014)** Desiccation provides photosynthetic protection for crust cyanobacteria Microcoleus vaginatus from high temperature. *Physiol. Plant.* 152(2), 345-54.

Lawrence, J.R., Swerhone, G.D.W., Leppard, G.G., Araki, T., Zhang, X., West, M.M., Hitchcock, A.P. **(2003)** Scanning Transmission X-Ray, Laser Scanning, and Transmission Electron Microscopy Mapping of the Exopolymeric Matrix of Microbial Biofilms. *Appl. Environ. Microbiol.* 69, 95543-95554.

Lebre, P.H., De Maayer, P., Cowan, D.A. **(2017)** Xerotolerant bacteria: surviving through a dry spell. *Nat. Rev. Microbiol.* 15(5), 285-296.

Leonardo, T., Farhi, E., Pouget, S., Motellier, S., Boisson, A.M., Banerjee, D., Rébeillé, F., den Auwer, C., Rivasseau, C. **(2016)** Silver Accumulation in the Green Microalga Coccomyxa actinabiotis: Toxicity, in Situ Speciation, and Localization Investigated Using Synchrotron XAS, XRD, and TEM. *Environ. Sci. Technol.* 50 (1), 359–367.

Leunert, F., Grossart, H.P., Gerhardt, Volkmar., Eckert, Werner. **(2013)** Toxicant induced changes on delayed fluorescence decay kinetics of cyanobacteria and green algae: a rapid and sensitive biotests. *PLoS One.* 8(4), e63127.

Levy, J.L., Stauber, J.L., Jolley, D.F. **(2007)** Sensitivity of marine microalgae to copper: The effect of biotic factors on copper adsorption and toxicity. *Sci. Total Environ.* 387, 141-154.

Liu, X.D., Shen, Y.G. **(2004)** NaCl-induced phophorylation of light harvesting chlorophyll *a/b* proteins in thylakoid membranes from the halotolcrant green alga. *Dunaliella salina. FEBS Lett.* 569, 337-340

Lu, C.M., Zhang, J.H. **(1999)** Effects of salt stress on PSII function and photoinhibition in the cyanobacterium Spirulina platensis. *J. Plant Physiol.* 155, 740-745.

Madigan, M.T., Marrs, B.L. **(1997)** Extremophiles. *Sci. Am.* 276, 82-87.

Magdaleno, A., Vélez, C.G., Wenzel, M.T., Tell, G. **(2014)** Effects of cadmium, copper and zinc on growth of four isolated algae from a highly polluted Argentina river. *Bull. Environ. Contam. Toxicol.* 92, 202-207.

Maldonado, J., Diestra, E., Huang, L., Domènech, A.M., Villagrasa, E., Puyen, Z.M., Duran, R., Esteve, I., Solé, A. **(2010a)** Isolation and identification of a bacterium with high tolerance to lead and copper from marine microbial mat in Spain. *Ann. Microbiol.* 60, 113-120.

Maldonado, J., de los Rios, A., Esteve, I., Ascaso, C., Puyen, Z.M., Brambilla, C., Solé, A. **(2010b)** Sequestration and *in vivo* effect of lead on DE2009 microalga, using high-resolution microscopic techniques. *J. Hazard. Mater.* 183, 44–50.

Maldonado, J., Solé, A., Puyen, Z.M., Esteve, I. **(2011)** Selection of bioindicators to detect lead pollution in Ebro delta microbial mats, using high-resolution microscopic techniques. *Aquat Toxicol.* 104, 135-144.

Mallick, N., Mohn, F.H. **(2003)** Use of chlorophyll fluorescence in metal-stress research: a case study with the green microalga *Scenedesmus. Ecotoxicol. Environ. Saf.* 55, 64-69.

Manahan, S.E. **(2009)** Environmental chemistry, 9th ed.; CRC Press LLC, Taylor and Francis Group, USA.

Mañosa, S., Mateo, R., Guitart, R. **(2001)** A review of the effects of agricultural and industrial contamination on the Ebro Delta biota and wildlife. *Environ. Monit. Assess.* 71, 187-205.

Mateo, R., Martinez-Vilalta, A. Guitart, R. **(1997)** Lead shot pellets in the Ebro delta, Spain: densities in sediments and prevalence of exposure in waterflow. *Environ. Pollut.* 96, 335-341.

Mehta, P., Jajoo, A., Mathur, S., Bharti, S. **(2010)** Chlorophyll *a* fluorescence study revealing effects of high salt stress on Photosystem II in wheat leaves. *Plant Physiol. Biochem.* 48, 16-20.

Merchant, S.S., Allen, M.D., Kropat, J., Moseley, J.L., Long, J.C., Tottey, S., Terauchi, A.M. **(2006)** Between a rock and a hard place: trace element nutrition in Chlamydomonas. *Biochim. Biophys. Acta.* 1763, 578-594.

Messaoudii, C., Boudier, T., Sanchez Sorzano, C.O., Marco, S. **(2007)** TomoJ: tomography software for three-dimensional reconstruction in transmission electron microscopy. *BMC Bioinformatics.* 8, 288.

Millach, L., Solé, A., Esteve, I. **(2015)** Role of *Geitlerinema* sp. DE2011 and *Scenedesmus* sp. DE2009 as bioindicators and immobilizers of chromium in a contaminated natural environment. *Biomed Res. Int.* Vol. 2015, Article ID 519769, 11 pages.

Millach, L., Obiol, A., Solé. A., Esteve, I. **(2017)** A novel method to analyze *in vivo* the physiological state and cell viability of phototrophic microorganisms by confocal laser scanning microscopy using a dual laser. *J. Microsc.* doi:10.1111/jmi.12586.

Millán de Kuhn, R., Streb, C., Breiter, R., Richter, P., Neeβe, T., Häder, D.-P. **(2006)** Screening for unicellular algae as possible bioassay organisms for monitoring marine water samples. *Water Res.* 40, 2695-2703.

Millonig, G. **(1961)** Advantages of phosphate buffer OsO_4 solutions in fixation. *J. Appl. Phys.* 32, 1637.

Miranda, P.J., McLain, N.K., Hatzenpichler, R., Orphan, V.J., Dillon, J.G. **(2016)** Characterization of chemosynthetic microbial mats associated with intertidal hydrothermal sulfur vents in White Point, San Pedro, CA, USA. *Front. Microbiol.* 7, 1163.

Mohanty, N., Vass, I., Demeter, S. **(1989)** Copper toxicity affects photosystem II electron transport at the secondary quinine acceptor, QB. *Plant Physiol.* 90, 175-179.

Morgan-Kiss, R.M., Priscu, J.C., Pocock, T., Gudynaite-Savitch, L., Huner, N.P.A. **(2006)** Adaptation and Acclimation of Photosynthetic Microorganisms to Permanently Cold Environments. *Microbiol. Mol. Biol. Rev.* 70(1), 222-252.

Mota, R., Guimarães, R., Büttel, Z., Rossi, F., Colica, G., Silva, C.J., Santos, C., Gales, L., Zille, A., De Philippis, R., Pereira, S.B., Tamagnini, P. **(2013)** Production and characterization of extracellular carbohydrate polymer from *Cyanothece* sp. CCY 0110. *Carbohydr Polym.* 92, 1408-1415.

Murata, N., Takahashi, S., Nishiyama, Y., Allakhverdiev, S.I. **(2007)** Photoinhibition of photosystem II under environmental stress. *Biochim. Biophys. Acta.* 1767, 414-421.

Naganuma, T. **(1996)** Differential enumeration of intact and damaged marine planktonic bacteria based on cell membrane integrity. *J. Aquat. Ecosystem Health.* 5, 217-222.

Nakagawa, T., Fukui, M. **(2002)** Phylogenetic characterization of microbial mats and streamers from a Japanese alkaline hot spring with a thermal gradient. *J. Gen. Appl. Microbiol.* 48, 211-222.

Nikolaou, A., Bernardi, A., Meneghesso, A., Bezzo, F., Morosinotto, T., Chachuat, B. **(2015)** A model of chlorophyll fluorescence in microalgae integrating photoproduction, photoinhibition and photoregulation. *J. Biotechnol.* 194, 91-99.

Nogales, B., Lanfranconi, M.P., Piña-Villalonga, J.M., Bosch, R. **(2011)** Anthropogenic perturbations in marine microbial communities. *FEMS Microbiol. Rev*. 35, 275-298.

Nziguheba, G., Smolders, E. **(2008)** Inputs of trace elements in agricultural soils via phosphate fertilizers in European countries. *Sci. Total Environ.* 390, 53-57.

Ohnishi, N., Murata, N. **(2006)** Glycine betaine counteracts the inhibitory effects of salt stress on the degradation and synthesis of the D1 protein during photo inhibition in *Synechococcus* sp. PCC 7942. *Plant Physiol.* 141, 758-765.

Otón, J., Sorzano, C.O.S., Pereiro, E., Cuenca-Alba, J., Navarro, R., Carazo, J.M., Marabini, R. **(2012)** Image formation in celular X-ray microscopy. *J. Struct. Biol.* 178, 29-37.

Otón, J., Pereiro, E., Pérez-Berná, A.J., Millach, L., Sorzano, C.O., Marabini, R., Carazo, J.M. **(2016)** Characterization of transfer function, resolution and depth of field of a soft X-ray microscope applied to tomography enhancement by Wiener deconvolution. *Biomed. Opt. Express.* 7(12), 5092-5103.

Otte, S., Kuenen, J.G., Nielsen, L.P., Paerl, H.W., Zopfi, J., Schulz, H.N., Teske, A., Strotmann, B., Gallardo, V.A., Jorgensen, B.B. **(1999)** Nitrogen, carbon, and sulfur metabolism in natural Thioploca samples. *Appl. Environ. Microbiol.* 65, 3148-3157.

Overmann, J., van Gemerden, H. **(2000)** Microbial interactions involving sulfur bacteria: implications for the ecology and evolution of bacterial communities. *FEMS Microbiol. Rev*. 24(5), 591-599.

Ozturk, S., Aslim, B. **(2008)** Relationship between chromium(VI) resistance and extracellular polymeric substances (EPS) concentration by some cyanobacterial isolates. *Environ. Sci. Pollut. Res.* 15, 478-480.

Ozturk, S., Aslim, B., Suludere, Z., Tan, S. **(2014)** Metal removal of cyanobacterial exopolysaccharides by uronic acid content and monosaccharide composition. *Carbohydr. Polym.* 101, 265-271.

Paerl, H.W., Pinckney, J.L, Steppe, T.F **(2000)** Cyanobacterial-bacterial mat consortia: examining the functional unit of microbial survival and growth in extreme environments. *Environ. Microbiol.* 2(1), 11-26.

Pal, S.W., Singh, N.K., Azam, K. **(2013)** Evaluation of relationship between light intensity (Lux) and growth of *Chaetoceros muelleri. Oceanography.* 1, 111.

Panof, J.M., Priem, B., Morvan, H., Joset, F. **(1988)** Sulphated exopoly-saccharides produced by two unicellular strains of cyanobacteria, *Synechocystis* sp. PCC 6803 and 6714. *Arch. Microbiol.* 150, 558-563.

Priester, J.H., Olson, S.G., Webb, S.M., Neu, M.P., Hersman, L.E., Holden, P.A. **(2006)** Enhanced exopolymer production and chromium stabilization in *Pseudomonas putida* unsaturated biofilms. *Appl. Environ. Microb.* 72(3), 1988-1996.

Paul, V.G., Wronkiewicz, D.J., Mormile, M.R., Foster, J.S. **(2016)** Mineralogy and Microbial Diversity of the Microbialites in the Hypersaline Storr's Lake, the Bahamas. *Astrobiology.* 16(4), 282-300.

Pereira, S., Micheletti, E., Zille, A., Santos, A., Moradas-Ferreira, P., Tamagnini, P., De Philippis, R. **(2011)** Using extracellular polymeric substances (EPS)-producing cyanobacteria for the bioremediation of heavy metals: do cations compete for the EPS functional groups and also accumulate inside the cell? *Microbiol.* 157, 451-458.

Pereiro, E., Chichón, F.J. **(2014)** Cryo-soft X ray tomography of the cell, in: eLS. John Wiley & Sons, Ltd: Chichester.

Perkins, R.G., Oxborough, K., Hanlon, A.R.M., Underwood, G.J.C., Baker, N.R. **(2002)** Can chlorophyll fluorescence be used to estimate the rate of photosynthetic electron transport within microphytobenthic biofilms? *Mar. Ecol. Prog. Ser.* 228, 47-56.

Pfennig, N., Trüpper, H.G. **(1992)** The family Chromatiaceae, in: Balows, A., Trüpper, H.G., Dworkin, M., Harder, W., Schleifer, K.H. (Eds.), *The Prokaryotes*, 2nd edn. Springer-Verlag, Berlin, pp. 3200-3221.

Portillo, M.C., Sririn, V., Kanoksilapatham, W., Gonzalez, J.M. **(2009)** Differential microbial communities in hot spring mats from Western Thailand. *Extremophiles.* 13(2), 321-331.

Potts, M. **(1994)** Desiccation tolerance of prokaryotes. *Microbiol. Rev.* 58, 755-805.

Pouneva, I. **(1997)** Evaluation of algal culture viability and physiological state by fluorescent microscopic methods. *Bulg. J. Plant Physiol.* 23(1-2), 67-76.

Prasad, S.M., Singh, J.B., Rai, L.C., Kumar, H.D. **(1991)** Metal-induced inhibition of photosynthetic electron transport chain of the cyanobacterium *Nostoc muscorum*. *FEMS Microbiol. Lett.* 82, 95-100.

Puyen, Z.M., Villagrasa, E., Maldonado, J., Diestra, E., Esteve, I., Solé, A. **(2012a)** Viability and biomass of *Micrococcus luteus* DE2008 at different salinity concentrations determined by specific fluorochromes and CLSM-image analysis. *Curr. Microbiol.* 64, 75-80.

Puyen, Z.M., Villagrasa, E., Maldonado, J., Diestra, E., Esteve, I., Sole, A. **(2012b)** Biosorption of lead and copper by heavy-metal tolerant Micrococcus luteus DE2008. *Bioresour. Technol.* 126, 233-237.

Puyen, Z.M., Villagrasa, E., Millach, L., Esteve, I., Maldonado, J., Solé., A. **(2017)** Multi-approach microscopy techniques to evaluate the cytotoxic effect of chromium (III) on the cyanobacterium Chroococcus sp. PCC 9106, in: Méndez-Vilas, A. (Ed.), *Microscopy and imaging science: practical approaches to applied research and education.* Microscopy Book Series, Formatex Research Center. Number, 7, pp. 602-609.

Puzon, G. J., Petersen, J. N., Roberts, A. G., Kramer, D. M., Xun, L. **(2002)** A bacterial flavin reductase system reduces chromate to a soluble chromium (III)-$NAD^{(+)}$ complex. *Biochem. Biophys. Res. Commun.* 294, 76–81.

Puzon, G. J., Tokala, R. K., Zhang, H., Yonge, D., Peyton, B. M., Xun, L. **(2008)** Mobility and recalcitrance of organo-chromium(III) complexes. *Chemosphere.* 70, 2054-2059.

Rai, D., Eary, L.E., Zachara, J.M. **(1989)** Environmental chemistry of chromium. *Sci. Total Environ.* 86, 15-23.

Rajeev, L., Nunes da Rocha, U., Klitgord, N., Luning, E.G., Fortney, J., Axen, S.D., et al. **(2013)** Dynamic cyanobacterial response to hydration and dehydration in a desert biological soil crust. *ISME J.* 7, 2178-2191.

Rasband, W.S. **(2014)** ImageJ. US National Institutes of Health, Bethesda, MD, USA. http://imagej.nih.gov/ij.

Ratnakumar, S., Tunnacliffe, A. **(2006)** Intracellular trehalose is neither necessary nor sufficient for desiccation tolerance in yeast. *FEMS Yeast Res.* 6 (6), 902-913.

Reynolds, E.S. **(1963)** The use of lead citrate at high pH as an electron-opaque stain in electron microscopy. *J. Cell Biol.* 17, 208-212.

Rivasseau, C., Farhi, E., Compagnon, E., de Gouvion Saint Cyr, D., van Lis, R., Falconet, D., Kuntz, M., Atteia, A. and Couté, A. **(2016)** *Coccomyxa actinabiotis* sp. nov. (Trebouxiophyceae, Chlorophyta), a new green microalga living in the spent fuel cooling pool of a nuclear reactor. *J. Phycol.* 52, 689–703.

Roane, T.M., Rensing, C., Pepper, I.L., Maier, R.M. **(2009)** Microorganisms and Metal Pollutants, in: *Environmental Microbiology*. Elsevier Inc., pp. 421-441. doi: 10.1016/B978-0-12-370519-8.00021-3.

Roeselers, G., Norris, T.B., Castenholz, R.W., Rysgaard, S., Glud, R.N., Kühl, M., Muyzer, G. **(2007)** Diversity of phototrophic bacteria in microbial mats from Arctic hot springs (Greenland). *Environ. Microbiol.* 9, 26–38.

Roldan, M., Thomas, F., Castel, S., Quesada, A., Hernandez-Marine, M. **(2004)** Noninvasive pigment identification in single cells from living phototrophic biofilms by confocal imaging spectrofluorometry. *Appl. Environ. Microbiol.* 70, 3745-3750.

Roldán, M., Ascaso, C., Wierzchos, J. **(2014)** Fluorescent fingerprints of endolithic phototrophic cyanobacteria living within halite rocks in the Atacama Desert. *Appl. Environ. Microbiol.* 80, 2998-3006.

Romero-Puertas, M.C., Rodriguez-Serrano, M., Corpas, F.J., Gomez, M., Del Rio, L.A., Sandalio, L.M. **(2004)** Cadmium induced subcellular accumulation of O_2 and H_2O_2 in pea fronds. *Plant Cell Environ.* 27, 1122-1134.

Rossi, F., De Philippis, R. **(2015)** Role of Cyanobacterial Exopolysaccharides in Phototrophic Biofilms and in Complex Microbial Mats. *Life.* 5, 1218-1238.

Rugnini, L., Costa, G., Congestri, R., Bruno, L. **(2017)** Testing of two different strains of green microalgae for Cu and Ni removal from aqueous media. *Sci. Total. Environ.* 2, 601-602, 959-967.

Sakai, H.D., Kurosawa, N. **(2016)** Exploration and isolation of novel thermophiles in frozen enrichment cultures derived from a terrestrial acidic hot spring. *Extremophiles.* 20(2), 207-214.

Šalamún, P., Kucanová, E., Brázová, T., Miklisová, D., Renčo, M., Hanzelová, V. **(2014)** Diversity and food web structure of nematode communities under high soil salinity and alkaline pH. *Ecotoxicology.* 23, 1367-1376.

Sánchez, O., van Gemerden, H., Mas, J. **(1998)** Utilization of reducing power in light-limited cultures of Chromatium vinosum DSM 185. *Arch. Microbiol.* 170(6), 411-417.

Sato, M., Murata, Y., Mizusawa, M., Iwahashi, H., Oka, S. **(2004)** A simple and rapid dual-fluorescence viability assay for microalgae. *Microbiol. Cult. Coll.* 20, 53-59.

Schiewer, S., Volesky, B. **(2000)** Biosorption processes for heavy metal removal, in: Lovley, D.R (Ed.), *Environmental microbe-metal interactions.* ASM Press, Washingon, D.C. USA, pp. 329-362.

Schreiber, U. **(1998)** Chlorophyll fluorescence: new instruments for special applications, in: Garag, G. (Ed.), Photosynthesis: Mechanisms and Effects. *Kluwer Academic Publishers*, Dordrecht, Vol. V, pp. 4253-4258.

Seder-Colomina, M., Burgos, A., Maldonado, J., Solé, A., Esteve, I. **(2013)** The effect of copper on different phototrophic microorganisms determined *in vivo* and at cellular level by confocal laser microscopy. *Ecotoxicol.* 22, 199-205.

Shanab, S., Essa, A., Shalaby, E. **(2012)** Bioremoval capacity of three heavy metals by some microalgae species (Egyptian Isolates). *Plant Sing. Behav.* 7(3), 1-8.

Shing, W. L., Heng, L. Y., Surif, S. **(2012)** The fluorometric response of cyanobacteria to short exposure of heavy metal. *Adv. Environ. Biol.* 6(1), 103-108.

Slobodkin, A., Wiegel, J. **(1997)** Fe(III) as an electron acceptor for H_2 oxidation in thermophilic anaerobic enrichment cultures from geothermal areas. *Extremophiles.* 1(2), 106-109.

Solé, A., Mas, J., Esteve, I. **(2007)** A new method base on image analysis for determining cyanobacterial biomass by CLSM in stratified benthic sediments. *Ultramicroscopy.* 107, 669-673.

Solé, A., Diestra, E., Esteve, I. **(2009)** Confocal laser scanning microscopy image analysis for cyanobacterial biomass determined at microscale level in different microbial mats. *Microb. Ecol.* 57, 649-656.

Sorrentino, A., Nicolás, J., Valcárcel, R., Chichón, F.J., Rosanes, M., Avila, J., Thachuk, A., Irwin, J., Ferrer, S., Pereiro, E. **(2015)** MISTRAL: a transmission soft X-ray microscopy beamline for cryo nano-tomography of biological samples and magnetic domains imaging. *J. Synchrotron Rad.* 22, 1112-1117.

Spurgeon, D.J., Hopkin, S.P. and Jones, D.T. **(1994)** Effects of cadmium, copper, lead and zinc on growth, reproduction and survival of the earthworm *Eisenia fetida* (Savigny): assessing the environmental impact of point source metal contamination in terrestrial ecosystems. *Environ. Pollut.* 84, 123-130.

Stauber, J.L., Davies, C.M. **(2000)** Use and limitations of microbial bioassays for assessing copper bioavailability in the aquatic environment. *Environ. Rev.* 8, 255-301.

Stevens, S.E., Nierzwicki-Bauer, S.A., Balkwill, D.L. **(1985)** Effect of nitrogen starvation on the morphology and ultrastructure of the cyanobacterium *Mastigocladus laminosus. J. Bacteriol.* 161, 1215-1218.

Stevenson, L.H. **(1978)** Case for bacterial dormancy in aquatic systems. *Microb. Ecol.* 4, 127-133.

Su, J., Liang, H., Gong, X.N., Lv, X.Y., Long, Y.F., Wen, Y.X. **(2017)** Fast Preparation of Porous MnO/C Microspheres as Anode Materials for Lithium-Ion Batteries. *Nanomaterials.* 7(6), 121.

Sudhir, P., Murthy, S.D.S. (**2004)** Effects of salt stress on basic processes of photosynthesis. *Photosynthetica.* 42, 481-486.

Sultan, S., Hasnain, S. **(2007)** Reduction of toxic hexavalent chromium by *Ochrobactrum intermedium* strain SDCr-5 stimulated by heavy metals. *Bioresour. Technol.* 98, 340-344.

Tamaru, Y., Takani, Y., Yoshida, T., Sakamoto, T. **(2005)** Crucial role of extracellular polysaccharides in desiccation and freezing tolerance in the terrestrial cyanobacterium *Nosctoc commune. Appl. Environ. Microbiol.* 71, 7327-7333.

Tang, Y.Z., Dobbs, F.C. **(2007)** Green autofluorescence in dinoflagellates, diatoms and other microalgae and its implications for vital staining and morphological studies. *Appl. Environ. Microbiol.* 73(7), 2306-2313.

Veldhuis, M.J.W., Kraay, G.W., Timmermans, K.R. **(2001)** Cell death in phytoplankton: correlation between changes in membrane permeability, photosynthetic activity, pigmentation and growth. *Eur. J. Phycol.* 36, 167-177.

Verma, P., Raghavan, R.V., Jeon, C.O., Lee, H.J., Priya, P.V., Dharani, G., Kirubagaran, R. **(2017)** Complex bacterial communities in the deep-sea sediments of the Bay of Bengal and volcanic Barren Island in the Andaman Sea. *Mar. Genomics.* 31, 33-41.

Wagenen, J.V., Holdt, S.L., Francisci, D.D., Valverde-Perez, B., Plósz, B.G., Angelidaki, I. **(2014)** Microplate-based method for high-throughput screening of microalgae growth potential. *Bioresour. Technol.* 169, 566-572.

Weidler, G.W., Dornmayr-Pfaffenhuemer, M., Gerbl, F.W., Heinen, W., Stan-Lotter, H. **(2007)** Communities of *Archaea* and *Bacteria* in a Subsurface Radioactive Thermal Spring in the Austrian Central Alps, and Evidence of Ammonia-Oxidizing *Crenarchaeota. Appl. Environ. Microbiol.* 73, 259-270.

Wierzchos, J., Ascaso, C., McKay, C.P. **(2006)** Endolithic cyanobacteria in halite rocks from the hyperarid core of the Atacama Desert. *Astrobiology.* 6(3), 415-422.

Willemann, R.L. **(2002)** Development of an application of the ECOTOX System in the Estuarine Zone of the Baía da Babitonga, SC, Brazil, Diplom, Friedrich-Alexander Universität, Erlangen-Nürnberg, pp. 1-72.

Wu, Y., Guan, K., Wang, Z., Xu, B., Zhao, F. **(2013)** Isolation, Identification and Characterization of an Electrogenic Microalgae Strain. *PLoS One* 8(9): e73442.

Zhang, T., Gong, H., Wen, X., Lu, C. **(2010)** Salt stress induces a decrease in excitation energy transfer from phycobilisomes to photosystem II but an increase to photosystem I in the cyanobacterium *Spirulina platensis. J. Plant Physiol.* 167(12), 951-958.

Zhou, G.J., Peng, F.Q., Zhang, L.J., Ying, G.G. **(2012)** Biosorption of zinc and copper from aqueous solutions by two freshwater green microalgae *Chlorella pyrenoidosa* and *Scenedesmus obliquus. Environ. Sci. Pollut. Res.* 19, 2918-2929.

Annex I

Journal of Microscopy

Journal of Microscopy, Vol. 00, Issue 0 2017, pp. 1–13
Received 31 December 2016; accepted 29 April 2017

doi: 10.1111/jmi.12586

A novel method to analyse *in vivo* the physiological state and cell viability of phototrophic microorganisms by confocal laser scanning microscopy using a dual laser

LAIA MILLACH, ALEIX OBIOL, ANTONIO SOLÉ & ISABEL ESTEVE
Departament de Genètica i Microbiologia, Facultat de Biociències, Universitat Autònoma de Barcelona, Bellaterra, Barcelona, Spain

Key words. Autofluorescence signals, cell viability, CLSM, environmental parameters, phototrophic microorganisms, *Scenedesmus* sp. DE2009.

Summary

Phototrophic microorganisms are very abundant in extreme environments, where are subjected to frequent and strong changes in environmental parameters. Nevertheless, little is known about the physiological effects of these changing environmental conditions on viability of these microorganisms, which are difficult to grow in solid media and have the tendency to form aggregates. For that reason, it is essential to develop methodologies that provide data in short time consuming, *in vivo* and with minimal manipulating the samples, in response to distinct stress conditions.

In this paper, we present a novel method using Confocal Laser Scanning Microscopy and a Dual Laser (CLSM-DL) for determining the cell viability of phototrophic microorganisms without the need of either staining or additional use of image treating software. In order to differentiate viable and nonviable *Scenedesmus* sp. DE2009 cells, a *sequential scan* in two different channels was carried out from each same *xyz* optical section. On the one hand, photosynthetic pigments fluorescence signal (living cells) was recorded at the red channel (625- to 785-nm fluorescence emission) exciting the samples with a 561-nm laser diode, and an acousto-optic tunable filter (AOTF) of 20%. On the other hand, nonphotosynthetic autofluorescence signal (dead cells) was recorded at the green channel (500- to 585-nm fluorescence emission) using a 405-nm UV laser, an AOTF of 15%. Both types of fluorescence signatures were captured with a hybrid detector.

The validation of the CLSM-DL method was performed with SYTOX green fluorochrome and electron microscopic techniques, and it was also applied for studying the response of distinct light intensities, salinity doses and exposure times on a consortium of *Scenedesmus* sp. DE2009.

Correspondence to: Isabel Esteve, Departament de Genètica i Microbiologia, Facultat de Biociències, Universitat Autònoma de Barcelona, Bellaterra, 08193, Spain. E-mail: isabel.esteve@uab.cat

Introduction

Oxygenic and anoxygenic photosynthetic microorganisms are very abundant in microbial mats. These ecosystems are widely distributed around the world, including extreme environments, where are subjected to periodic and strong changes in environmental parameters (Green *et al.*, 2008; Antibus *et al.*, 2012; de los Ríos *et al.*, 2015; Cuadrado *et al.*, 2015; Hoffmann *et al.*, 2015).

Over a considerable period of time, our group has been studying microbial mats, hypersaline ecosystems located in the Ebro Delta, Tarragona, Spain (Esteve *et al.*, 1994; Guerrero *et al.*, 2002; Solé *et al.*, 2009; Millach *et al.*, 2015). These mats are developed in water-sediment interfaces and, are formed by multilayered benthic microbial communities that are distributed along vertical microgradients of different physicochemical parameters. Cyanobacteria and microalgae, located mainly in the upper green layers, play an important role in primary production in these mats, where they stabilise deltaic sediments over large areas. Among them, *Scenedesmus* sp. DE2009 has been isolated (Maldonado *et al.*, 2010) and identified by molecular biology methods (Burgos *et al.*, 2013). This microorganism is very abundant in Ebro Delta microbial mats and their cells are spherical, with a diameter of 7–9 μm, and their chloroplasts are distributed laterally in the cell.

However, it is important to highlight that most phototrophic microorganisms isolated from natural habitats do not grow in solid laboratory cultures; additionally, they have a tendency to form aggregates. In this current work, therefore, *Scenedesmus* sp. DE2009 was selected as a model because it grows with difficulty in a solid medium and forms a consortium with heterotrophic bacteria.

Various studies have been made to analyse changes in microbial diversity in stress conditions such us desiccation and high salinity by means molecular techniques (Garcia-Pichel *et al.*, 2001; Rajeev *et al.*, 2013; Lan *et al.*, 2014), nevertheless, less is known about the impact on cell viability that changes in different environmental conditions may cause, mainly in the

microorganisms that colonise extreme habitats, and particularly in those that usually show increased survival in stress conditions. Among diverse stressing factors, high light intensity and dry conditions, which in turn increase salinity, are very important parameters that should be considered in ecosystems subjected to long periods of annual drought.

For this reason, it is essential to develop methodologies that characterise the physiological state of microbial cells and provide valuable information about the viability and functioning of microbial communities. Plate counting is one of the most fundamental microbiological techniques in determining the number of viable cells in a sample (Buck, 1979). However, as we have already mentioned, most isolated microorganisms from natural environments do not grow in solid media.

The analysis of pigment excitation/absorption spectra (Roldan *et al.*, 2004) and quantification of the chlorophyll content are frequently used to quantify and identify microorganisms (Gregor & Maršálek, 2004; Wagenen *et al.*, 2014). The Pulse–Amplitude–Modulation (PAM) fluorometry can also be used for ultrasensitive fluorescence measurements in distinct layers of photosynthetically active material (Schreiber, 1998). This technique is noninvasive and has frequently been used to estimate the photosynthetic efficiency within oxygenic organisms (Genty *et al.*, 1989; Perkins *et al.*, 2002). For that, *in vivo* chlorophyll fluorescence methods have for a long time been used for nondestructive estimation of biomass and growth rates (Büchel & Wilhelm, 1993; Huot & Babin, 2011) and for the detection and quantification of changes induced in the photosynthetic apparatus (Mehta *et al.*, 2010). Nevertheless, all these methods are suitable for pigment analysis or photophysiology studies, but cannot be applied to distinguish between viable and nonviable cells.

Finally, other alternative and common viability assays are fluorescent staining like DNA-specific SYTOX green dye (Sato *et al.*, 2004) or other fluorochromes (Pouneva, 1997), and flow cytometry (Dorsey *et al.*, 1989; Al-Rubeai *et al.*, 1997; Veldhuis *et al.*, 2001); but in both methods staining is required and, in the second one is difficult to apply in filamentous cyanobacteria and in microorganisms that tend to form aggregates.

In this article, a novel, simple, nonintrusive, rapid and *in vivo* method was developed for determining the cell viability of phototrophic microorganisms without the need of prior staining by confocal laser scanning microscopy (CLSM). This method is based on a *sequential scan* using a dual laser (CLSM-DL) that allows the capturing of different and specific wavelengths within the spectrum at the same time. High-resolution images are obtained that can help to clearly distinguish living cells from dead ones, overlapping and separately, and without the need of a subsequent analysis of the generated images.

The objectives of this work are (i) to set up a fast and easy CLSM-DL method for differentiating living and dead microbial cells; (ii) to validate the method by means of other microscopy techniques and (iii) to justify its applicability to the study of *Scenedesmus* sp. DE2009 response to light and salinity treatment.

Material and methods

Strain and culture conditions

The microalga *Scenedesmus* sp. DE2009 was isolated from Ebro Delta microbial mats (0°35' E–0°56' E; 40°33' N–40°47' N), Tarragona, Spain. This microorganism was grown in liquid mineral Pfennig medium (Pfennig & Trüpper, 1992) in 100 mL flasks with a salinity condition of 2.65 g NaCl L^{-1}. Cultures were exposed and maintained at the optimal growth temperature at 27 °C in a growth chamber (Climas Grow 180, ClimasLab, Barcelona) under continuous illumination with a light intensity of 6 $\mu E\ m^{-2}\ s^{-1}$, provided by cold white fluorescence lights (Philips TL-D 18W-865). These cultures were used as control in all the experiments performed.

Experimental conditions

Various experiments were made applying the CLSM-DL and complemented with CLSM-λ*scan* function to assess the effect of light and salinity at single-cell level on *Scenedesmus* sp. DE2009 consortium. For this end, the cultures were exposed to distinct light intensities (2, 4, 6, 8, 10 and 12 $\mu E\ m^{-2}\ s^{-1}$). These conditions were controlled accurately throughout all the experiments measuring every day the light intensity with a Luxmeter C.A. 811 (Chauvin Arnoux, Metrix Paris, France).

On the other hand, different salinity doses (10, 35, 75 and 100 g L^{-1}) were selected considering changes in salinity detected in flood and dry (crust formation) periods in Ebro Delta sampling site. Furthermore, all experiments were performed for short periods (7 days) and long-term (30 days) under the same growth conditions mentioned in 'Strain and culture conditions' section.

Pigment analysis by CLSM-λscan function

Scenedesmus sp. DE2009 cultures were evaluated *in vivo* to determine the emission spectra of microalga pigments by λ*scan* function of Leica LAS AF Software using a Leica TCS-SP5 CLSM (Leica Microsystems Heidelberg GmbH, Mannheim, Germany). This technique, based on a fluorescence method, shows the complete spectral distribution of the fluorescence signals emitted by photosynthetic pigments of phototrophic microorganisms. Statistically changes in the spectrum of Chlorophyll *a* (Chl $a = 684$ nm), used as a biomarker, was considered to evaluate the state of pigments by means of the Maximum Intensity Fluorescence (MIF).

In this paper, CLSM-λ*scan* method was optimised to differentiate plainly between red and green fluorescence signals. In this sense, each image sequence was obtained by scanning the same *xy* optical section throughout the visible spectrum using

an ×63 (1.4 numerical aperture) oil immersion objective. Images were acquired at the *z* position at which the fluorescence was maximal and acquisition settings were constant throughout the experiment. Photosynthetic pigments excitation was carried out with an UV Laser at 405 nm and an acousto-optic tunable filter (AOTF) of 5% for PAF and 15% for NPAF. Both types of fluorescence emissions were captured with a hybrid detector, in 10 nm bandwidth increments, with a λ step size of 3 nm and in the range from 420 nm to 750 nm.

On the other hand, the mean fluorescence intensity (MFI) was obtained through the average fluorescence intensity for each wavelength within the studied range. For that, a set of 70 regions of interest (ROIs) of 1 μm^2 for photosynthetic pigments autofluorescence signal (PAF) and 20 ROIs for non-photosynthetic autofluorescence signal (NPAF) were selected in the thylakoid area of *Scenedesmus* sp. DE2009 to analyse the spectral signature at cell level and the peak emission range.

CLSM-DL method for viability assay

The CLSM-DL method has been tested in *Scenedesmus* sp. DE2009 consortium for differentiating dead and living microalga cells. For that reason, to capture both fluorescence signatures, separated and combined, a *sequential scan* in two channels was carried out from each same *xyz* optical section. On the one hand, PAF was recorded in the red channel (625- to 785-nm fluorescence emission) exciting the samples with a 561-nm laser diode and an AOTF of 20%. On the other hand, NPAF was viewed in the green channel (500- to 585-nm fluorescence emission) using a 405-nm UV laser, an AOTF of 15%. Both types of fluorescence signals were captured with a hybrid detector. A set of 20 red and 20 green CLSM images (1024 × 1024 pixels) was obtained from all cultures analysed. To determine the number of living (red signal) and dead cells (green signal) per condition, cell count and statistical analysis were calculated.

Furthermore, in order to characterise the distribution of both fluorescence signatures on *Scenedesmus* sp. DE2009 cells, a series of optical sections (CLSM stack) were acquired, at the same conditions described above. The 17.25 μm thick stack was scanned from up to down in 69 optical sections, in *x*–*y* planes every 0.25 μm along the optical axis with a 1-Airy-unit confocal pinhole. Various projections were generated by the Leica LAS AF software and the IMARIS software package (version 7.2.1, Bitplane AG, Zürich, Switzerland) for three-dimensional (3D) reconstructions of *Scenedesmus* sp. DE2009 cells.

SYTOX green nucleic acid stain

To validate the CLSM-DL method and quantify *Scenedesmus* sp. DE2009 dead cells, the samples were incubated at 6 μE m^{-2} s^{-1} and 100 g NaCl L^{-1} for 7 days. Later, one aliquot was used as a control (without fluorochrome) and the other one was stained using a specific-fluorescence SYTOX Green dye (Molecular Probes Inc., Eugene, OR, USA). The original fluorescent probe containing 5 mM stock solution in DMSO was diluted in deionised Milli-Q water for a final dye concentration of 5 μM and added to the cell suspension of microalga. The mixture was incubated for 30 min at room temperature in the dark and then observed by CLSM-DL method. No washing was required before or after SYTOX Green staining.

Electron microscopy techniques

Electron microscopy techniques were used to analyse changes on the morphology and ultrastructure of living and dead *Scenedesmus* sp. DE2009 cells. The samples were incubated at 6 μE m^{-2} s^{-1} and 100 g NaCl L^{-1} for 7 days.

For SEM analysis, cultures were filtrated in Nucleopore™ polycarbonate membranes (Whatman, Ltd.) and then were fixed in 2.5% glutaraldehyde diluted in Milloning phosphate buffer (0.1 M pH 4) at 4 °C for 2 h. Later, samples were washed in the same buffer, dehydrated in increasing concentrations of ethanol and dried by critical point (CPD 030 Critical Point Drier, BAL-TEC GmbH D – 58579 Schalksmühle). Finally, samples were coated with a 5-μm gold–palladium layer (K550 Sputter Coater, Emitech, Ashford, UK) for better image contrast. A Zeiss EVO®MA 10 SEM (Carl Zeiss NTS GmbH, Oberkochen, Germany) was used to observe the samples.

For TEM analysis, cultures were fixed in 2.5% glutaraldehyde diluted in Milloning phosphate buffer. Samples were postfixed in 1% OsO_4 at 4 °C for 2 h and washed in the same buffer. They were then dehydrated in a graded series of acetone and embedded in Spurr's resin. Ultrathin sections (70 nm), obtained with a Leica EM UC6 Ultramicrotome (Leica Microsystems), were mounted on carbon-coated copper grids and stained with uranyl acetate and lead citrate. Samples were viewed in a JEM-1400 TEM (JEOL, USA).

Statistical analysis

Statistical analyses were performed by one-way analysis of variance (ANOVA) and Tukey and Bonferroni's comparison *post hoc* tests. Differences were considered significant at $p < 0.05$. The analyses were performed using IBM SPSS Statistics software (version 20.0 for Windows 7).

Results and discussion

Autofluorescence emission spectra of Scenedesmus sp. DE2009 cells

Previously, the fluorescence emitted by the photosynthetic pigments and other nonspecific molecules of *Scenedesmus* sp.

DE2009 was characterised, identified and evaluated by means of λ*scan* function of CLSM. Three types of fluorescence signatures were detected when microalga cells were excited with a 405-nm UV laser diode: (1) photosynthetic pigments autofluorescence signal (PAF) emitted in the red range, (2) nonphotosynthetic autofluorescence signal (NPAF) emitted within the green range and (3) a mixture of both autofluorescence signals.

The emission profiles correspond to individual cells of *Scenedesmus* sp. DE2009 showing only PAF signal are represented in Figure 1(A). The PAF spectra recorded indicated a high-intensity emission peak at 684 nm, produced by Chl *a* (Fig. 1B). The results obtained by CLSM-λ*scan* function demonstrated that the differences were not statistically significant ($p < 0.05$) among 6, 8 and 10 $\mu E\, m^{-2}\, s^{-1}$. An *xyz* optical section corresponding to PAF detected in the microalga growing at 12 $\mu E\, m^{-2}\, s^{-1}$ is shown in Figure 1(C).

In the same conditions, some cells of *Scenedesmus* sp. DE2009 emitted only NPAF. The spectra recorded in these cells showed irregular curves, with a maximum fluorescence intensity at the range of 460–530 nm (Fig. 1D). This type of green emission was confirmed by CLSM images (Fig. 1E). Generally, NPAF was distributed evenly across the cell cytoplasm and cells showed a disorganisation of the thylakoids and a lack of pigment. These cellular differences were observed by bright-field microscopy (Fig. 1F).

Finally, a few cells also emitted both autofluorescence signals: PAF and NPAF. In this case, the emission spectra recorded showed two distinct fluorescence intensities: (i) a low-intensity uneven peak at 684 nm (Chl *a*) and (ii) a wide and irregular fluorescence intensity in the green region (Fig. 1G). These cells were considered an intermediate physiological state between viable and nonviable (Figs. 1E, F and H), because the Chl *a* peak still emitted fluorescence, but their cell integrity was damaged.

To evaluate the optimal light intensity for the growth of *Scenedesmus* sp. DE2009 during a long period of time, an analogous experiment was carried out under the same light conditions for 30 days (Fig. 2). The λ*scan* plots corresponding to PAF emission showed differences in the MIF in response to varying light intensities (Fig. 2A). In this case, the highest MIFs correspond to 6 and 8 $\mu E\, m^{-2}\, s^{-1}$ and no statistically significant differences ($p < 0.05$) were found between them, using the Tukey's and Bonferroni comparison test. A decrease in the MIF was observed in the rest of the light intensities tested for a month. An *xyz* optical section from PAF detected in cultures of *Scenedesmus* sp. DE2009 growing at 8 $\mu E\, m^{-2}\, s^{-1}$ is shown in Figure 2(B).

Finally, when comparing the MIF results obtained at 7 and 30 days, no statistically significant differences ($p < 0.05$) were found between 6 and 8 $\mu E\, m^{-2}\, s^{-1}$. These results suggest that the optimum light intensity for the growth of *Scenedesmus* sp. DE2009 is in this range, because the exposure time does not alter the MIFs.

Set up of CLSM-DL method

In this work, it is described a novel, fast and *in vivo* method to identify and quantify viable and nonviable *Scenedesmus* sp. DE2009 cells without manipulation of the samples. This technique allows us to differentiate clearly two types of fluorescence signatures at cell level observed previously in the CLSM-λ*scan* studies. A simultaneous scan of the same *xyz* optical section is showed for PAF corresponding to living cells (Fig. 3A), for NPAF representing dead cells (Fig. 3B) and an overlap of both autofluorescence signals (Fig. 3C). The percentages of living and dead cells were calculated from these CLSM images.

For determining the *in vivo* effect of light on cellular viability of *Scenedesmus* sp. DE2009 by means of CLSM-DL, two experiments at different light intensities were performed. Changes in microalga viability growing for 7 days are represented in Figure 3(D). These results showed low significant differences ($p < 0.05$) in all the light intensities tested, which indicated a slight effect of light. However, there were no significant differences ($p < 0.05$) among 6, 8 and 10 $\mu E\, m^{-2}\, s^{-1}$, which also represent the highest values of viable cells in this experiment: 93.52%, 93.11% and 93.18%, respectively. A similar experiment was performed in cultures growing for 30 days (Fig. 3E). In this case, it is important to highlight that, even at 10 $\mu E\, m^{-2}\, s^{-1}$ (67.48%) and 12 $\mu E\, m^{-2}\, s^{-1}$ (58.81%), a high percentage of viable cells was also remained. These results confirm the high viability level was maintained in all the light intensities assayed.

Finally, a reduction of cell viability at 10 $\mu E\ m^{-2}\ s^{-1}$ (25.69%) and 12 $\mu E\ m^{-2}\ s^{-1}$ (29.80%) was observed for light exposure experiments between 7 and 30 days using the Tukey's and Bonferroni comparison test. However, no statistically significant differences ($p < 0.05$) were only found at 6 $\mu E\, m^{-2}\, s^{-1}$, which also corresponds to the highest percentage of living cells. Hence, it was considered important to fix the light parameter at 6 $\mu E\, m^{-2}\, s^{-1}$ in salinity experiments.

In the same way, our results in light experiments agree with those obtained in other microalgae studies at low light intensities. In this case, Ferreira *et al.* (2016) demonstrated an increase in chlorophyll content at 16.91 ± 0.45 μmol photons $m^{-2}\, s^{-1}$ to capture light in a more efficient manner in *Scenedesmus dimorphus* (UTEX 1237); and Pal *et al.* (2013) indicated that 1000–1500 lux (6–9 $\mu E\ m^{-2}\ s^{-1}$) were the best light intensities in order to produce maximum yield in *Chaetoceros muelleri* (CS-178).

Validation of the CLSM-DL method

First, to validate the CLSM-DL method, SYTOX green nucleic acid stain and electron microscopic techniques were applied to study the response of this microorganism to the highest salinity condition (100 g NaCl L^{-1}), considering this parameter as inductor of damage in the cells. The objective was to compare whether NPAF corresponded to *Scenedesmus* sp. DE2009 dead cells.

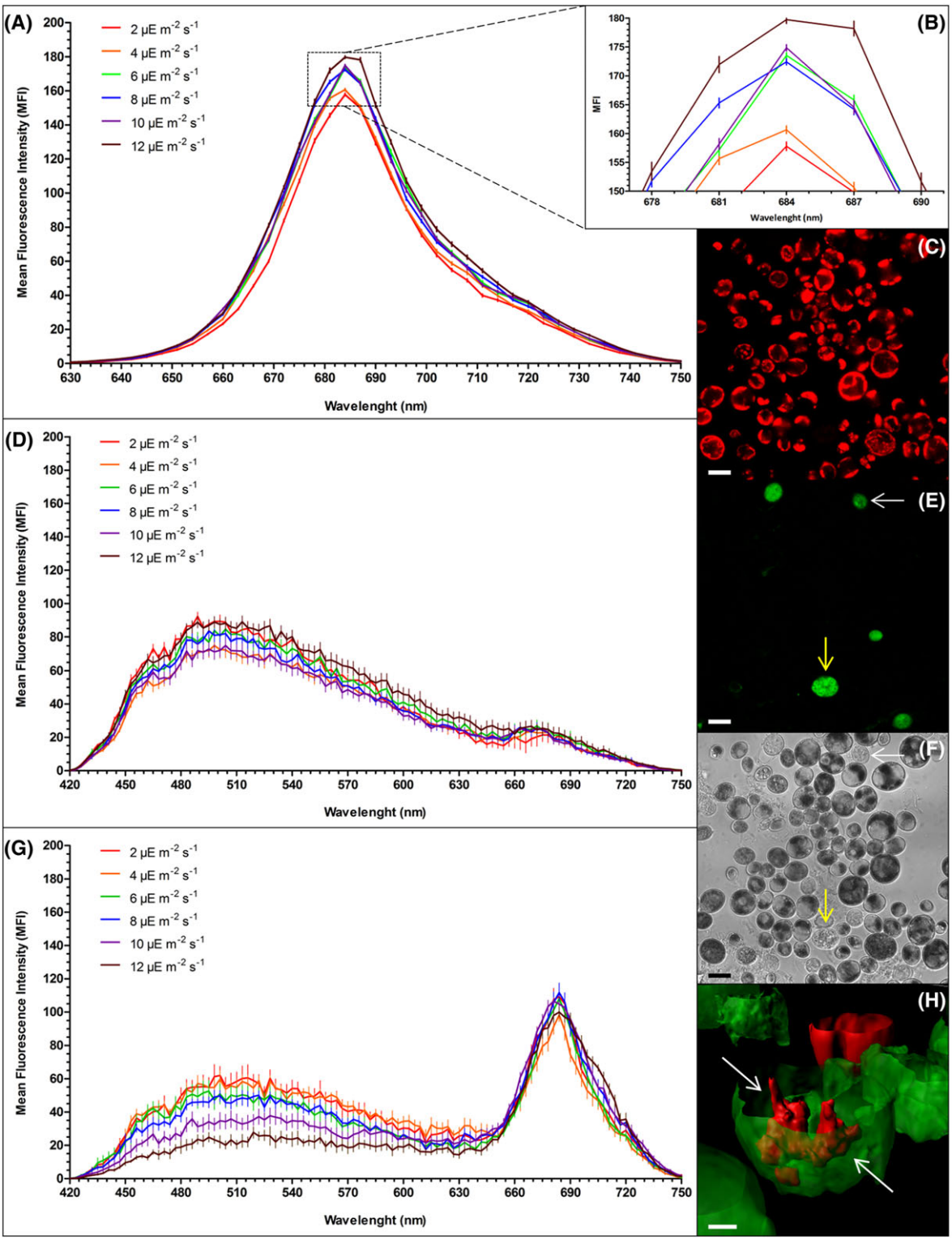

Fig. 1. *λscan* plots of *Scenedesmus* sp. DE2009 cultures grown at different light intensities for 7 days. Spectral profiles corresponding to cells emitting PAF (A). Detail of the emission peak at 684 nm for chlorophyll *a*, used as biomarker (B). Spectral profiles corresponding to cells emitting NPAF (yellow arrows) (D). Spectral profiles corresponding to an intermediate physiological stage of the cells (white arrows) (G). 2D plots represent the MFI data ± SE: emission wavelength, *x* axis; MFI, *y* axis. CLSM images from the same *xyz* optical section of *Scenedesmus* sp. DE2009 grown at 12 μE m^{-2} s^{-1}: PAF emission (C), NPAF emission (E) and bright-field micrograph (F). Scale bars represent 10 μm. 3D reconstruction of *Scenedesmus* sp. cells (H). Scale bars represent 2.5 μm.

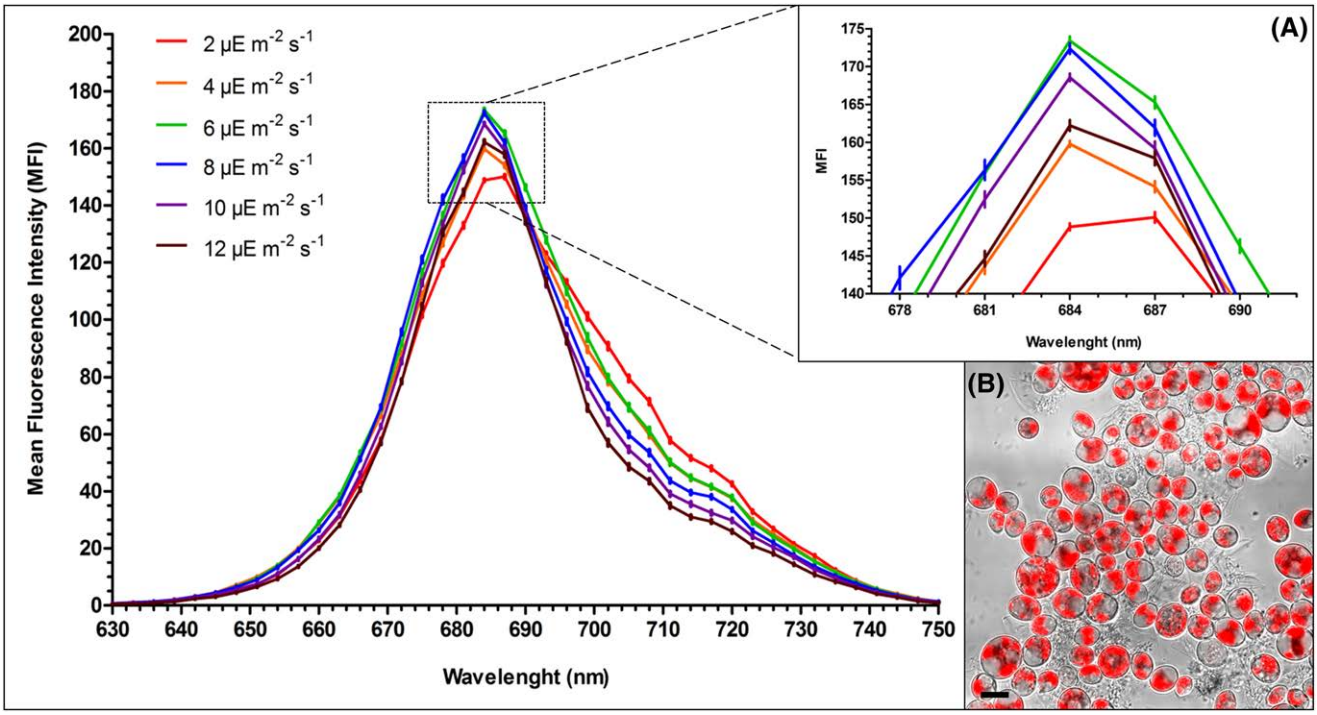

Fig. 2. λ*scan* plots of *Scenedesmus* sp. DE2009 cultures grown at different light intensities for 30 days. Spectral profiles corresponding to cells emitting PAF. Detail of the emission peak at 684 nm for chlorophyll *a*, used as biomarker (A). 2D plots represent the MFI data ± SE: emission wavelength, *x* axis; MFI, *y* axis. Summa projection of PAF emission and bright-field microscopy of microalga sp. DE2009 grown at 8 µE m^{-2} s^{-1} (B). Scale bars represent 10 µm.

Second, the CLSM-DL method was applied for assessing the effect of salinity at different doses over a long period of time on photosynthetic pigments and cell viability.

Analysis of the correlation between NPAF and dead cells. Samples were stained using a specific-fluorescence SYTOX green nucleic acid fluorochrome. The results demonstrated that the differences were not statistically significant ($F = 1.367$) ($p > 0.05$) between the cells stained by SYTOX green (45.79%) and NPAF cells (50.95%). Hence, a very good correlation was established between the cells stained by SYTOX green (Fig. 4A) and cells emitting NPAF (Fig. 4B), being the second one a more accurate technique, because heterotrophic bacteria showed no fluorescent signal.

In addition, electron microscopy techniques (SEM and TEM) were also used to analyse the changes in morphology and cellular ultrastructure in cells that emitted in NPAF. This was done to check if these cells had clear symptoms of degradation, which would confirm the nonviability of the microalga. Changes in cell morphology can be clearly observed between healthy cells (Fig. 5A) and collapsed cells, which present invagination of the cell wall, a reduction of cell volume and an irregular morphology (Fig. 5B). Moreover, various pleomorphic cells showed a rupture of the cell wall and intracytoplasmic membrane, and a retraction of the cytoplasm were viewed in the same growth conditions in ultrathin sections (Figs. 5C and D). According Kroemer *et al.* (1995) and Naganuma (1996), the loss of membrane integrity is a late stage of the automortality process resulting in the total disintegration of the alga cell.

Effect of salt stress. The results related to PAF demonstrated that MIFs peaks (Chl *a*) decreased, mainly between 35 and 75 g L^{-1}, whereas the concentrations of salinity increased from control culture to 100 g NaCl L^{-1}. In some cases, a displacement of the Chl *a* peak towards 684 nm (at 35 g L^{-1}) and 681 nm (at 75 and 100 g L^{-1}) was produced. On the contrary, the λ*scan* plots corresponding to NPAF showed irregulars curves with an evident plateau from 460 nm to 530 nm and a positive correlation between NPAF intensity and all the salinity doses (Fig. 6A).

The second experiment was performed at the same conditions mentioned above, but maintaining *Scenedesmus* sp. DE2009 cultures for 30 days. The Chl *a* peak at distinct salinities followed the same pattern as the obtained in the previous experiment, but in this case, the MIF peak was drastically reduced from 10 g NaCl L^{-1}. The NPAF also followed the same pattern as in the previous experiment (Fig. 6B).

However, in both experiments, the salt impact on photosynthetic pigments varied significantly according to the salinity doses assayed. Highly statistically significant differences on MIF ($p < 0.05$) were observed between control and all

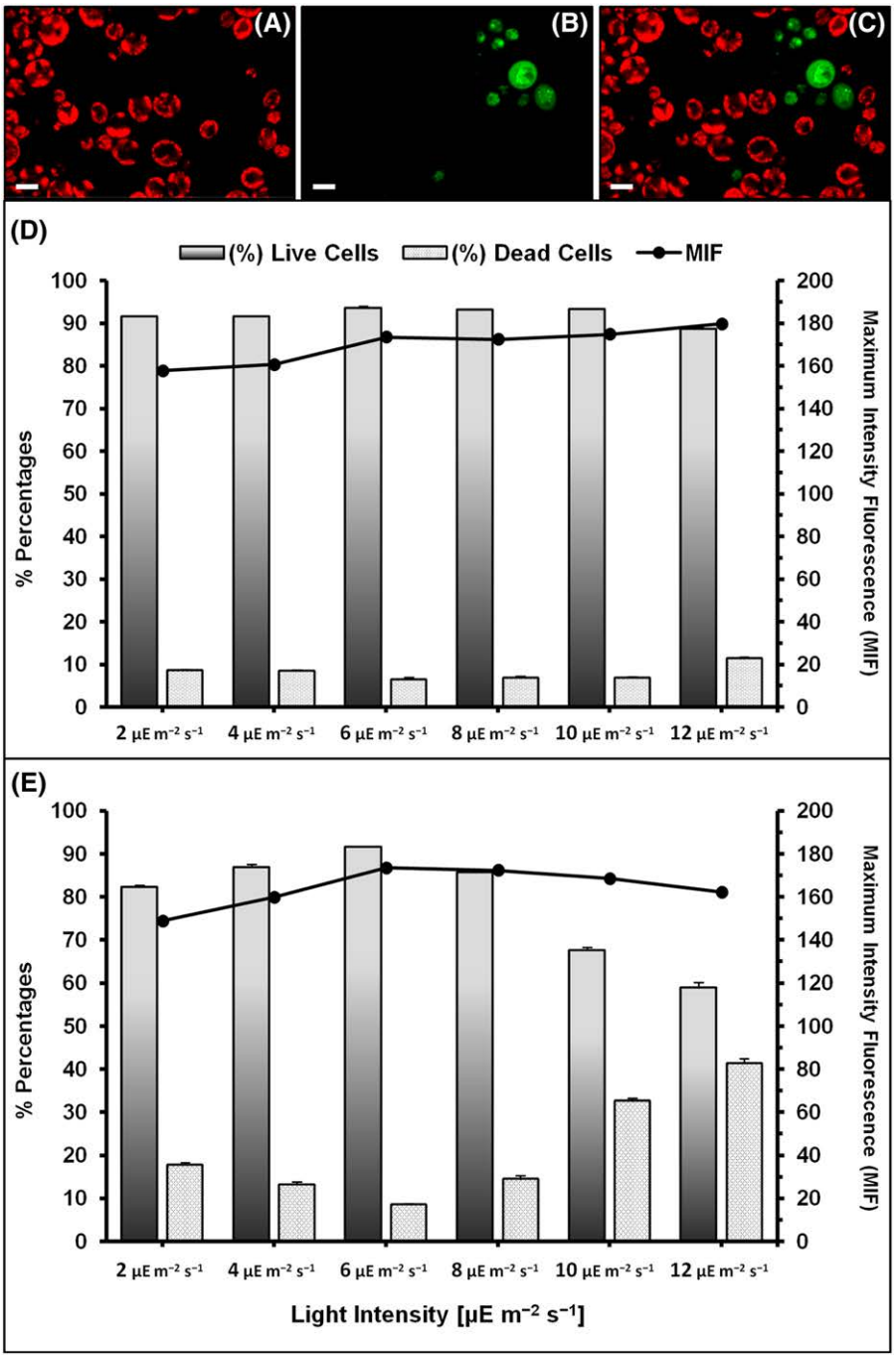

Fig. 3. CLSM images from the same *xyz* optical section of *Scenedesmus* sp. DE2009 grown at 6 µE m^{-2} s^{-1}: PAF (A), NPAF (B) and summa projection of both autofluorescence signals (C). Scale bars represent 10 µm. MIF and relative abundance of living and dead *Scenedesmus* sp. DE2009 cells at distinct light intensities (expressed as a percentage) for 7 days (D) and 30 days (E). The bars indicate the standard error of the mean.

the NaCl concentrations tested, both at 7 days and at 30 days. The result also indicated that, in short periods of time (7 days) the differences were not statistically significant between the highest concentrations: 75 g L^{-1} and 100 g L^{-1}, while for long periods (30 days), the differences were significant and the MIF peak was not detected at the maximum concentration tested at 100 g L^{-1}. These results demonstrate that, at these high concentrations, there is a clear effect of salinity on *Scenedesmus* sp. DE2009 and this effect also increases with time.

Likewise, a viability assay applying the CLSM-DL method was carried to investigate the cell viability in response to

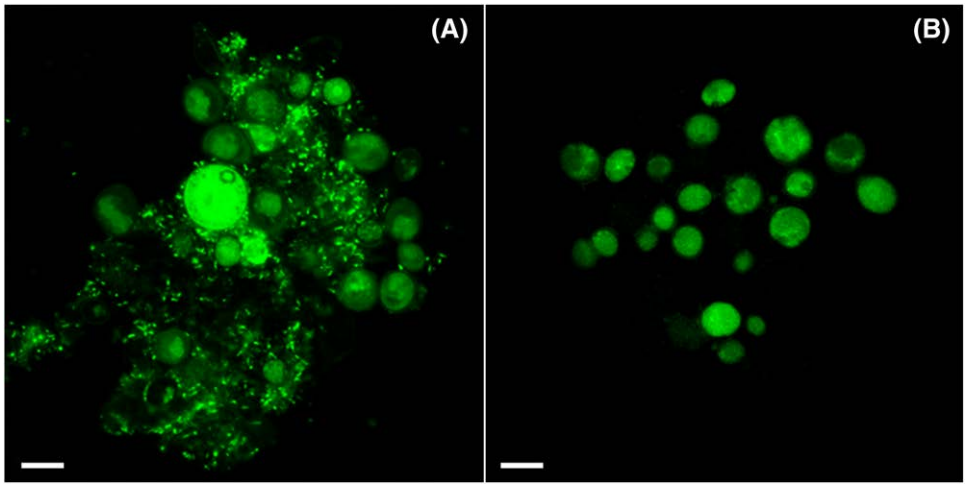

Fig. 4. CLSM images of *Scenedesmus* sp. DE2009 grown at 6 μE m^{-2} s^{-1} and 100 g NaCl L^{-1} for 7 days. Cells stained by SYTOX Green nucleic acid fluorochrome (A) and cells emitting NPAF by CLSM-DL (B). Scale bars represent 10 μm.

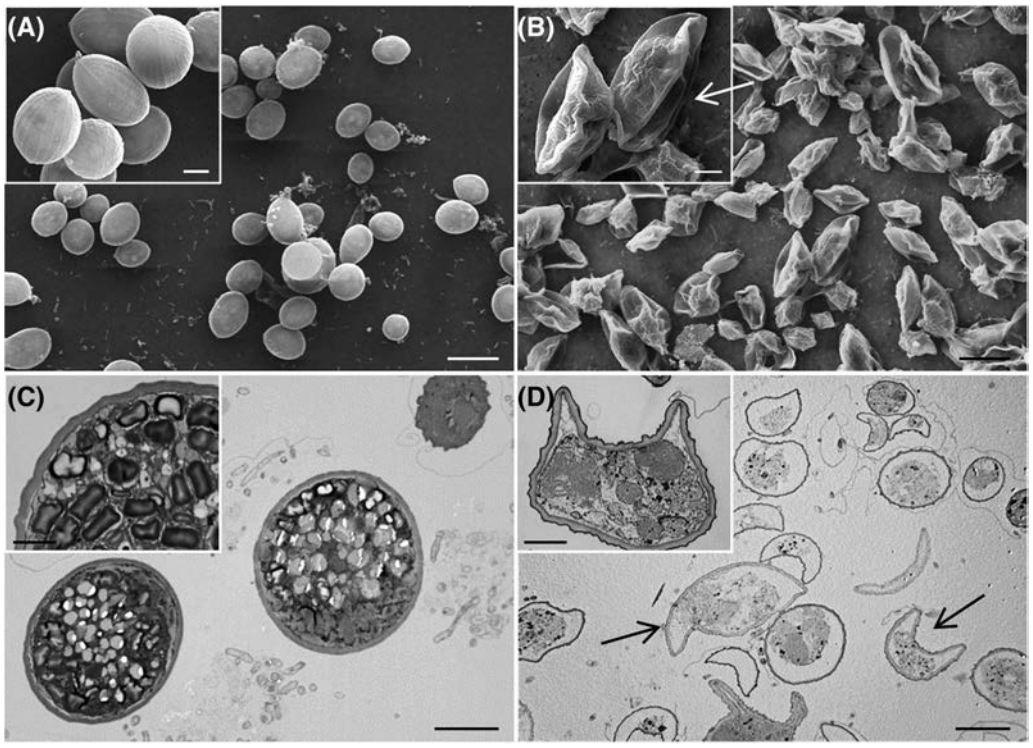

Fig. 5. SEM micrographs of *Scenedesmus* sp. DE2009 grown at 6 μE m^{-2} s^{-1} for 7 days in control cultures (A) and in cultures grown at 100 g NaCl L^{-1} (B) (white arrow). Scale bars represent 10 μm (general) and 2 μm (close up images). Ultrathin sections of the same microorganism in control cultures (C) and in cultures grown at 100 g NaCl L^{-1} (D) (black arrows). Scale bars represent 5 μm (general) and 2 μm (close up images).

varying salinities. The same *xyz* optical section is showed for PAF corresponding to living cells (Fig. 7A), for NPAF representing dead cells (Fig. 7B) and an overlap of both autofluorescence signals (Fig. 7C). The conversion of this data into relative frequency made it possible to observe that the percentage of viable cells decreased when the salinity doses increased.

Changes in viability for 7 days are shown in Figure 7(D). These values showed high significant differences ($p < 0.05$) between the control and all the salinities tested, which indicate a negative effect of salt on the cellular viability of the microalga. However, at low salinity concentrations (10 and 35 g L^{-1}), viable cells remained in high levels (81.73%

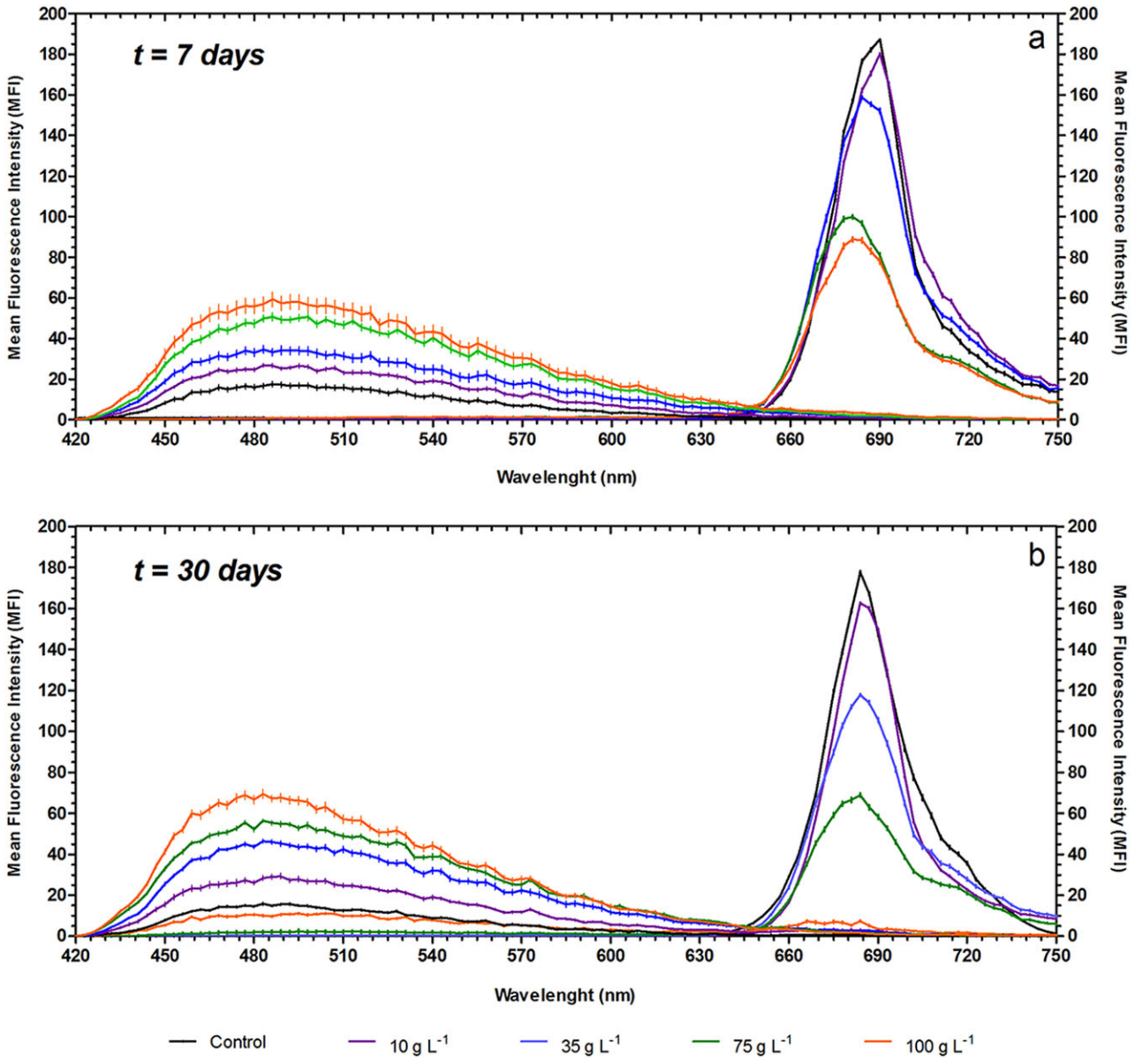

Fig. 6. λ*scan* plots of *Scenedesmus* sp. DE2009 cultures grown at different salinity doses during 7 days (A) and 30 days (B). Overlay of the spectral profiles corresponding to cells emitting PAF (living cells) and NPAF (dead cells). 2D plots represent the MFI data ± SE: emission wavelength, *x* axis; MFI, *y* axis.

and 74.12%, respectively). On the contrary, no statistically significant differences ($p < 0.05$) were found between the highest salinity doses (75 and 100 g L^{-1}), and although the percentage of living cells decreased (57.39% and 52.54%, respectively), it remained still fairly high.

For 30 days of salinity exposure, high statistically significant differences ($p < 0.05$) were also found between the control and all the salinities tested, nevertheless the trend was different (Fig. 7E). In this case, viable cells decreased drastically from 10 g L^{-1} (79.24%) to 100 g L^{-1} (8.27%), corresponding to a reduction of 70.9%, being the exposure time a very important variable to consider on cell viability. These results indicated that the salinity had a great influence on the percentage of living and dead Scenedesmus sp. DE2009 cells; although a small proportion of the community was still active.

Another important advantage to the application of the CLSM-DL method is that it allows characterising the distribution of distinct fluorescent signals within the microalga cells through 3D reconstructions. In Figure 8, it was observed that PAF and NPAF were distributed externally on *Scenedesmus* sp. DE2009 cells, which correspond to a nondegraded and degraded pigment, respectively (Fig. 8A). Some of cells also presented NPAF externally and PAF internally, which correspond to an intermediate state of pigment degradation, probably due

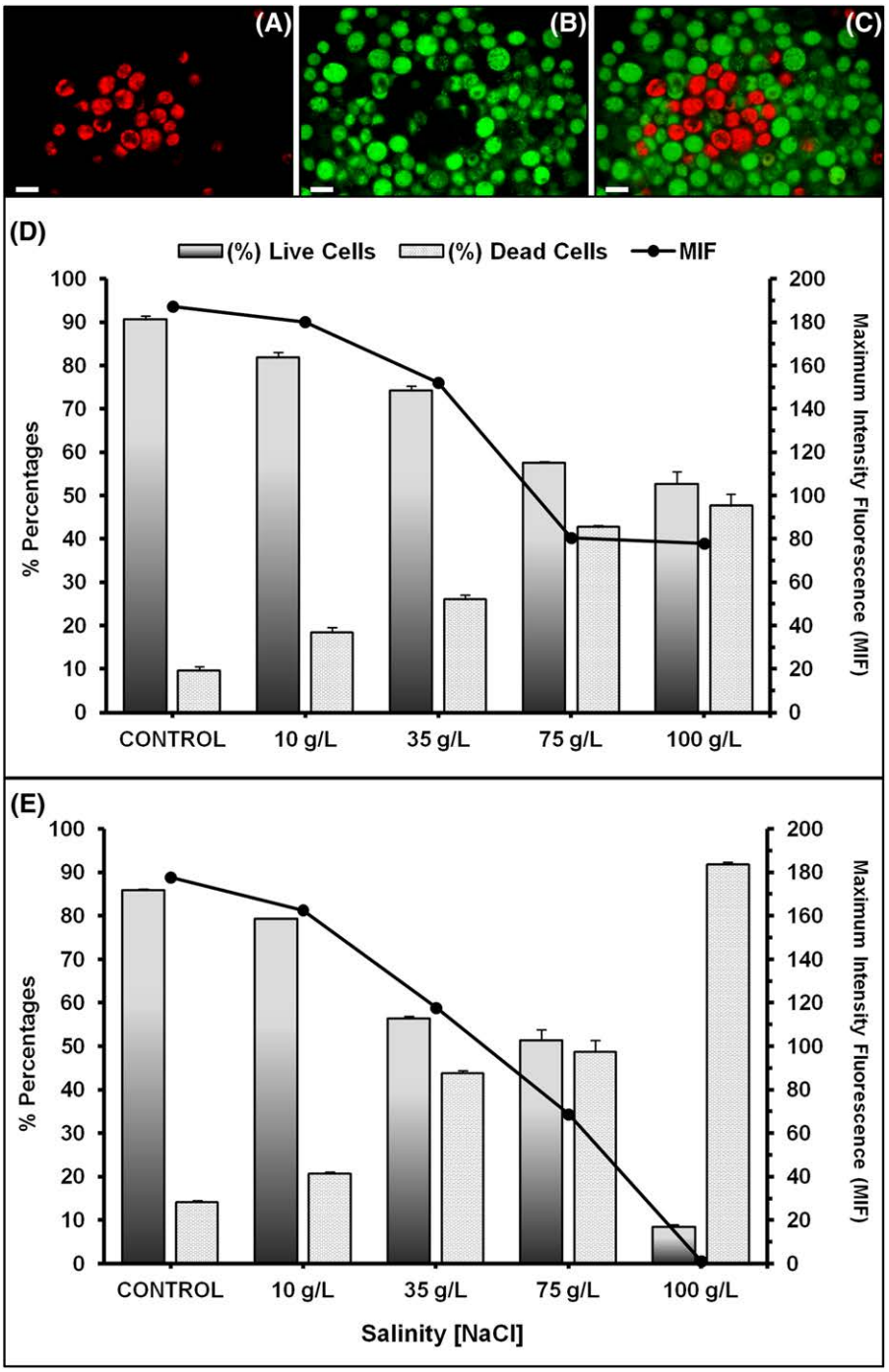

Fig. 7. CLSM images from the same *xyz* optical section of *Scenedesmus* sp. DE2009 grown at 100 g NaCl L^{-1}: PAF (A), NPAF (B) and summa projection of both autofluorescence signals (C). Scale bars represent 10 μm. MIF and relative abundance of living and dead *Scenedesmus* sp. DE2009 cells at distinct salinity doses (expressed as a percentage) for 7 days (D) and 30 days (E). The bars indicate the standard error of mean.

to a displacement and relocation of thylakoids within the cells (Figs. 8B and 1G).

3D easy projections also confirmed that the healthy cells (PAF) are very abundant in control cultures (Fig. 8C), whilst damaged cells (NPAF) are dominant in cultures exposed at the highest salinity (Fig. 8D). Other authors considered autofluorescence intensity as an indicator of integrity of the photosynthetic apparatus (Billi *et al.*, 2011), whereas green autofluorescence was considered by Tang and Dobbs (2007) a common feature in diverse organisms and that its presence

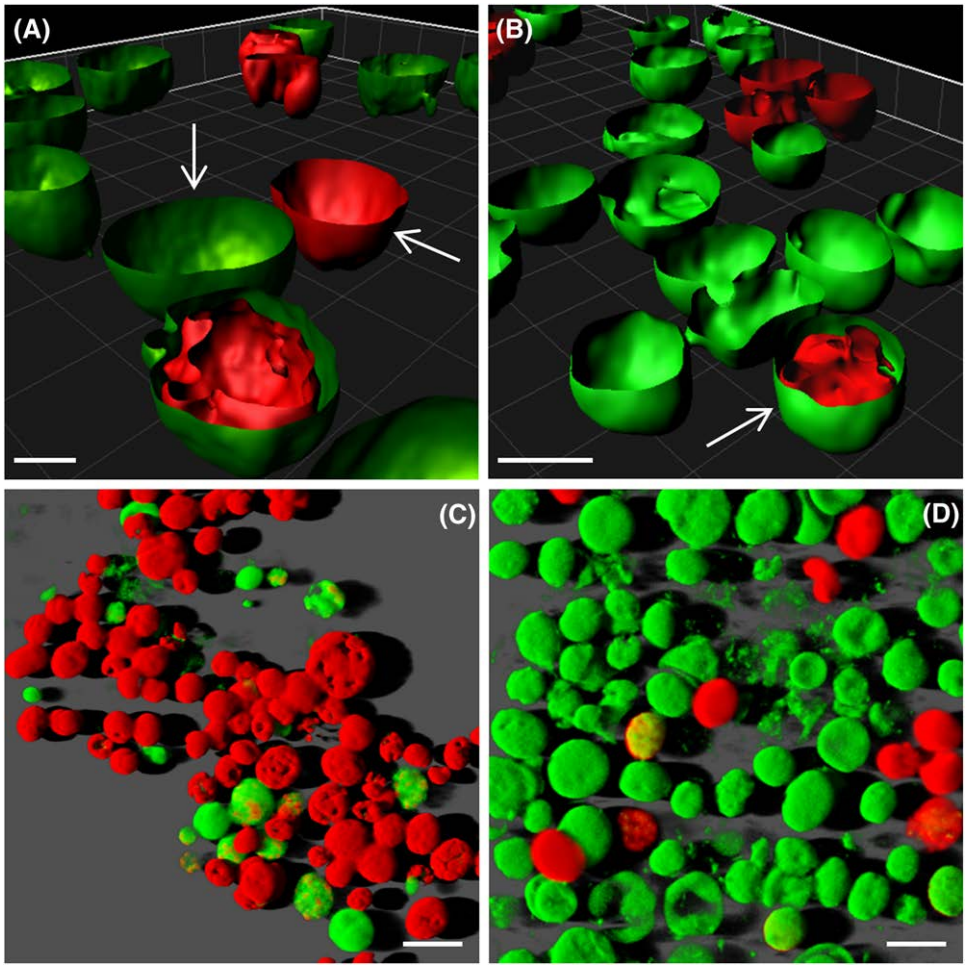

Fig. 8. Red and green autofluorescence patterns observed for *Scenedesmus* sp. DE2009. 3D reconstructions of microalga cells at 75 g NaCl L^{-1} (A) and 100 g NaCl L^{-1} (B). PAF and NPAF are indicated by arrows. Scale bars represent 5 μm. 3D easy projection for control culture (C) and 100 g NaCl L^{-1} (D). Scale bars represent 10 μm.

was independent of the cells physiological status. Nevertheless, we disagree with this last hypothesis, because NPAF was detected only in a few cells in control cultures. Moreover, a direct correlation was found between NPAF and nonviable cells, as demonstrated in light and salinity experiments.

Finally, in accordance with all the advantages described, the CLSM-DL method can be applied to assessing viability in other photosynthetic microorganism, whether these form aggregates or as individual cells. In addition, this method could be especially useful in characterising the physiological state of individual cells within microbial communities in extreme environments, in which dead and living cells coexist.

Conclusions

In conclusion, the newly developed CLSM-DL method can be providing data in short time consuming, *in vivo* and at cellular level without the need of either staining or additional use of image treating software.

This technique can be useful to distinguish cultivable and noncultivable phototrophic microorganisms, including those that form consortia with heterotrophic bacteria, because it rules out any interference with these microorganisms.

The CLSM-DL method combined with the CLSM-λ*scan* function confirms that there is a strong and good correlation of both the cells' physiological state and the performance of photosynthetic pigments with the percentages of individual living cells.

Acknowledgements

We express our thanks to the staff of the *Servei de Microscòpia* for technical assistance with the confocal and electron microscopes and the *Servei de Llengües,* both at the Universitat Autònoma de Barcelona. We also thank Eneko Mitxelena for

his support on images digital processing and Marc Alamany, who provided valuable comments on the manuscript. Finally, we acknowledge Cristina Sosa for her help in this work.

Fundings

This work was supported by the Spanish Ministry of Education and Science [grant DGICYT CGL2008-01891/BOS]; and the Universitat Autònoma de Barcelona (UAB) research fellowship for young scientists [to L.M.].

Disclosures

The authors have no conflicts of interest to declare.

References

Al-Rubeai, M., Welzenbach, K., Lloyd, D.R. & Emery, A.N. (1997) A rapid method for evaluation of cell number and viability by flow cytometry. *Cytotechnology* **24**(2), 161–168.

Antibus, D.E., Leff, L.G., Hall, B.L., Baeseman, J.L. & Blackwood, C.B. (2012) Cultivable bacteria from ancient algal mats from the McMurdo Dry Valleys, Antarctica. *Extremophiles* **16**, 105–114.

Billi, D., Viaggiu, E., Cockell, C.S., Rabbow, E., Horneck, G. & Onofri, S. (2011) Damage escape and repair in dried *Chroococcidiopsis* spp. from hot and cold deserts exposed to simulate space and Martian conditions. *Astrobiology* **11**, 65–73.

Büchel, C. & Wilhelm, C. (1993) In vivo analysis of slow chlorophyll fluorescence induction kinetics in algae: progress, problems and perspectives. *Photochem. Photobiol.* **58**, 137–148.

Buck, J. D. (1979) The plate count in aquatic microbiology. *Native Aquatic Bacteria: Enumeration, Activity, and Ecology* (ed. by J.W. Costerton & R.R. Colwell), pp. 19–28. ASTM STP 695, Baltimore.

Burgos, A., Maldonado, J., de los Ríos, A., Solé, A. & Esteve, I. (2013) Effect of copper and lead on two consortia of phototrophic microorganisms and their capacity to sequester metals. *Aquat. Toxicol.* **140–141**, 324–336.

Cuadrado, D.G., Pan, J., Gómez, E.A. & Maisano, L. (2015) Deformed microbial mat structures in a semiarid temperate coastal setting. *Sediment. Geol.* **325**, 106–118.

de los Ríos, A., Ascaso, C., Wierzchos, J., Vicent, W.F. & Quesada, A. (2015) Microstructure and cyanobacterial composition of microbial mats from the High Arctic. *Biodivers. Conserv.* **24**(4), 841–863.

Dorsey, J., Yentsch, C.M., Mayo, S. & McKenna, C. (1989) Rapid analytical technique for the assessment of cell metabolic activity in marine microalgae. *Cytometry* **10**, 622–628.

Esteve, I., Ceballos, D., Martínez-Alonso, M., Gaju, N. & Guerrero, R. (1994) Development of versicolored microbial mats: succession of microbial communities. *Microbial Mats: Structure, Development and Environmental Significance* (ed. by L.J. Stal & P. Caumette), pp. 415–420, NATO ASI Series G: Ecological Sciences, Springer-Verlag, Berlin, Heidelberg.

Ferreira, V.S., Pinto, R.F. & Sant'Anna, C. (2016) Low light intensity and nitrogen starvation modulate the chlorophyll content of *Scenedesmus dimorphus*. *J. Appl. Microbiol.* **120**(3), 661–670.

Garcia-Pichel, F., López-Cortés, A. & Nübel, U. (2001) Phylogenetic and morphological diversity of cyanobacteria in soil desert crusts from Colorado plateau. *Appl. Environ. Microbiol.* **67**(4), 1902–1910.

Genty, B., Briantais, J.M. & Baker, N.R. (1989) The relationship between the quantum yield of photosynthetic electron transport and quenching of chlorophyll fluorescence. *Biochim. Biophys. Acta.* **990**, 87–92.

Green, S.J., Blackford, C., Bucki, P., Jahnke, L.L. & Prufert-Bebbout, L. (2008) A salinity and sulfate manipulation of hypersaline microbial mats reveals stasis in the cyanobacterial community structure. *ISME J.* **2**, 457–470.

Gregor, J. & Maršálek, B. (2004) Freshwater phytoplankton quantification by chlorophyll *a*: a comparative study of in vitro, in vivo and in situ methods. *Water Res.* **38**, 517–522.

Guerrero, R., Piqueras, M. & Berlanga, M. (2002) Microbial mats and the search for minimal ecosystems. *Int. Microbiol.* **5**, 177–188.

Hoffmann, D., Maldonado, J., Wojciechowski, M.F. & Garcia-Pichel, F. (2015) Hydrogen export from intertidal cyanobacterial mats: sources, fluxes and the influence of community composition. *Environ. Microbiol.* **17**(10), 3738–3753.

Huot, Y., Babin, M. (2011) Overview of fluorescence protocols: theory, basic concepts and practice. *Chlorophyll a Fluorescence in Aquatic Sciences: Methods and Applications* (ed. by D.J. Suggett, O. Prášil & M.A. Borowizka), pp. 31–74. Springer, Dordrecht.

Kroemer, G., Petit, P., Zamzami, N., Vayssière, J.L. & Mignotte, B. (1995) The biochemistry of programmed cell death. *FASEB J.* **9**, 1277–1287.

Lan, S., Wu, L., Zhang, D. & Hu, C. (2014) Desiccation provides photosynthetic protection for crust cyanobacteria *Microcoleus vaginatus* from high temperature. *Physiol. Plant.* **152**(2), 345–354.

Maldonado, J., de los Ríos, A., Esteve, I., Ascaso, C., Puyen, Z.M., Brambilla, C. & Solé, A. (2010) Sequestration and *in vivo* effect of lead on DE2009 microalga, using high-resolution microscopic techniques. *J. Hazard. Mater.* **183**, 44–50.

Mehta, P., Jajoo, A., Mathur, S. & Bharti, S. (2010) Chlorophyll *a* fluorescence study revealing effects of high salt stress on Photosystem II in wheat leaves. *Plant Physiol. Biochem.* **48**, 16–20.

Millach, L., Solé, A. & Esteve, I. (2015) Role of *Geitlerinema* sp. DE2011 and *Scenedesmus* sp. DE2009 as bioindicators and immobilizers of chromium in a contaminated natural environment. *Biomed Res. Int.* 2015, Article ID 519769, 11 pages.

Naganuma, T. (1996) Differential enumeration of intact and damaged marine planktonic bacteria based on cell membrane integrity. *J. Aquat. Ecosyst. Health* **5**, 217–222.

Pal, S.W., Singh, N.K. & Azam, K. (2013) Evaluation of relationship between light intensity (Lux) and growth of *Chaetoceros muelleri*. *Oceanography* **1**, 111. https://doi.org/10.4172/2332-2632.1000111

Perkins, R.G., Oxborough, K., Hanlon, A.R.M., Underwood, G.J.C. & Baker, N.R. (2002) Can chlorophyll fluorescence be used to estimate the rate of photosynthetic electron transport within microphytobenthic biofilms? *Mar. Ecol. Prog. Ser.* **228**, 47–56.

Pfennig, N. & Trüpper, H.G. (1992) The family chromatiaceae. *The Prokaryotes* (ed. by A. Balows, H.G. Trüpper, M. Dworkin, W. Harder & K.H. Schleifer), pp. 3200–3221. Springer-Verlag, Berlin.

Pouneva, I. (1997) Evaluation of algal culture viability and physiological state by fluorescent microscopic methods. *Bulg. J. Plant Physiol.* **23**(1–2), 67–76.

Rajeev, L., Nunes da Rocha, U., Klitgord, N. *et al.* (2013) Dynamic cyanobacterial response to hydration and dehydration in a desert biological soil crust. *ISME J.* **7**, 2178–2191.

Roldan, M., Thomas, F., Castel, S., Quesada, A. & Hernandez-Marine, M. (2004) Noninvasive pigment identification in single cells from living

phototrophic biofilms by confocal imaging spectrofluorometry. *Appl. Environ. Microbiol.* **70**, 3745–3750.

Sato, M., Murata, Y., Mizusawa, M., Iwahashi, H. & Oka, S. (2004) A simple and rapid dual-fluorescence viability assay for microalgae. *Microbiol. Cult. Coll.* **20**, 53–59.

Schreiber, U. (1998) Chlorophyll fluorescence: new instruments for special applications. *Photosynthesis: Mechanisms and Effects*, Vol. **V** (ed. by G. Garag), pp. 4253–4258. Kluwer Academic Publishers, Dordrecht.

Solé, A., Diestra, E. & Esteve, I. (2009) Confocal laser scanning microscopy image analysis for cyanobacterial biomass determined at microscale level in different microbial mats. *Microb. Ecol.* **57**, 649–656.

Tang, Y.Z. & Dobbs, F.C. (2007) Green autofluorescence in dinoflagellates, diatoms and other microalgae and its implications for vital staining and morphological studies. *Appl. Environ. Microbiol.* **73**(7), 2306–2313.

Veldhuis, M.J.W., Kraay, G.W. & Timmermans, K.R. (2001) Cell death in phytoplankton: correlation between changes in membrane permeability, photosynthetic activity, pigmentation and growth. *Eur. J. Phycol.* **36**, 167–177.

Wagenen, J.V., Holdt, S.L., Francisci, D.D., Valverde-Perez, B., Plósz, B.G. & Angelidaki, I. (2014) Microplate-based method for high-throughput screening of microalgae growth potential. *Bioresour. Technol.* **169**, 566–572.

Hindawi Publishing Corporation
BioMed Research International
Volume 2015, Article ID 519769, 11 pages
http://dx.doi.org/10.1155/2015/519769

Research Article

Role of *Geitlerinema* sp. DE2011 and *Scenedesmus* sp. DE2009 as Bioindicators and Immobilizers of Chromium in a Contaminated Natural Environment

Laia Millach, Antoni Solé, and Isabel Esteve

Departament de Genètica i Microbiologia, Facultat de Biociències, Universitat Autònoma de Barcelona, Bellaterra, Cerdanyola del Vallès, 08193 Barcelona, Spain

Correspondence should be addressed to Isabel Esteve; isabel.esteve@uab.cat

Received 25 March 2015; Revised 25 May 2015; Accepted 31 May 2015

Academic Editor: Qaisar Mahmood

The aim of this work was to study the potential of the two phototrophic microorganisms, both isolated from Ebro Delta microbial mats, to be used as bioindicators and immobilizers of chromium. The results obtained indicated that (i) the Minimum Metal Concentration (MMC) significantly affecting Chlorophyll *a* intensity in *Geitlerinema* sp. DE2011 and *Scenedesmus* sp. DE2009 was 0.25 μM and 0.75 μM, respectively, these values being lower than those established by current legislation, and (ii) *Scenedesmus* sp. DE2009 was able to immobilize chromium externally in extracellular polymeric substances (EPS) and intracellularly in polyphosphate (PP) inclusions. Additionally, this microorganism maintained high viability, including at 500 μM. Based on these results, we postulate that *Geitlerinema* sp. DE2011 and *Scenedesmus* sp. DE2009 are good chromium-indicators of cytotoxicity and, further, that *Scenedesmus* sp. DE2009 plays an important role in immobilizing this metal in a contaminated natural environment.

1. Introduction

Metal contamination is a serious environmental problem that affects life forms and changes the natural microbiota of aquatic ecosystems. Currently, metals are released from natural and anthropogenic sources (e.g., industry, transport, fossil fuel combustion, the mining industry, and agriculture) into natural aquatic environments [1]. These metals are accumulated in waters, sediments, and biota, generating resistance in microorganisms that leads to environmental and public health problems. To study and predict the effects and removal of heavy metals on different ecosystems, nematode [2], plants [3], and algae [4], among others, have been used. Cyanobacteria and algae are particularly very abundant in aquatic ecosystems, playing an important role in primary production in rivers and their deltas, where metals very often accumulate.

The Ebro River is 928 km long, flows from the north of the Iberian Peninsula to the Mediterranean Sea, and drains an area of 85,000 km^2 approximately. The Ebro Delta, located at the outfall of the Ebro River, is the second most important wetland in Spain after Guadalquivir River marshes and the second one of the Mediterranean area after the Camargue (France). The Ebro Delta is also considered the third largest delta in the Mediterranean with a 320 km^2 triangular surface and it is located at the northeastern coastline of the Iberian Peninsula (0°35′E–0°56′E; 40°33′N–40°47′N) [5]. In 1983, some of the most outstanding natural areas of the delta were included in the Ebro Delta Natural Park (*Parc Natural del Delta de l'Ebre*) because of its ornithological importance, as well as for other geological, biological, economic, and cultural aspects [6].

Microbial mats, developed in water-sediment interfaces, are formed by multilayered benthic microbial communities that are distributed along vertical microgradients of different physical-chemical parameters. These ecosystems are widely distributed around the world in different extreme environments, such as lakes [7], marine waters [8], and cold waters [9], among others. Ebro Delta microbial mats are formed by different microorganisms; principally cyanobacteria and microalgae are the most abundant prokaryotic bacteria located mainly in the upper layers of microbial mats [10].

The e microbial mats receive waters and contaminants, including heavy metals dragged by the River Ebro into its estuary (delta). For this reason, in the last few years, our work group has isolated various microorganisms of this ecosystem and has developed several methods, in particular Confocal Laser Scanning Microscopy (CLSM), to determine their capacity to tolerate or resist metals, as well as evaluate the effect of these *in vivo* at both cell and population levels. The e methods used for the *in vivo* study of phototrophic microorganisms have led to obtaining quantitative results more quickly. Thi is mainly due to the minimal necessary manipulation of the specimens, and since these emit natural fluorescence, they do not require staining protocols. Furthermore, the majority of works have evaluated the effect of lead and copper toxicity in isolated microorganisms [11] and the capacity of various microorganisms to uptake these metals extra- and/or intracellularly using Scanning Electron Microscopy (SEM) and Transmission Electron Microscopy (TEM), both coupled to an Energy Dispersive X-Ray (SEM-EDX and TEM-EDX) [12].

However, the role that microorganisms play in this same habitat on chromium detoxification is still unknown. Chromium can exist in the environment as Cr(III) or Cr(VI) [13, 14] and particularly in the Cr(VI) form is extremely toxic, mutagenic, and carcinogenic. In the environment, chromium is introduced as the by-product of industries [15] and phosphate fertilizers [16]. In highly contaminated habitats [17, 18], the reduction of Cr(VI) to Cr(III) is an effective method of Cr(VI) detoxific tion. Nevertheless, the immobilization efficie y of Cr(III) is still unclear and different reports suggest that soluble organo-Cr(III) complexes are present in various chromate-reducing bacterial systems [19, 20]. Th permanence of soluble forms of Cr(III) causes a serious problem, since they can be reoxidized to Cr(VI). It is for this reason that there is great interest in studying the immobilization of Cr(III) in pilot-scale experiments [21].

Nowadays, there is little information on this process in the natural environment, where the levels of contamination by chromium are very low, as in the River Ebro ($<2\,\mu g\,L^{-1}$ Cr, according to data from the Ebro Hydrographic Association, in the last 10 years). In these cases, although the same probably occurs, the Cr(VI) is biotransformed to Cr(III), and this can remain in ecosystems, immobilized or not, and could have a toxic effect on life forms. Likewise, very little is known about the role of indigenous microorganisms in these natural environments with low levels of chromium and also with a prolonged permanence of the metal in the ecosystem.

Th aim of this work is to determine the role of *Geitlerinema* sp. DE2011 and *Scenedesmus* sp. DE2009, both isolated from Ebro Delta microbial mats, as bioindicators and immobilizers of chromium and, additionally, to analyse the effect of this metal on their biomass and cellular viability.

2. Material and Methods

2.1. Microorganisms and Culture Conditions. *Geitlerinema* sp. DE2011 (cyanobacterium) and *Scenedesmus* sp. DE2009 (microalga) were isolated from Ebro Delta microbial mats (Tarragona), Spain. Isolation and purific tion of the isolates were performed by dilution and plating of microbial mats samples. Isolated microorganisms were grown in liquid mineral Pfennig medium [22] in 100 mL flasks. Cultures were exposed and maintained at 27°C in a growth chamber (Climas Grow 180, ClimasLab, Barcelona) under continuous illumination with a light intensity of $3.5\,\mu E\,m^{-2}\,s^{-1}$ for the cyanobacterium and $10\,\mu E\,m^{-2}\,s^{-1}$ for the microalga, provided by cold white fluorescence lights. The e cultures were used as control in all the experiments performed.

2.2. Preparation of Chromium Stock Solution. Th stock solution of chromium was prepared by dissolving $Cr(NO_3)_3$ (Sigma-Aldrich, Bellefonte, PA, US) in deionized Milli-Q water at the concentration of 1 mM Cr(III) and sterilized by filtration in Millex-GP 0.2 μm filters (Millipore, USA). Working concentrations of Cr(III) were obtained by serial dilution. This solution was stored in the dark at 4°C.

2.3. Pigment Analysis of the Strains Using Confocal Laser Scanning Microscopy. Th tolerance and the *in vivo* effect of chromium on cultures of *Geitlerinema* sp. DE2011 and *Scenedesmus* sp. DE2009 were determined by *λscan* function of CLSM (CLSM Leica TCS SP5; Leica Heidelberg, Germany). Moreover, in order to evaluate the effect of chromium on the biomass and viability of *Scenedesmus* sp. DE2009, a modific tion of the FLU-CLSM-IA (Fluorochrome-CLSM-Image Analysis) method described by Puyen et al. [23] was used.

2.3.1. λscan Function. Cultures of *Geitlerinema* sp. DE2011 and *Scenedesmus* sp. DE2009 were contaminated at different $Cr(NO_3)_3$ concentrations: 0.025, 0.050, 0.1, 0.25, 0.50, 0.75, 1, and 5 μM for the cyanobacterium DE2011 and 0.25, 0.50, 0.75, 1, 5, 10, 15, and 25 μM for the microalga DE2009. All experiments were performed for 9 days under the same conditions mentioned in Section 2.1.

Pigment analysis was realized by the *λscan* function of CLSM. This technique provides information on the state of the photosynthetic pigments of phototrophic microorganisms on the basis of the emission wavelength region and the fluorescence intensity emitted (autofluorescence). Each image sequence was obtained by scanning the same *xy* optical section throughout the visible spectrum. Images were acquired at the *z* position at which the fl orescence was maximal, and acquisition settings were constant throughout each experiment. Th sample excitation was carried out with an Argon Laser at 488 nm (*λ*exe 488) with a *λ* step size of 3 nm for an emission wavelength between 550 and 748 nm.

In order to measure the mean fluorescence intensity (MFI) of the *xyλ* data sets, the Leica Confocal Software (Leica Microsystems CMS GmbH) was used. In these confocal images the pseudocolour palette 4 was selected, where warm colours represented the maximum intensities and cold colours represented the low intensities of fluorescence. The regions-of-interest (ROIs) function of the software was used to measure the spectral signature. For each sample, 70 ROIs of 1 μm^2 taken from cells were analysed.

This method allowed us to evaluate the physiological state of the phototrophic microorganisms at single-cell level, considering changes in the spectrum of Chlorophyll *a* (Chl *a*) used as a marker. For this purpose, the state of pigments was considered by means of the Maximum Intensity Fluorescence (MIF) signal detected at 661 nm (Chl *a*) for *Geitlerinema* sp. DE2011 and 685 nm for *Scenedesmus* sp. DE2009 (Chl *a*).

2.3.2. FLU-CLSM-IA Modified Method. To determine the effect of chromium on biomass and cellular viability of *Scenedesmus* sp. DE2009 cultures, experiments at different $Cr(NO_3)_3$ concentrations, 0.75, 25, 100, 200, and 500 μM, were performed for a period of 9 days under the same conditions mentioned in Section 2.1 following a modific tion of the FLU-CLSM-IA method [23]. Thi method combines the use of specific fluorochrome, the CLSM microscope, and the *ImageJ v1.48s* software.

In this study, *Scenedesmus* sp. DE2009 autofluorescence (emission at 616–695 nm) and SYTOX Green Nucleic Acid Stain fluorescence (emission at 520–580 nm; Invitrogen, Life Technologies) were used simultaneously as markers for live and dead cells, respectively, in a simple dual-fluorescence viability assay [24]. Both the red and green fluorescence signals were captured separately in a *sequential scan* process in two channels from each same *xyz* optical section (Figures 1(a) and 1(c)).

In order to differentiate between living and dead cells, red (live cells) and green (dead cells) pseudocolors were used and 20 red and green confocal images were acquired from every culture of *Scenedesmus* sp. DE2009 to determine the biomass and cellular viability at each Cr-concentration.

Th CLSM images were transformed to binary images (black/white) applying fluorescence threshold values of 30 (red pixels) and 35 (green pixels) by means of the *ImageJ v1.48s* softw re (Figures 1(b) and 1(d)). To minimize the background detected in every pair of images a smoothing fi ter was used.

To obtain biovolume values, the Voxel Counter plug-in was applied to these filtered images [25]. Thi specifi application calculates the ratio between the thresholded voxels (red and green fluorescent voxel counts) to all voxels from every binary image analysed. The biovolume value (volume fraction) was finally multiplied by a conversion factor of 310 fgC μm^3 to convert it to biomass [26].

2.4. Ascertaining Chromium Immobilization through Electronic Microscopy Techniques. With the aim of determining whether *Geitlerinema* sp. DE2011 and *Scenedesmus* sp. DE2009 could immobilize metals extra- and intracellularly, cells from cultures growing with and without chromium were analysed by EDX coupled to SEM and TEM.

2.4.1. Scanning Electron Microscopy and Energy Dispersive X-Ray Analysis. Phototrophic microorganisms cultures were contaminated at different $Cr(NO_3)_3$ concentrations, 1, 5, 10, 25, 50, 100, and 200 μM Cr(III), and incubated under the same conditions as mentioned above for a period of 9 days.

For SEM analysis, cultures were filtrated in Nuclepore polycarbonate membranes (Whatman, Ltd.) and then were fi ed in 2.5% glutaraldehyde diluted in Millonig phosphate buffer (0.1 M pH 4) at 4°C for 2 hours and washed four times in the same buffer, dehydrated in increasing concentrations of ethanol (30%, 50%, 70%, 90%, and 100%), and dried by critical-point (CPD 030 Critical Point Drier, BAL-TEC GmbH, 58579 Schalksmühle). Finally, samples were mounted on aluminium metal stubs and coated with a 5 μm gold layer (K550 Sputter Coater, Emitech, Ashford, UK) for better image contrast. A Zeiss EVOMA 10 scanning electron microscope (Carl Zeiss NTS GmbH, Oberkochen, Germany) was used to view the images.

For EDX microanalysis, cells were homogenously distributed and filtered on polycarbonate membrane filters. Th se filters were fixed, dehydrated, and dried by critical-point drying and then coated with gold. An EDX spectrophotometer Link Isis-200 (Oxford Instruments, Bucks, England) coupled to the microscope operating at 20 kV was used. Finally, EDX-SEM spectra from individual cells were obtained.

2.4.2. Transmission Electron Microscopy and Energy Dispersive X-Ray Analysis. TEM was used in order to observe the ultrastructure of the phototrophic microorganisms and TEM-EDX to assess whether *Geitlerinema* sp. DE2011 and *Scenedesmus* sp. DE2009 were able to bioaccumulate chromium intracellularly. So, cyanobacterium DE2011 and the microalga DE2009 were contaminated with 200 μM $Cr(NO_3)_3$ for a period of 9 days. Culture conditions were the same as described for SEM.

For TEM analysis, samples were fixed in 2.5% glutaraldehyde diluted in Millonig phosphate buffer (0.1 M pH 4) at 4°C for 2 hours and washed four times (15 min) in the same buffer at 4°C. The samples were postfi ed in 1% OsO_4 at 4°C for 2 hours, washed in the same buffer, and centrifuged in order to obtain a pellet. Th y were then dehydrated in a graded series of acetone (50%, 70%, 90%, 95%, and 100%) and embedded in Spurr's resin. Once the samples were included in the resin, ultrathin sections (70 nm), obtained with a Leica EM UC6 Ultramicrotome (Leica Microsystems, GmbH, Heidelberg, Germany), were mounted on carbon-coated titanium grids and stained with uranyl acetate and lead citrate. Samples were viewed in a Hitachi H-7000 transmission electron microscope (Hitachi Ltd., Tokyo, Japan).

For EDX microanalysis, sections 200 nm thick were also stained with uranyl acetate and mounted on carbon-coated titanium grids. Samples were analysed with an EDX spectrophotometer Link Isis-200 (Oxford Instruments, Bucks, England) coupled to a Jeol Jem-2011 (Jeol Ltd., Tokyo, Japan) operating at 20 kV. Finally, EDX-TEM spectra from individual cells were obtained.

2.5. Statistical Analysis. Statistical analyses were carried out by one-way analysis of variance (ANOVA) and Tukey and Bonferroni's comparison *post hoc* tests. Significant diff rences were accepted at $P < 0.05$. The analyses were performed using IBM SPSS Statistics software (version 20.0 for Windows 7).

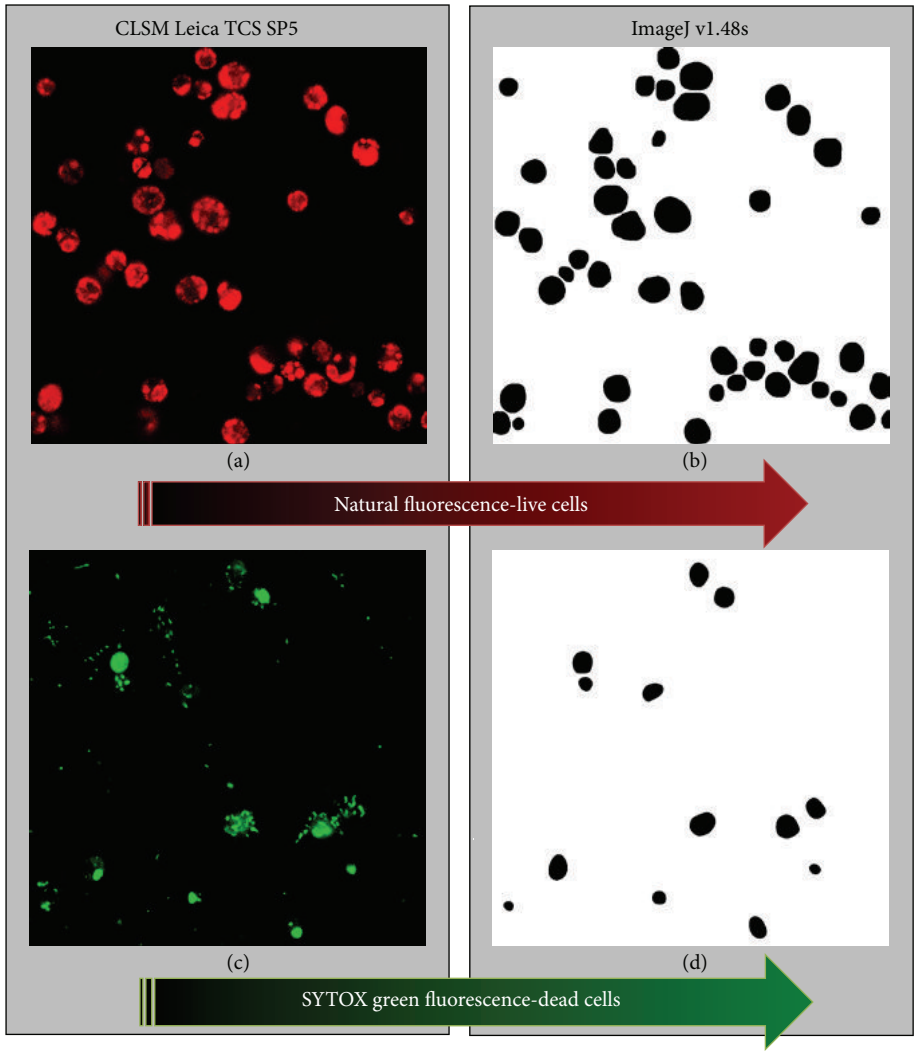

Figur e 1: *xyz* CLSM optical sections (a) and (b) and their corresponding binary images of live (b) and dead (d) *Scenedesmus* sp. DE2009 cells analysed using the modifie FLU-CLSM-IA method.

3. Results and Discussion

3.1. Morphological Characteristics of Geitlerinema sp. DE2011 and Scenedesmus sp. DE2009. The phototrophic microorganisms, isolated from Ebro Delta microbial mats, were identifi d as *Geitlerinema* sp. DE2011 [27] and *Scenedesmus* sp. DE2009 [12] by molecular biology methods. Both microorganisms are very abundant in Ebro Delta microbial mats and play an important role in the stabilization of deltaic sediments.

Geitlerinema sp. DE2011 is a cyanobacterium, which forms individual filaments, sometimes densely packed and surrounded by a sheath. Cells from filaments vary in size from 3.13 to 3.75 μm. On the other hand, *Scenedesmus* sp. DE2009 is a microalga, which like *Geitlerinema* sp. DE2011 forms a consortium with diff rent heterotrophic bacteria. The microalga cells are spherical, with a diameter of 7–9 μm and their chloroplasts are distributed laterally in the cell.

3.2. Chromium Tolerance in Phototrophic Microorganisms. In order to calculate the Minimum Metal Concentration (MMC) that signific ntly affects pigment intensity in *Geitlerinema* sp. DE2011 and *Scenedesmus* sp. DE2009, two experiments were performed. In the preliminary experiment, a wide range of chromium concentrations was assayed. Displacement of the fluorescence peak was observed only in *Geitlerinema* sp. DE2015 from 661 nm (MIF) towards to 670 nm, at maximum Cr-concentration assayed (5 μM fluorescence spectrum). In both cases, highly statistically signific nt differences ($P < 0.05$) were found between the control and all the concentrations tested (Figures 2(a) and 2(b)).

For this reason, a second experiment was carried out on *Geitlerinema* sp. DE2011 with lower doses from 25 nM to 0.75 μM Cr(III). The *xyz* optical sections of this microorganism, corresponding to the autofluorescence detected in control and contaminated cultures, were shown in Figures 3(a) and 3(b). The results indicated that the MMC of chromium (when compared with the control) that significantly ($P < 0.05$) affected the intensity of the pigment (Chl *a*)

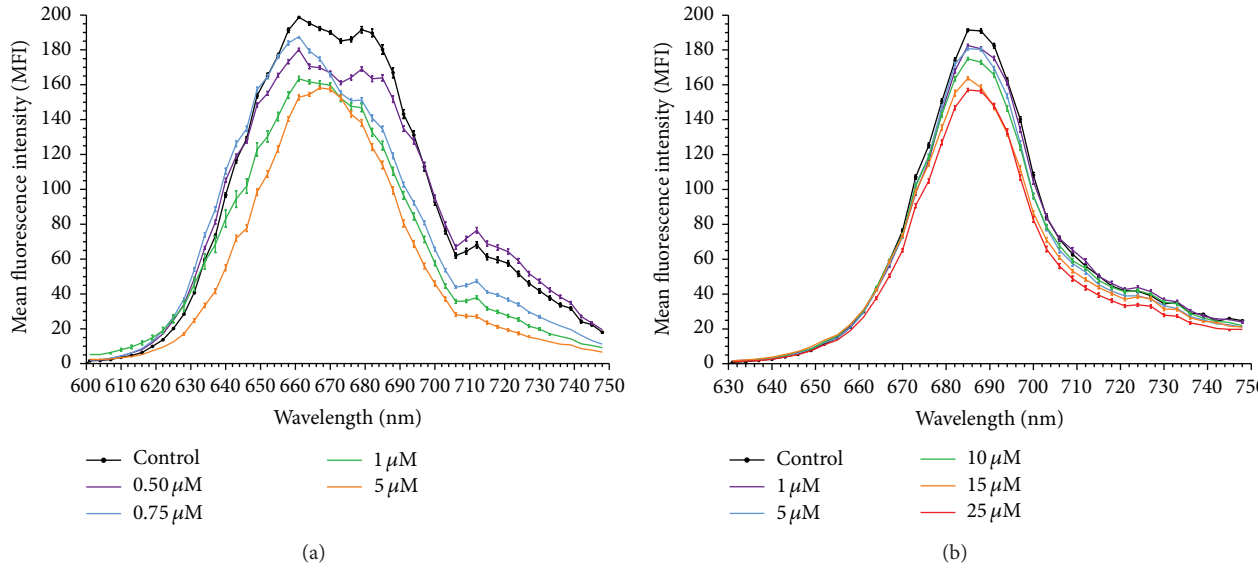

Figur e 2: *λscan* plots of *Geitlerinema* sp. DE2011 (a) and *Scenedesmus* sp. DE2009 (b) contaminated with a wide range of chromium concentrations.

of *Geitlerinema* sp. DE2011 was 0.25 μM Cr. An analogous experiment to that mentioned above was performed with lower doses from 0.25 μM to 5 μM Cr(III) on cultures of *Scenedesmus* sp. DE2009. Th autofluorescence detected in control and contaminated cultures was shown in Figures 4(a) and 4(b). In this case, the MMC that significantly ($P < 0.05$) affected the intensity of the pigment in *Scenedesmus* sp. DE2009 was 0.75 μM Cr, and therefore this microorganism was more tolerant to chromium than *Geitlerinema* sp. DE2011 (0.25 μM Cr).

On the other hand, the *λscan* plots graphs of both microorganisms indicated how the MIF peak (Chl *a*) decreased while the Cr-concentration increased following mainly the same pattern as the control culture (Figures 3(c) and 4(c)). These results are in agreement with those obtained by different authors, which demonstrated, in *Scenedesmus obliquus* and *Nostoc muscorum*, respectively, that metal stress results in direct inactivation of the photosystem II (PS II) reaction center and consequently a decrease of Chlorophyll *a* fluorescence intensity (F_{685}) [28, 29]. Furthermore, other authors have demonstrated that in response to varying physical-chemical parameters photosynthetic microorganisms undergo changes in their physiological characteristics, mainly changing the quality and concentration of their light-harvesting pigments [30].

It is worth highlighting that the MMC values obtained were below the level permitted in continental surface waters (50 μg L^{-1} Cr) (in accordance with the Directive 2008/105/CE of the European Parliament and the Council on Environmental Quality Standards in the field of Water Policy, transposed into Spanish law "Real Decreto 60/2011, Anexo II"), which demonstrated that both microorganisms should be considered as good indicators of cytotoxicity.

3.3. Metal Immobilization in Phototrophic Microorganisms. Cr-contaminated cultures of *Geitlerinema* sp. DE2011 were analysed by SEM-EDX and chromium was not detected in the extracellular polymeric substances (EPS) (Figures 3(d), 3(e), and 3(f)). Nevertheless, in the contaminated samples of *Scenedesmus* sp. DE2009, the results confirmed that the microalga had the ability to sequester chromium in the EPS (Figures 4(d), 4(e), and 4(f)). Different parts of the filter were also tested as a control in all samples, to be sure that chromium was retained only in cells.

Both microorganisms have dense EPS envelopes, which explain the external uptake of heavy metals. Various authors have suggested that the overall negative charge of EPS may be essential for sequestering metal cations that are necessary for cell growth but present at low concentrations in their surroundings and/or preventing the direct contact between the cells and toxic heavy metals dispersed in the environment [31]. Th functions of EPS in metal uptake are known, but other roles have been proposed for these polymers, such as protection against dehydration or UV radiation, biomineralization, phagocytosis, and adhesion capacity to the surrounding substrate [32].

Although *Geitlerinema* sp. DE2011 gave a negative result for chromium uptake, in previous studies it has been shown that this cyanobacterium was able to capture lead and copper extracellularly [27]. The e differences in metal immobilization were probably due to the fact that the same microorganism can capture distinct metals using diff rent functional groups in the EPS. In accordance with studies carried out by Ozturk et al. [33] an increase in uronic acid, glucuronic acid, and galacturonic acid content was shown in the EPS of *Synechocystis* sp. BASO671 cultures contaminated by chromium. In addition, Çelekli et al. [34] also confirmed

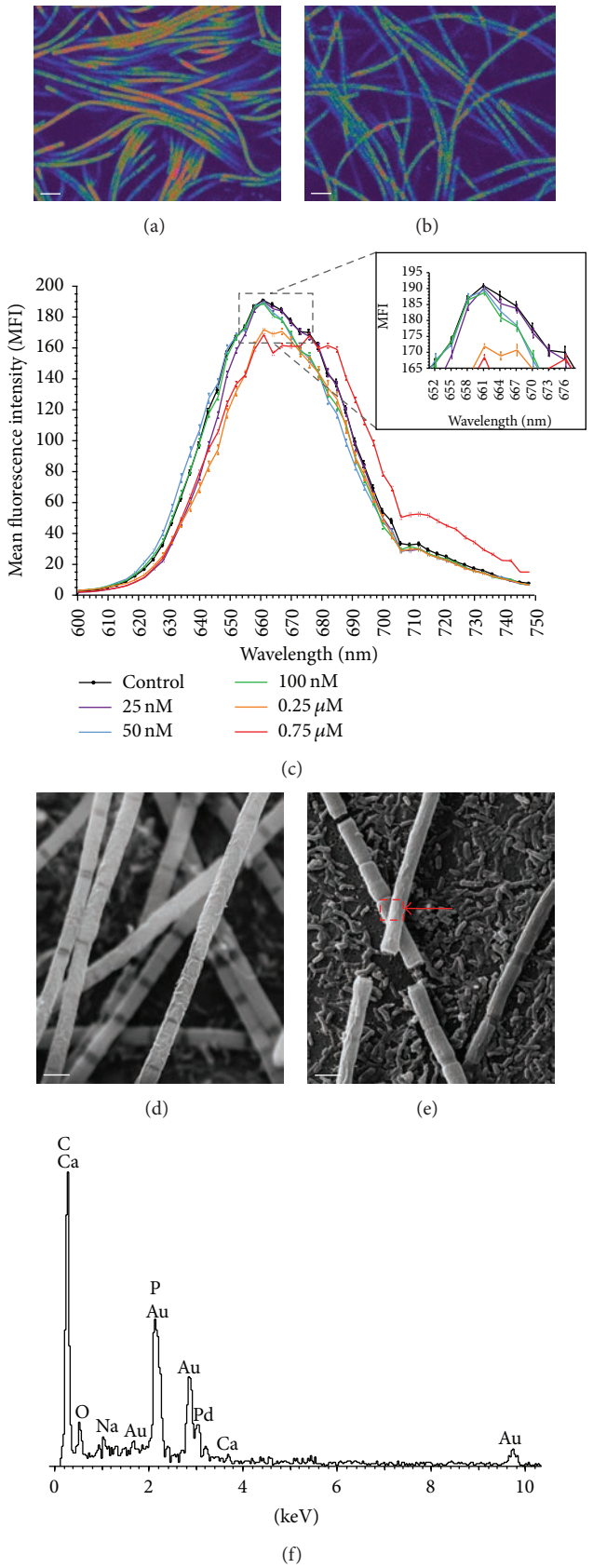

Figur e 3: Continued.

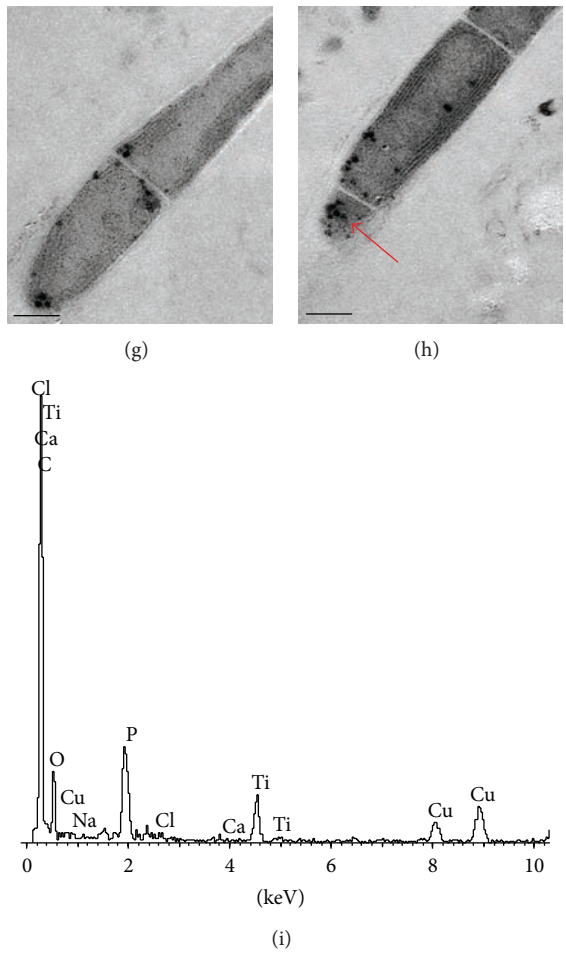

Figure 3: CLSM images of control (a) and chromium contaminated (b) cultures of *Geitlerinema* sp. DE2011 (scale bars represent 10 μm) and *λscan* plot (c). SEM images of control (d) and 200 μM chromium contaminated (e) cultures. Scale bars represent 2 μm. Contaminated EDX spectrum (f). TEM images of control (g) and 200 μM chromium contaminated (h) cultures. Scale bars represent 1 μm. Contaminated EDX spectrum (i).

that specifi anionic groups played a signific nt role in the biosorption of Cd^{2+} by *Scenedesmus quadricauda* var. *longispina*.

On the other hand, TEM micrographs of the ultrathin sections of *Geitlerinema* sp. DE2011 and *Scenedesmus* sp. DE2009 growing at 200 μM Cr showed abundant high electron dense intracytoplasmic inclusions of different sizes in their cytoplasm identifi d as polyphosphate inclusions (PP) (Figures 3(h) and 4(h)). In many cases, similar inclusions have been found when cells are grown in adverse culture conditions [35]. Chromium was not detected internally in *Geitlerinema* sp. DE2011 or *Scenedesmus* sp. DE2009 in control cultures (Figures 3(g) and 4(g)).

Th results obtained through EDX analysis of the inclusions demonstrated that *Geitlerinema* sp. DE2011 did not have the capacity to accumulate chromium as no Cr peak was detected (Figure 3(i)). In contrast to this, a signific nt Cr peak was detected in *Scenedesmus* sp. DE2009, demonstrating that this microorganism was able to immobilize this metal internally in PP inclusions (Figure 4(i)). The e results agree with studies of Goldberg et al. [36], which suggested that this kind of inclusions has a detoxifying effect and a large affinity by sequestering heavy metals. In general, algae seem to be more effective than cyanobacteria in capturing heavy metals [37, 38] and, as has been shown in this work, *Scenedesmus* sp. DE2009, due to its ability to capture chromium both extra- and intracellularly, probably plays an important role in chromium detoxific tion in Ebro Delta microbial mats.

3.4. Effect of Chromium on Biomass and Cellular Viability of Scenedesmus sp. DE2009. For this objective, previously, the red and green fluorescent voxels counts were measured as mentioned in Section 2.3.2. The red voxels (live cells) ranged from 162097 ± 9220 (control experiment) to 143390 ± 6638 (at 500 μM) and the green voxels (dead cells) varied from 23450 ± 1822 (control experiment) to 32113 ± 2277 (at 500 μM). The conversion of this data into biomass values made it possible to observe that the live biomass slightly decreased from 47.92 ± 2.73 mgC cm^{-3} in the control culture to 42.39 ± 1.96 mgC cm^{-3} at 500 μM Cr.

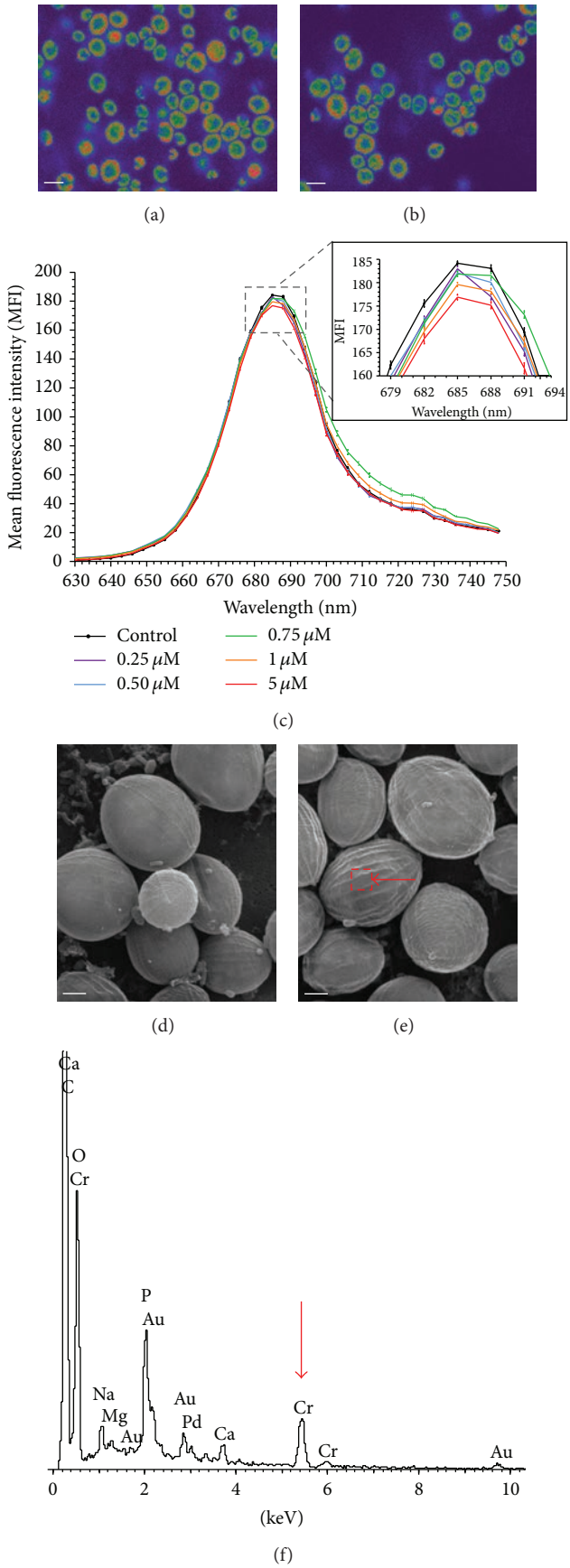

Figur e 4: Continued.

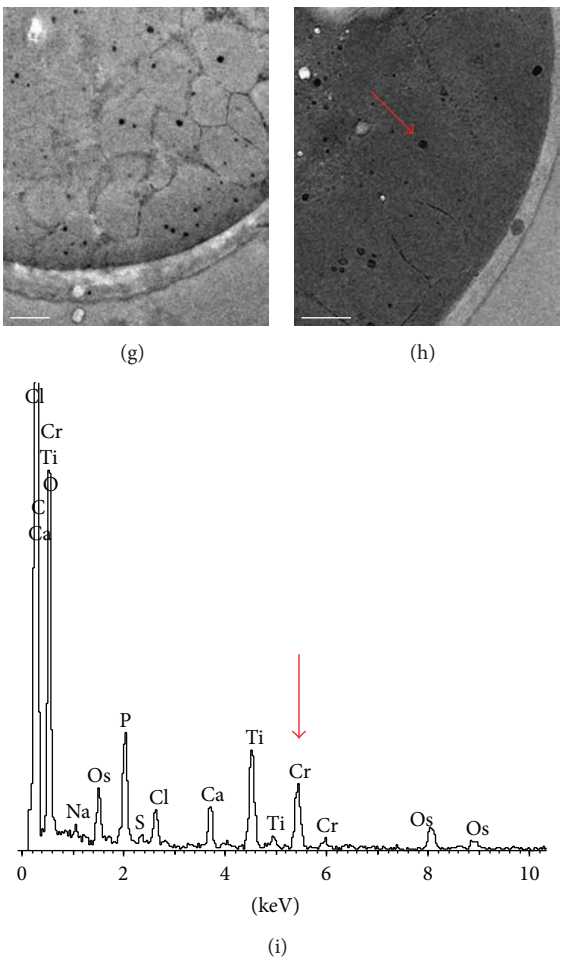

Figur e 4: CLSM images of control (a) and chromium contaminated (b) cultures of *Scenedesmus* sp. DE2009 (scale bars represent 10 μm) and *λscan* plot (c). SEM images of control (d) and 200 μM chromium contaminated (e) cultures. Scale bars represent 2 μm. Contaminated EDX spectrum (f). Arrow indicates the main Cr peak at 5.4 keV. TEM images of control (g) and 200 μM chromium contaminated (h) cultures. Scale bars represent 1 μm. Contaminated EDX spectrum (i). Cr peaks are indicated by arrows.

The changes in viability were shown in Figure 5. These results were expressed as the percentages (%) of live cells and dead cells for each contaminated culture. These values showed low signific nt differences ($P < 0.05$) for all of them compared to the control culture, which indicated a slight effect of the metal in the viability of *Scenedesmus* sp. DE2009. However, there were no significant diff rences ($P < 0.05$) between the various concentrations tested, with the percentage of viable cells in all the Cr-concentrations tested remaining stable.

Thus, on comparing the growth of *Scenedesmus* sp. DE2009 in control culture and the maximum tested concentration (500 μM), it was observed that in the control experiment live cells represented 87.19% and dead cells 12.81%, and in the contaminated culture live cells represented 81.61% and dead cells 18.39% (Figure 5). The e results confi med that a high level of viability of the microalga is maintained, even at the highest concentration of chromium tested.

4. Conclusions

Th results obtained in this paper lead to the conclusion that *Scenedesmus* sp. DE2009 is more tolerant to chromium than *Geitlerinema* sp. DE2011 and that both microorganisms could be considered as good indicators of chromium toxicity in low contaminated natural ecosystems.

On the other hand, *Scenedesmus* sp. DE2009 maintains an elevated biomass and viability at high Cr-concentrations and also has the ability to capture chromium extracellularly in EPS and intracellularly in PP inclusions, which demonstrates its capacity to immobilize this metal.

Conflict of Interests

The authors declare that there is no conflict of interests regarding the publication of this paper.

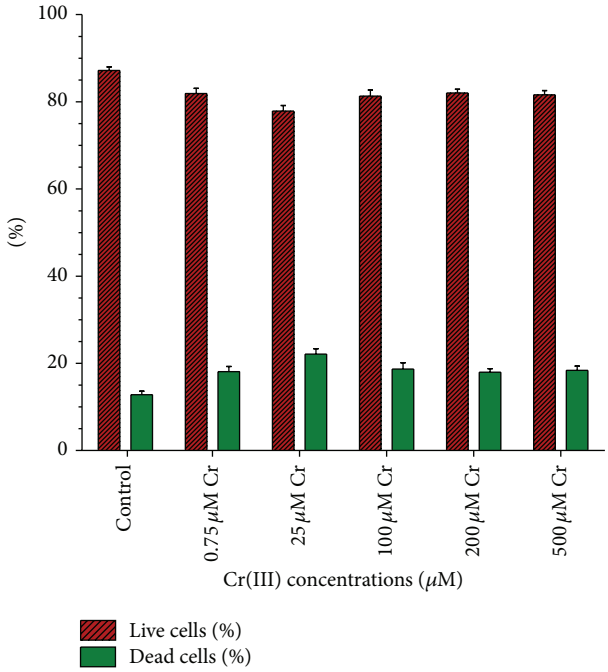

Figur e 5: Percentages of live and dead *Scenedesmus* sp. DE2009 cells at different Cr(III) concentrations. The bars indicate the Standard Error of the Means (S.E.M.).

Acknowledgments

Thi research was supported by the following grants: DGICYT (CGL2008-01891/BOS) and the UAB postgraduate scholarship to Laia Millach. The authors express their gratitude to the staff of *Servei de Microscòpia* for technical assistance with the confocal and electron microscopes and *Servei de Llengües* both at Universitat Autònoma de Barcelona. They also thank Eneko Mitxelena for his support on images digital processing and Cristina Sosa for her help in this work.

References

[1] B. Nogales, M. P. Lanfranconi, J. M. Piña-Villalonga, and R. Bosch, "Anthropogenic perturbations in marine microbial communities," *FEMS Microbiology Reviews*, vol. 35, no. 2, pp. 275–298, 2011.

[2] P. Šalamún, E. Kucanová, T. Brázová, D. Miklisová, M. Renčo, and V. Hanzelová, "Diversity and food web structure of nematode communities under high soil salinity and alkaline pH," *Ecotoxicology*, vol. 23, no. 8, pp. 1367–1376, 2014.

[3] F. C. Chang, C. H. Ko, M. J. Tsai, Y. N. Wang, and C. Y. Chung, "Phytoremediation of heavy metal contaminated soil by *Jatropha curcas*," *Ecotoxicology*, vol. 23, no. 10, pp. 1969–1978, 2014.

[4] A. Magdaleno, C. G. Vélez, M. T. Wenzel, and G. Tell, "Effects of cadmium, copper and zinc on growth of four isolated algae from a highly polluted Argentina river," *Bulletin of Environmental Contamination and Toxicology*, vol. 92, no. 2, pp. 202–207, 2014.

[5] R. Guerrero, M. Piqueras, and M. Berlanga, "Microbial mats and the search for minimal ecosystems," *International Microbiology*, vol. 5, no. 4, pp. 177–188, 2002.

[6] S. Mañosa, R. Mateo, and R. Guitart, "A review of the effects of agricultural and industrial contamination on the Ebro delta biota and wildlife," *Environmental Monitoring and Assessment*, vol. 71, no. 2, pp. 187–205, 2001.

[7] J. K. Cole, J. R. Hutchison, R. S. Renslow et al., "Phototrophic biofilm assembly in microbial-mat-derived unicyanobacterial consortia: model systems for the study of autotroph-heterotroph interactions," *Frontiers in Microbiology*, vol. 5, article 109, 2014.

[8] D. Hoffmann, J. Maldonado, M. F. Wojciechowski, and F. Garcia-Pichel, "Hydrogen export from intertidal cyanobacterial mats: sources, fluxes and the influence of community composition," *Environmental Microbiology*, 2015.

[9] D. E. Antibus, L. G. Leff, B. L. Hall, J. L. Baeseman, and C. B. Blackwood, "Cultivable bacteria from ancient algal mats from the McMurdo Dry Valleys, Antarctica," *Extremophiles*, vol. 16, no. 1, pp. 105–114, 2012.

[10] I. Esteve, D. Ceballos, M. Martínez-Alonso, N. Gaju, and R. Guerrero, "Development of versicolored microbial mats: succession of microbial communities," in *Microbial Mats*, L. J. Stal and P. Caumette, Eds., vol. 35 of *NATO ASI Series*, pp. 415–420, Springer, Berlin, Germany, 1994.

[11] M. Seder-Colomina, A. Burgos, J. Maldonado, A. Solé, and I. Esteve, "Th effect of copper on different phototrophic microorganisms determined in vivo and at cellular level by confocal laser microscopy," *Ecotoxicology*, vol. 22, no. 1, pp. 199–205, 2013.

[12] J. Maldonado, A. de los Rios, I. Esteve et al., "Sequestration and *in vivo* effect of lead on DE2009 microalga, using high-resolution microscopic techniques," *Journal of Hazardous Materials*, vol. 183, no. 1–3, pp. 44–50, 2010.

[13] D. Rai, L. E. Eary, and J. M. Zachara, "Environmental chemistry of chromium," *Science of the Total Environment*, vol. 86, no. 1-2, pp. 15–23, 1989.

[14] V. Gómez and M. P. Callao, "Chromium determination and speciation since 2000," *TrAC Trends in Analytical Chemistry*, vol. 25, no. 10, pp. 1006–1015, 2006.

[15] S. E. Manahan, *Environmental Chemistry*, CRC Press, Taylor and Francis Group, Boca Raton, Fla, USA, 9th edition, 2009.

[16] G. Nziguheba and E. Smolders, "Inputs of trace elements in agricultural soils via phosphate fertilizers in European countries," *Science of the Total Environment*, vol. 390, no. 1, pp. 53–57, 2008.

[17] M. Faisal and S. Hasnain, "Comparative study of Cr(VI) uptake and reduction in industrial effluent by *Ochrobactrum intermedium* and *Brevibacterium* sp.," *Biotechnology Letters*, vol. 26, no. 21, pp. 1623–1628, 2004.

[18] S. Sultan and S. Hasnain, "Reduction of toxic hexavalent chromium by *Ochrobactrum intermedium* strain SDCr-5 stimulated by heavy metals," *Bioresource Technology*, vol. 98, no. 2, pp. 340–344, 2007.

[19] G. J. Puzon, J. N. Petersen, A. G. Roberts, D. M. Kramer, and L. Xun, "A bacterial flavin reductase system reduces chromate to a soluble chromium (III)-NAD^+ complex," *Biochemical and Biophysical Research Communications*, vol. 294, no. 1, pp. 76–81, 2002.

[20] G. J. Puzon, R. K. Tokala, H. Zhang, D. Yonge, B. M. Peyton, and L. Xun, "Mobility and recalcitrance of organo-chromium(III) complexes," *Chemosphere*, vol. 70, no. 11,pp. 2054–2059, 2008.

[21] Y. Cheng, F. Yan, F. Huang et al., "Bioremediation of Cr(VI) and immobilization as Cr(III) by *Ochrobactrum anthropi*," *Environmental Science and Technology*, vol. 44, no. 16, pp. 6357–6363, 2010.

[22] N. Pfennig and H. G. Trüpper, "The family Chromatiaceae," in *Th Prokaryotes*, A. Balows, H. G. Trüpper, M. Dworkin, and K. H. Schleifer, Eds., pp. 3200–3221, Springer, Berlin, Germany, 2nd edition, 1992.

[23] Z. M. Puyen, E. Villagrasa, J. Maldonado, I. Esteve, and A. Solé, "Viability and biomass of *Micrococcus luteus* DE2008 at different salinity concentrations determined by specifi fluorochromes and CLSM-image analysis," *Current Microbiology*, vol. 64, no. 1, pp. 75–80, 2012.

[24] M. Sato, Y. Murata, M. Mizusawa, H. Iwahashi, and S. Oka, "A simple and rapid dual-fluorescence viability assay for microalgae," *Microbiology and Culture Collections*, vol. 20, pp. 53–59, 2004.

[25] W. S. Rasband, *ImageJ*, US National Institutes of Health, Bethesda, Md, USA, 1997–2014, http://imagej.nih.gov/ij.

[26] J. C. Fry, "Direct methods and biomass estimation," *Methods in Microbiology*, vol. 22, pp. 41–85, 1990.

[27] A. Burgos, J. Maldonado, A. de los Rios, A. Solé, and I. Esteve, "Effect of copper and lead on two consortia of phototrophic microorganisms and their capacity to sequester metals," *Aquatic Toxicology*, vol. 140-141, pp. 324–336, 2013.

[28] N. Mallick and F. H. Mohn, "Use of chlorophyll fluorescence in metal-stress research: a case study with the green microalga *Scenedesmus*," *Ecotoxicology and Environmental Safety*, vol. 55, no. 1, pp. 64–69, 2003.

[29] S. M. Prasad, J. B. Singh, L. C. Rai, and H. D. Kumar, "Metal-induced inhibition of photosynthetic electron transport chain of the cyanobacterium *Nostoc muscorum*," *FEMS Microbiology Letters*, vol. 82, no. 1, pp. 95–100, 1991.

[30] M. Roldán, C. Ascaso, and J. Wierzchos, "Fluorescent fingerprints of endolithic phototrophic cyanobacteria living within halite rocks in the atacama desert," *Applied and Environmental Microbiology*, vol. 80, no. 10, pp. 2998–3006, 2014.

[31] S. Pereira, E. Micheletti, A. Zille et al., "Using extracellular polymeric substances (EPS)-producing cyanobacteria for the bioremediation of heavy metals: do cations compete for the EPS functional groups and also accumulate inside the cell?" *Microbiology*, vol. 157, no. 2, pp. 451–458, 2011.

[32] R. de Philippis and M. Vincenzini, "Outermost polysaccharidic investments of cyanobacteria: nature, signific nce and possible applications," *Recent Research Developments in Microbiology*, vol. 7, pp. 13–22, 2003.

[33] S. Ozturk, B. Aslim, Z. Suludere, and S. Tan, "Metal removal of cyanobacterial exopolysaccharides by uronic acid content and monosaccharide composition," *Carbohydrate Polymers*, vol. 101, no. 1, pp. 265–271, 2014.

[34] A. Çelekli, M. Kapı, and H. Bozkurt, "Effect of cadmium on biomass, pigmentation, malondialdehyde, and proline of *Scenedesmus quadricauda* var. *longispina*," *Bulletin of Environmental Contamination and Toxicology*, vol. 91, no. 5, pp. 571–576, 2013.

[35] T. E. Jensen and L. M. Sicko, "Phosphate metabolism in blue green algae. I. Fine structure of the 'polyphosphate overplus' phenomenon in Plectonema boryanum," *Canadian Journal of Microbiology*, vol. 20, no. 9, pp. 1235–1239, 1974.

[36] J. Goldberg, H. González, T. E. Jensen, and W. A. Corpe, "Quantitative analysis of the elemental composition and the mass of bacterial polyphosphate bodies using STEM EDX," *Microbios*, vol. 106, no. 415, pp. 177–188, 2001.

[37] G.-J. Zhou, F.-Q. Peng, L.-J. Zhang, and G.-G. Ying, "Biosorption of zinc and copper from aqueous solutions by two freshwater green microalgae *Chlorella pyrenoidosa* and *Scenedesmus obliquus*," *Environmental Science and Pollution Research*, vol. 19, no. 7, pp. 2918–2929, 2012.

[38] J. Kováčik, P. Babula, J. Hedbavny, O. Kryštofová, and I. Provaznik, "Physiology and methodology of chromium toxicity using alga *Scenedesmus quadricauda* as model object," *Chemosphere*, vol. 120, pp. 23–30, 2015.

Research Article | Vol. 7, No. 12 | 1 Dec 2016 | BIOMEDICAL OPTICS EXPRESS 5092
Biomedical Optics EXPRESS

Characterization of transfer function, resolution and depth of field of a soft X-ray microscope applied to tomography enhancement by Wiener deconvolution

JOAQUÍN OTÓN,[1,*] EVA PEREIRO,[2] ANA J. PÉREZ-BERNÁ,[2] LAIA MILLACH,[3] CARLOS OSCAR S. SORZANO,[1] ROBERTO MARABINI,[4] AND JOSÉ M. CARAZO[1]

[1]*Centro Nacional de Biotecnología (CNB-CSIC), Cantoblanco, 28049, Madrid, Spain*
[2]*ALBA Synchrotron Light Source, Cerdanyola del Vallès, 08290, Barcelona, Spain*
[3]*Facultat de Biociències. Departament de Genètica i Microbiologia. UAB. Cerdanyola del Vallès, 08193, Barcelona, Spain*
[4]*Escuela Politecnica Superior, Univ. Autonoma de Madrid, Cantoblanco, 28049, Madrid, Spain*
[*]*joton@cnb.csic.es*
http://biocomp.cnb.csic.es

Abstract: Full field soft X-ray microscopy is becoming a powerful imaging technique to analyze whole cells preserved under cryo conditions. Images obtained in these X-ray microscopes can be combined by tomographic reconstruction to quantitatively estimate the three-dimensional (3D) distribution of absorption coefficients inside the cell. The impulse response of an imaging system is one of the factors that limits the quality of the X-ray microscope reconstructions. The main goal of this work is to experimentally measure the 3D impulse response and to assess the optical resolution and depth of field of the Mistral microscope at ALBA synchrotron (Barcelona, Spain). To this end we measure the microscope apparent transfer function (ATF) and we use it to design a deblurring Wiener filter, obtaining an increase in the image quality when applied to experimental datasets collected at ALBA.

OCIS codes: (340.0340) X-ray optics; (040.7480) X-rays, soft X-rays; (110.7440) X-ray imaging; (180.7460) X-ray microscopy; (110.6960) Tomography; (110.4100) Modulation transfer function; (350.5730) Resolution; (100.1830) Deconvolution.

References and links

1. G. Schneider, P. Guttmann, S. Heim, S. Rehbein, F. Mueller, K. Nagashima, J. B. Heymann, W. G. Muller, J. G. McNally, and W. G. Müller, "Three-dimensional cellular ultrastructure resolved by X-ray microscopy," Nat. Methods **7**, 985–987 (2010).
2. J. Kirz, C. Jacobsen, and M. Howells, "Soft X-ray microscopes and their biological applications," Q. Rev. Biophys. **28**, 33–130 (1995).
3. M. Bertilson, O. von Hofsten, U. Vogt, A. Holmberg, and H. M. Hertz, "High-resolution computed tomography with a compact soft X-ray microscope," Opt. Express **17**, 11057–11065 (2009).
4. D. B. Carlson, J. Gelb, V. Palshin, and J. E. Evans, "Laboratory-based cryogenic soft X-ray tomography with correlative cryo-light and electron microscopy," Microsc. Microanal. **19**, 22–29 (2013).
5. W. Chao, P. Fischer, T. Tyliszczak, S. Rekawa, E. Anderson, and P. Naulleau, "Real space soft X-ray imaging at 10 nm spatial resolution," Opt. Express **20**, 9777–9783 (2012).
6. S. Rehbein, P. Guttmann, S. Werner, and G. Schneider, "Characterization of the resolving power and contrast transfer function of a transmission X-ray microscope with partially coherent illumination," Opt. Express **20**, 1–3 (2012).
7. J. Lehr, J. B. Sibarita, and J. M. Chassery, "Image restoration in X-ray microscopy: PSF determination and biological applications," in *IEEE transactions on image processing* **7**, 258–263 (1998).
8. D. Schäfer, M. Benk, K. Bergmann, T. Nisius, U. Wiesemann, and T. Wilhein, "Optical setup for tabletop soft X-ray microscopy using electrical discharge sources," Journal of Physics: Conference Series **186**, 012033 (2009).
9. Q. Yuan, K. Zhang, Y. Hong, W. Huang, K. Gao, Z. Wang, P. Zhu, J. Gelb, A. Tkachuk, B. Hornberger, M. Feser, W. Yun, and Z. Wu, "A 30 nm-resolution hard X-ray microscope with X-ray fluorescence mapping capability at BSRF," J. Synchrotron Radiat. **19**, 1021–1028 (2012).

#275785 http://dx.doi.org/10.1364/BOE.7.005092
Journal © 2016 Received 13 Sep 2016; revised 18 Oct 2016; accepted 22 Oct 2016; published 14 Nov 2016

Biomedical Optics EXPRESS

10. Y. S. Chu, J. M. Yi, F. De Carlo, Q. Shen, W.-K. Lee, H. J. Wu, C. H. L. H. L. Wang, J. Y. Wang, C. J. Liu, C. H. L. H. L. Wang, S. R. Wu, C. C. Chien, Y. Hwu, A. Tkachuk, W. Yun, M. Feser, K. S. Liang, C. S. Yang, J. H. Je, and G. Margaritondo, "Hard-X-ray microscopy with Fresnel zone plates reaches 40 nm Rayleigh resolution," Appl. Phys. Lett. **92**, 103119 (2008).
11. J. Chen, K. Gao, X. Ge, Z. Wang, K. Zhang, Y. Hong, Z. Pan, Z. Wu, P. Zhu, W. Yun, and Z. Wu, "Scattering imaging method in transmission X-ray microscopy," Opt. Lett. **38**, 2068–2070 (2013).
12. M. Uchida, G. McDermott, M. Wetzler, M. a. Le Gros, M. Myllys, C. Knoechel, A. E. Barron, and C. a. Larabell, "Soft X-ray tomography of phenotypic switching and the cellular response to antifungal peptoids in Candida albicans," P. Natl. Acad. Sci. USA **106**, 19375–19380 (2009).
13. E. M. H. Duke, M. Razi, A. Weston, P. Guttmann, S. Werner, K. Henzler, G. Schneider, S. A. Tooze, and L. M. Collinson, "Imaging endosomes and autophagosomes in whole mammalian cells using correlative cryo-fluorescence and cryo-soft X-ray microscopy (cryo-CLXM)," Ultramicroscopy **143**, 77–87 (2014).
14. C. Hagen, S. Werner, and S. Carregal-Romero, "Multimodal nanoparticles as alignment and correlation markers in fluorescence/soft X-ray cryo-microscopy/tomography of nucleoplasmic reticulum and apoptosis in mammalian cells," Ultramicroscopy **146**, 46–54 (2014).
15. K. C. Dent, C. Hagen, and K. Grünewald, "Critical step-by-step approaches toward correlative fluorescence/soft X-ray cryo-microscopy of adherent mammalian cells," Methods Cell Biol. **124**, 179–216 (2014).
16. J. J. Conesa, J. Otón, M. Chiappi, J. M. Carazo, E. Pereiro, F. J. Chichón, and J. L. Carrascosa, "Intracellular nanoparticles mass quantification by near-edge absorption soft X-ray nanotomography," Sci. Rep.**6**, 22354 (2016).
17. A. J. Pérez-Berná, M. J. Rodríguez, F. J. Chichón, M. F. Friesland, A. Sorrentino, J. L. Carrascosa, E. Pereiro, and P. Gastaminza, "Structural Changes In Cells Imaged by Soft X-Ray Cryo-Tomography During Hepatitis C Virus Infection," ACS Nano **10** (7), 6597–6611 (2016).
18. M. Chiappi, J. J. Conesa, E. Pereiro, C. O. S. Sorzano, M. J. Rodríguez, K. Henzler, G. Schneider, F. J. Chichón, and J. L. Carrascosa, "Cryo-soft X-ray tomography as a quantitative three-dimensional tool to model nanoparticle:cell interaction," J. Nanobiotechnology **14**, 15 (2016).
19. J. Oton, C. O. S. Sorzano, E. Pereiro, J. Cuenca-Alba, R. Navarro, J. M. Carazo, and R. Marabini, "Image formation in cellular X-ray microscopy," J. Struct. Biol. **178**, 29–37 (2012).
20. H. N. Chapman, "Phase-retrieval X-ray microscopy by Wigner-distribution deconvolution," Ultramicroscopy **66**, 153–172 (1996).
21. R. Burge, X.-C. Yuan, G. Morrison, P. Charalambous, M. Browne, and Z. An, "Incoherent imaging with the soft X-ray microscope," Ultramicroscopy **83**, 75–92 (2000).
22. E. Pereiro, J. Nicolás, S. Ferrer, and M. R. Howells, "A soft X-ray beamline for transmission X-ray microscopy at ALBA," J. Synchrotron Radiat. **16**, 505–512 (2009).
23. A. Sorrentino, J. Nicolás, R. Valcárcel, F. J. Chichón, M. Rosanes, J. Avila, A. Tkachuk, J. Irwin, S. Ferrer, and E. Pereiro, "MISTRAL: a transmission soft X-ray microscopy beamline for cryo nano-tomography of biological samples and magnetic domains imaging," J. Synchrotron Radiat. **22**, 1112–1117 (2015).
24. X. Zeng, F. Duewer, M. Feser, and C. Huang, "Ellipsoidal and parabolic glass capillaries as condensers for X-ray microscopes," Appl. Opt. **47**, 2376–2381 (2008).
25. D. Attwood, *Soft X-Rays and Extreme Ultraviolet Radiation: Principles and Applications* (Cambridge University, 2000).
26. W. Chao, B. D. Harteneck, J. A. Liddle, E. H. Anderson, and D. T. Attwood, "Soft X-ray microscopy at a spatial resolution better than 15 nm," Nature **435**, 1210–1213 (2005).
27. O. Mendoza-Yero, G. Minguez-Vega, R. Navarro, J. Lancis, and V. Climent, "PSF analysis of nanometric Fresnel zone plates," in "Proceeding of the EOS Topical Meeting on Diffractive Optics," 2428 (2010).
28. M. Born and E. Wolf, *Principles of Optics: Electromagnetic Theory of Propagation, Interference and Diffraction of Light* (Cambridge University, 1999).
29. J. W. Goodman, *Introduction to Fourier Optics* (McGraw-Hill, 1996).
30. C. Chang and T. Nakamura, "Partially coherent image formation theory for X-ray microscopy," in "Microscopy: Science, Technology, Applications and Education," 4th ed. M.-V. A. and D. J., eds. (Formatex Research Center, 2010), Chap. 3, pp. 1897–1904.
31. J. W. Goodman, *Statistical Optics*, A Wiley-Interscience publication (Wiley, 2000).
32. J. Otón, C. O. S. Sorzano, R. Marabini, E. Pereiro, and J. M. Carazo, "Measurement of the modulation transfer function of an X-ray microscope based on multiple Fourier orders analysis of a Siemens star," Opt. Express **23**, 9567 (2015).
33. H. Hopkins and P. Barham, "The influence of the condenser on microscopic resolution," Proceedings of the Physical Society Section B **63**, 737 (1950).
34. J. Oton, C. O. S. Sorzano, F. J. Chichón, J. L. Carrascosa, J. M. Carazo, and R. Marabini, "Soft X-ray Tomography Imaging for Biological Samples," in "Computational Methods for Three-Dimensional Microscopy Reconstruction," (2014), Chap. 8, p. 260.
35. I. G. Kazantsev, J. Klukowska, G. T. Herman, and L. Cernetic, "Fully three-dimensional defocus-gradient corrected backprojection in cryoelectron microscopy," Ultramicroscopy **110**, 1128–1142 (2010).
36. B. Gunturk, "Fundamentals of Image Restoration," in "Image Restoration: Fundamentals and Advances," B. K. Gunturk; and X. Li, eds. (CRC, 2012), pp. 25–62.

37. J. Frank, *Three Dimensional Electron Microscopy of Macromolecular Assemblies* (Oxford University, 2006).
38. S. Gabarda and G. Cristóbal, "Blind image quality assessment through anisotropy," J. Opt. Soc. Am. A Op.t Image Sci. Vis. **24**, B42–B51 (2007).

1. Introduction

Full field soft X-ray tomography (SXT) refers to an emerging microscopy technique in which photons of wavelengths of a few nanometers are used to obtain images of objects of interest. Applied to biology, we refer to cryo-microscopes imaging whole cells at resolutions in the order of 50 nm and lower [1]. The contrast in these images can be relatively higher than in electron tomography, specially if photons with energy in the so called water window are used (between 284 and 543 eV) [2]. In this situation, images are formed mostly by absorption, being typical absorption values for biological specimens (carbon) an order of magnitude greater than the one of water (oxygen). Furthermore, these 2D image projections can be combined to obtain a quantitative estimation of the 3D structure of the cell by tomographic reconstruction techniques. This kind of microscopes needs a high photon flux, typical of synchrotron facilities, as can be found in ALBA (Spain), HZB-Bessy II (Germany), Diamond (UK) or ALS (US). Recently, the use of soft X-rays emitted from laser-produced plasmas rather than synchrotron radiation is becoming more popular [3, 4].

In order to characterize the X-ray microscope optical resolution, the impulse response function needs to be measured. To achieve this goal, several methods have been proposed based on: qualitative assessment [5, 6], specific contrast decay [7–9] and Rayleigh criteria [10, 11]. We have favoured this last one because it is obtained using parameters related with the microscope instead of visual inspection or a pure mathematical definition. Moreover, if these impulse response profiles are acquired along the optical axis at different defocus positions, it is possible to characterize the depth of field (DOF) of the microscope.

Most work performed on SXT microscopes addresses samples a few microns thick [4, 12–18]. Depending on the ratio between the sample thickness and the DOF, standard reconstruction algorithms introduce different artifacts which can be better estimated once the experimental DOF is known [19]. Even if the specimen is fully in focus, images are not perfect projections but they are blurred by the microscope impulse response. Although image deblurring by deconvolution is a well-known tool in image processing and, in fact, it has already been applied in scanning transmission X-ray microscopy [20, 21], this step has never been used in SXT before. Here, taking into account the experimental impulse response, we apply deconvolution techniques to experimental data.

In this work, we introduce the definitions of the apparent point spread function (APSF) and pseudo-apparent point spread function (PAPSF) that allow for the analysis of the impulse response of an optical system. Both functions are derived from the apparent transfer function (ATF). We provide the first experimental characterization of these profiles for the typical optical schemes used at the Mistral microscope, at ALBA synchrotron (Barcelona) [22, 23]. Using the experimental PAPSF 3D distribution, we calculate the Rayleigh resolution and depth of field of the microscope. Finally, we design a Wiener deconvolution filter which, once applied to experimental image projections prior to 3D reconstruction, results in an quality increase in the final tomograms.

2. Methods

In this section we describe a transmission X-ray microscope and the different magnitudes needed to characterize the optical system response. When these magnitudes cannot be directly measured we suggest and justify how to derive them from alternative measurements.

Biomedical Optics EXPRESS

2.1. Microscope optical system

The typical optical scheme of a full field transmission X-ray microscope is shown in Fig. 1. It is composed by both a condenser and objective lenses. The latest microscopes make use of achromatic single-bounce ellipsoidal glass capillaries as condensers [24]. In the case of objective lenses, Fresnel zone plates (FZP) are used [25]. These FZP are rotationally symmetric diffractive gratings, composed by radially decreasing width rings. The spatial resolution is intrinsically related to the width of the last ring which, at present, can reach up to 15 nm resolution [26]. Theoretical expressions that characterize the optics of an X-ray microscope are easily found in the literature [25, 27]. However, the manufacturing of these two kind of lenses is a rather complicated microfabrication process, so the final lenses will be an approximation to the ideal ones. Additionally, glass capillaries and FZPs are not the only optical elements used in these microscopes and other elements, as beam central stoppers, also take part in the scheme. As the FZP is a diffractive element, its zero order takes 25% of the incident energy, behaving this direct light as background noise in the projection. Therefore, this inefficient fraction of energy is removed by placing a central stopper just before the capillary condenser. The light source, usually the monochromator exit slit, is imaged by the condenser onto the sample plane in a scheme known as *critical illumination* [28] and, in general, the beam underfills the sample, problem that is overcome by wobbling the capillary.

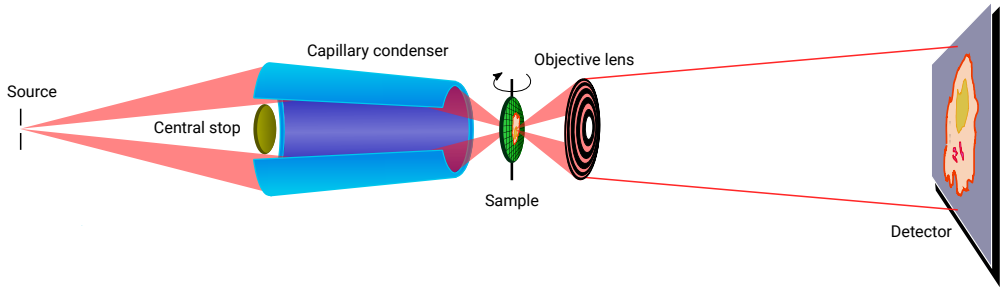

Fig. 1. Optical system scheme of a full field transmission X-ray microscope. The exit slit of a monochromator used to select the proper photon energy acts as light source. Beam is then condensed by an ellipsoidal glass capillary onto the sample plane, while a central stopper blocks the center part of the beam that is not reflected by the capillary. Finally, images are obtained by FZP objective lens.

In the case of the Mistral full-field transmission X-ray microscope, which was built by Xradia Inc. (now Zeiss), the single bounce glass capillary condenser is characterized by a length of 100 mm, with inner entrance and exit diameters of 1.82 and 0.58 mm, respectively, and works as a single reflection achromatic lens with a focal length of 10.05 mm. The exit slit of the monochromator is imaged and demagnified with a typical dimension of 2 μm onto the sample. To reach a field of view that covers the whole sample, in the range of 10×10–16×16 μm^2, the condenser is mounted on a x-y scanner and can be used at variable frequencies for adjusting exposure time. Two Ni FZP lenses, made also by Xradia Inc., are available. They are characterized by outermost zone widths of 40 and 25 nm (named hereafter, ZP40 & ZP25), 937 and 1,500 zones, that give 2.52 and 1.57 mm theoretical focal lengths, respectively, at 520 eV energy of illumination.

2.2. Apparent transfer function

Linear systems are characterized in Fourier domain by a transfer function. In optical systems, the concrete magnitude that establishes the relationship between input and output varies: *amplitude*

Biomedical Optics EXPRESS

transfer function for electric field amplitude in coherent systems and *optical transfer function* for intensity in totally incoherent systems [29]. Partially coherent systems are not linear neither in amplitude nor in intensity [28, 30]. In these systems, the *apparent transfer function* (ATF) has been introduced to accurately predict the system response [31]. ATF is defined as:

$$\mathcal{H}_A(\mathbf{f_x}) = \frac{\tilde{I}_{out}(\mathbf{f_x})}{\tilde{I}_{in}(\mathbf{f_x})}, \tag{1}$$

where $\mathbf{f_x} = (f_x, f_y)$ represents the frequency variable, $\tilde{I}_{in}(\mathbf{f_x})$ and $\tilde{I}_{out}(\mathbf{f_x})$ are the Fourier transforms of the input and output intensity distributions of a test pattern, respectively. In this work we have experimentally calculated the ATF using an approach we had previously introduced in [32]. This approach, in a nutshell, requires a Siemens star as test pattern from which a rotationally averaged ATF is obtained.

2.3. Apparent point spread function

Another magnitude used to characterize optical systems is the impulse response in spatial domain. This magnitude is known as point spread function for pure coherent or incoherent systems. For partially coherent systems we will refer to it as *apparent point spread function* (APSF), defined as

$$h_A(\mathbf{x}) = \mathcal{F}^{-1}\left\{\mathcal{H}_A(\mathbf{f_x})\right\}, \tag{2}$$

where $\mathcal{F}^{-1}$ denotes the inverse *Fourier* transform operation in the plane (f_x, f_y).

One of the advantages of the APSF over the ATF is that the former can be used to directly calculate the optical resolution and the DOF for partially coherent systems. Unfortunately, the experimental ATF measurement does not include the phase information and, therefore, the information required to fully recover the APSF is not available [32]. We define here the *pseudo-apparent point spread function* (PAPSF) where the phase content is removed:

$$h_{PA}(\mathbf{x}) = \mathcal{F}^{-1}\left\{\left|\mathcal{H}_A(\mathbf{f_x})\right|\right\}. \tag{3}$$

This new function, as we show in the next subsections, can be used to compute the optical resolution and the DOF.

2.4. Rayleigh resolution criterion

In optics, resolution is usually measured according to Rayleigh criterion. This value is defined for totally incoherent illumination as the distance where the first minimum of the Airy intensity pattern of one source point coincides with the maximum of another. Its theoretical expression is $\delta = \frac{0.61\lambda}{NA_O}$, where λ is the wavelength of the illumination and NA_O is the numerical aperture of the objective lens [29]. In the case of partially coherent illumination, defined by the ratio between numerical apertures of condenser and objective lenses $m = \frac{NA_C}{NA_O} < 1$, there is no closed form and numerical calculations must be done [33]. However, we note that the resolution definition for incoherent illumination can also be inversely applied to an APSF profile to calculate the *critical resolution* of an optical system: at the midpoint in the intensity profile addition between two source points separated by Rayleigh resolution distance δ there is an intensity decay from 100% of its maximum to 73.5 % [28]. Therefore, we can measure the critical resolution as the distance in the APSF profile where the intensity decays to 36.75 % (73.5/2), as one can obtain from the PSF intensity profile of a single source point under totally incoherent illumination.

However, the proposed characterization method does not recover the APSF but the PAPSF, which misses the phase from the ATF profiles. Therefore, to validate the feasibility of using PAPSF profiles instead of APSF ones, we show in Fig. 2 transverse profiles of numerical simulation of both APSF and PAPSF at different values of numerical apertures ratio m, being the transverse spatial units normalized to $\frac{\lambda}{NA_O}$. We see that both profiles, APSF and PAPSF, match

along all x-positions, independently of m. That is, for the in-focus plane the APSF is real and therefore there is not phase modulation.

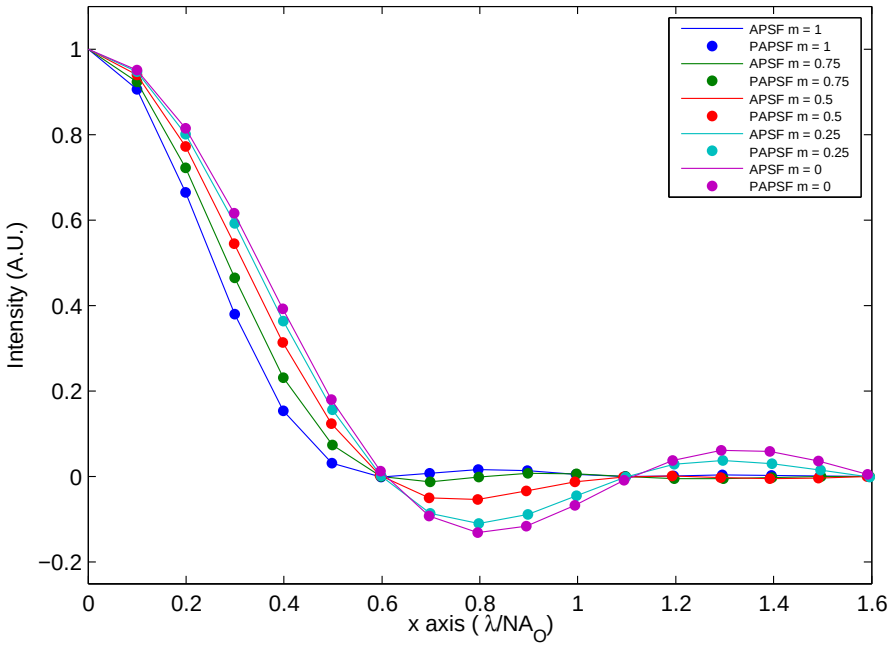

Fig. 2. Transverse profiles of the APSF and PAPSF calculated for different numerical apertures ratio m values. Axial units has been normalized to $\frac{\lambda}{NA_O}$.

2.5. Depth of field

Current 3D reconstructions in soft X-ray tomography are implemented by using tomographic standard reconstruction algorithms, which do not consider the 3D PSF of the optical system and assume that the whole sample is in focus. Therefore, for a proper evaluation of the error related to the ratio between specimen thickness and DOF, it is important to quantify this latter magnitude.

The depth of field is defined as the distance along the optical axis around the best focusing plane where the axial intensity of the PSF decays to 80 % and, as Rayleigh resolution, the analytical expression we find in the literature, $\Delta z = \frac{\lambda}{NA_O^2}$, is only defined for totally incoherent illumination [28, 34]. Therefore, akin to the critical resolution measurement, the DOF can be experimentally calculated from the APSF along the optical axis.

In the previous subsection, we showed a perfect match between PAPSF and APSF profiles for in-focus planes (see Fig. 2), which does not have to occur at every unfocused plane. Thus, to validate the DOF obtained from PAPSF, we show in Fig. 3 the numerical simulation of the profile along the optical axis (that is, at different defocus) of both APSF and PAPSF for different values of numerical apertures ratio m. We note that, for those intensity values used for estimating the DOF (intensities greater than 80 %), both APSF and PAPSF profiles practically match. The discrepancy increases with defocus because the ATF phase component is not negligible for medium and large defoci.

Calculations show that the DOF obtained from the PAPSF introduces an error lower than 1 %

for $m \geq 0.25$, which increases to 6% for the totally coherent case ($m = 0$). We also note that, as m decreases, the DOF clearly varies, which allows to assess that the theoretical definition of the DOF is only valid for a totally incoherent illumination.

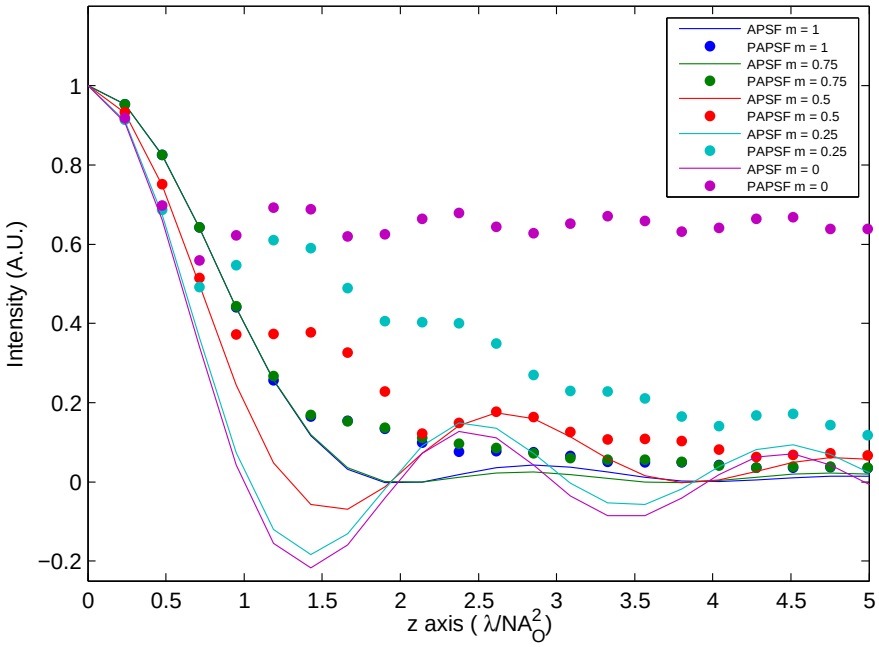

Fig. 3. Axial profiles of the APSF and PAPSF calculated for different numerical apertures ratio m values. Axial units has been normalized to $\frac{\lambda}{NA_O^2}$.

2.6. Deconvolution

Even if we assume that the specimen is fully in focus, images are blurred by the microscope impulse response. Consequently, reconstruction will improve if standard deconvolution is applied to experimental data. The image formation process within this assumption, known as the X-ray transform, is described as [35]:

$$I_s(\mathbf{x}) = \left[I_0(\mathbf{x}) \mathrm{e}^{-\int_{z_0}^{z_s} \mu(\mathbf{x},z)\mathrm{d}z} \right] \otimes h_A(\mathbf{x}), \tag{4}$$

where $\mathbf{x} = (x, y)$, $I_0(\mathbf{x})$ and $I_s(\mathbf{x})$ are the projections acquired without and with the sample (that is, the flatfield reference and projection images), respectively; $\mu(\mathbf{x}, z)$ is the volume that describes the 3D distribution of the sample absorption coefficients, with $\mu > 0 \; \forall \; z \in [z_0, z_S]$ and $\otimes$ denotes the convolution operation in $(\mathbf{x})$. The inversion of Eq. (4) has already been proved to recover the information of the standard projection [35]:

$$\int_{z_0}^{z_s} \mu(\mathbf{x}, z)\mathrm{d}z = -\ln \left[\frac{I_s(\mathbf{x}) \otimes h_A^{-1}(\mathbf{x})}{I_0(\mathbf{x}) \otimes h_A^{-1}(\mathbf{x})} \right], \tag{5}$$

where $h_A^{-1}(\mathbf{x})$, defined as $h_A(\mathbf{x}) \otimes h_A^{-1}(\mathbf{x}) = \delta(\mathbf{x})$, is the deconvolution kernel. Equation (5) shows that when applying a deconvolution operation on both projection and flatfield images a better

Biomedical Optics EXPRESS

estimation of the ideal projections is obtained. Furthermore, as flatfield projections of the background illumination pattern are slowly varying along x-y plane, the flatfield deconvolution can be ignored.

To properly deconvolve the image projections, we must consider the quantum nature of the photons when they interact with detection devices. Wiener filtering has been proved to be an efficient implementation of the deconvolution process under the presence of shot noise [36]. Thus, the estimated projection is calculated in Fourier space as

$$\tilde{I}_s^e(\mathbf{f_x}) = W(\mathbf{f_x})\tilde{I}_s(\mathbf{f_x}), \tag{6}$$

where $\tilde{I}_s^e(\mathbf{f_x})$ and $\tilde{I}_s(\mathbf{f_x})$ are the Fourier transforms of the estimated and true image projections, respectively, and $W(\mathbf{f_x})$ is the Wiener estimator defined as

$$W(\mathbf{f_x}) = \frac{\mathcal{H}_A^*(\mathbf{f_x})}{|\mathcal{H}_A(\mathbf{f_x})|^2 + \frac{S_n(\mathbf{f_x})}{S_I(\mathbf{f_x})}}, \tag{7}$$

where $S_n(\mathbf{f_x}) = \mathcal{F}\{\Phi_N(\mathbf{x})\}$ and $S_I(\mathbf{f_x}) = \mathcal{F}\left\{\Phi_{\tilde{I}_s}(\mathbf{x})\right\}$ are the power spectral densities of the noise and true projections, respectively, calculated as the Fourier transform of the autocorrelation function of the noise, N, or signal, $\tilde{I}_s$, images and their ratio is the SNR. In practice, as photon noise is statistically independent (i.e. white noise), the SNR can be easily obtained as the ratio between the variance of the background illumination (as instance, from the flatfield projections) and estimated projections.

3. Results

In this work, we show the characteristic ATF and PAPSF experimental profiles of the Mistral microscope. In Fig. 4(a) we show the experimentally measured ATF for both ZP40 and ZP25. The profiles for both lenses are similar, being the cut-off frequency of ZP25 greater than ZP40's, as expected by theory. ATF coefficients when f_x approaches zero are not achievable by the measurement method based on the Siemens star test pattern. However, as the normalization in the method recovers the modulation without considering any energy lost, ATF should reach 1 at $f_x = 0$.

To calculate the PAPSF distributions, the 1D profiles depicted in Fig. 4(a) are extrapolated for low frequencies. After that, a 2D-ATF is created assuming rotational symmetry and, finally, Eq. (3) is applied. In Fig. 4(b) the PAPSF profiles for the in-focus plane are shown, being ZP25 profile clearly tighter than ZP40. From these PAPSF profiles, we have obtained critical resolution values of 61.9 and 51.8 nm for the ZP40 and ZP25 lenses, respectively, whereas theoretical resolution values for both ZP40 and ZP25 ideal lenses are 48.8 and 30.5 nm, respectively, in the totally incoherent case.

From the PAPSF intensity along the optical axis we obtain the axial profiles plotted in Fig. 4(c). We clearly note the tighter peak corresponding to ZP25, consequence of the smaller DOF. We have obtained DOF values of 3.3 and 1.6 μm for the ZP40 and ZP25 lenses respectively, whereas theoretical values for both ZP40 and ZP25 ideal lenses are 2.69 and 1.05 μm respectively, in the totally incoherent case. Again, experimental DOF values differ from theoretical ones, enlarged probably by a smaller numerical aperture ratio m than expected, in both cases.

3.1. Tomographic reconstruction

We have used the experimental PAPSF profiles shown in Fig. 4(b) to implement our deblurring Wiener filter. In the following, we show the result of deblurring two experimental datasets, one acquired with each of the two FZPs. The first reconstructed volume by SXT was obtained on a *Scenedesmus* cells sample using ZP40 (*Scenedesmus* is a phototrophic microorganism isolated

Biomedical Optics EXPRESS

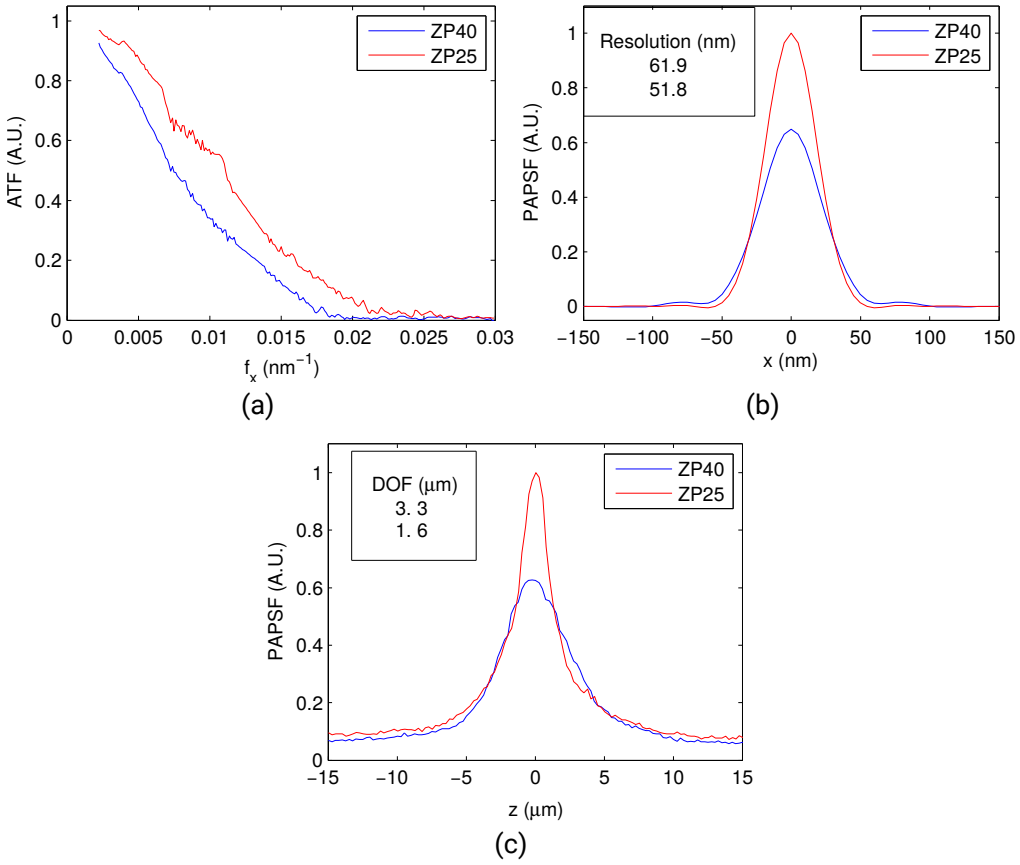

Fig. 4. Experimental characterization of the Mistral microscope when using: ZP40, 937 zones, 2.52 mm theoretical focal length (blue); and ZP25, 1,500 zones, 1.57 mm theoretical focal length (red). Profiles have been calculated for 520 eV. (a) Apparent transfer function profiles; (b) Pseudo apparent transfer function profile calculated at in-focus plane. Applying Rayleigh criteria results in critical resolution values of 61.9 and 51.8 nm for ZP40 and ZP25 lenses, respectively; (c) Axial apparent transfer function profiles. Experimental DOF are 3.3 and 1.6 µm for ZP40 and ZP25, respectively.

from Ebro delta (Spain) microbial mats in 2009), while the second reconstructed volume case, Huh-7 cells (human hepatoma cell line), was collected using ZP25. Both datasets were acquired at 520 eV photon energy. Collection geometry was single-tilt axis in the range [-60°, 70°] in 1° steps, with variation of exposure time between 2 and 3 s and pixel size of 13 nm for ZP40; and in the range [-65°, 65°], using 1° steps, exposure time between 2 and 3 s and 11.3 nm pixel size for ZP25. Comparing the local variance in these projections to the variance of the flatfield image projections, we obtained a value of $SNR \approx 20$ to be used in the Wiener filter.

We show the results for the reconstructed tomograms using ZP40 and ZP25 in Figs. 5 and 6, respectively. We compared an x-z slice (normal to tilt axis) where no deconvolution has been applied (Figs. 5(a) and 6(a)) to the same x-z slice enhanced by deconvolution (Figs. 5(e) and 6(e)). We also compared distinct x-y slices at the same z positions from the standard reconstruction (Figures 5(b-d) and 6(b-d)) with reconstructed slices from deconvolved tomograms (Figures 5(f-h) and 6(f-h)). Clearly, details are enhanced by a contrast increase in the deconvolved case, as shown in the profiles depicted in Figs. 5(i) and 6(i). We note in the case of *Scenedesmus* that details in the slice at $z = 2$ µm, out of the DOF, are also enhanced.

Biomedical Optics EXPRESS

For quantitative assessment of the deconvolution improvement, since the Fourier ring correlation is invariant against deconvolution [37], we applied a blind image quality assessment (AQI) [38] to evaluate absolute image quality without a reference. We analyzed these AQI measures at the different z planes when FZPs ZP40 and ZP25 are used in Figs. 5(j) and 6(j), respectively. AQI shows that, in all the slices, the quality of the images has been increased after the application of the tailored deconvolution.

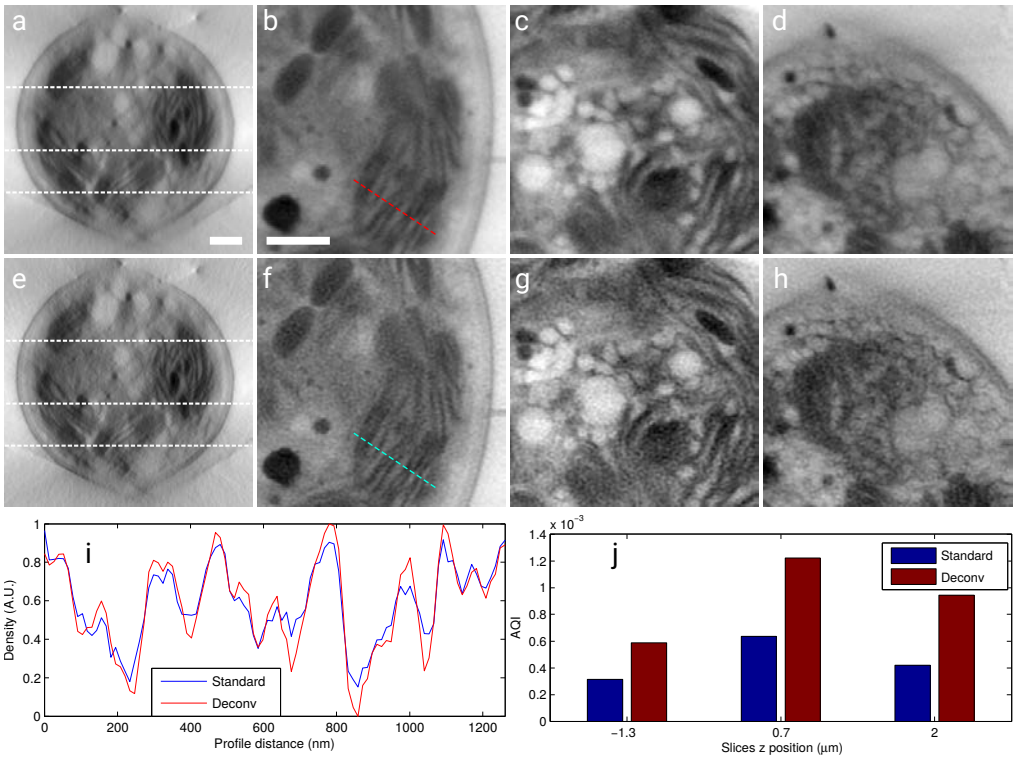

Fig. 5. Comparison of *Scenedesmus* cells tomograms obtained using ZP40. The first row shows standard tomographic results (non-deconvolved), while the second row presents the reconstruction from deconvolved tilt series tomogram. (a, e) Sections perpendicular to the tilt axis where three dashed lines are drawn, corresponding to slices in x-y plane at different distances in z: (b, f) z=-1.3 μm, (c, g) z=0.7 μm and (d, h) z=2 μm. Scale bars = 1 μm; (i) Density profile along the dashed red line marked in (b) compared to the same profile, dashed blue line, in (f); (j) Anisotropic quality index (AQI) comparison of slice pairs (b,f), (c,g) and (d,h). In all the cases the visibility of the slices is enhanced in the case when deconvolution is applied.

Biomedical Optics EXPRESS

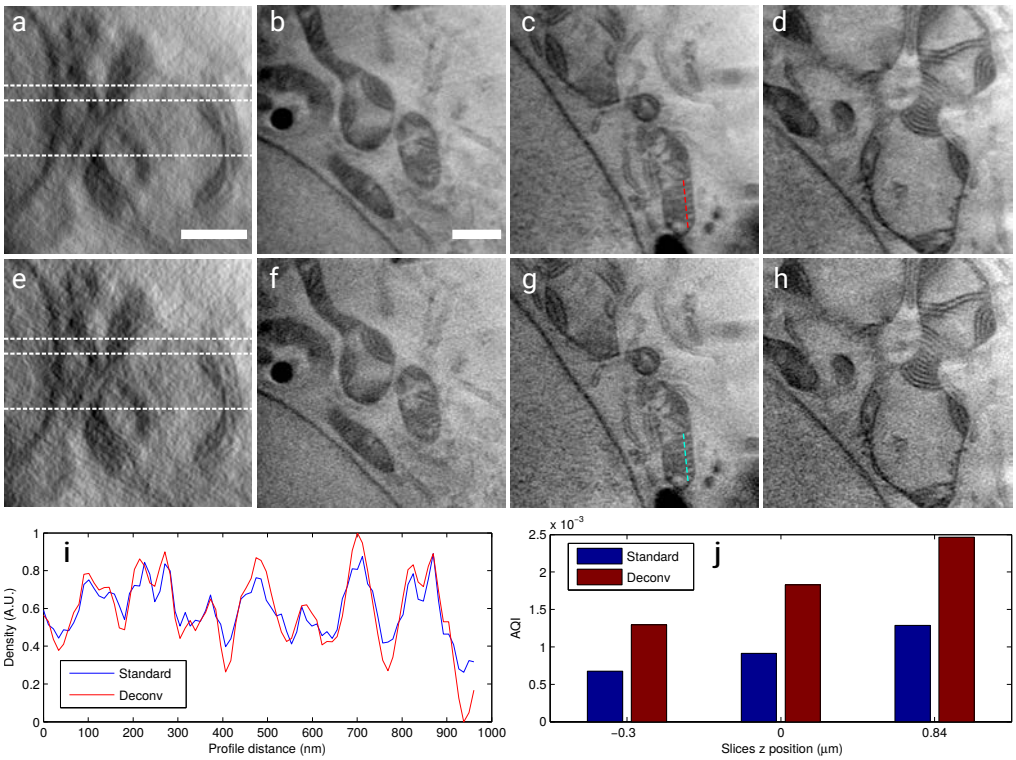

Fig. 6. Comparison of Huh-7 cells tomograms obtained using ZP25. The first row shows standard tomographic results (non-deconvolved), while the second row presents the reconstruction from deconvolved tilt series tomogram. (a, e) Sections perpendicular to the tilt axis where three dashed lines are drawn, corresponding to slices in x-y plane at different distances in z: (b, f) z=-0.3 μm, (c, g) z=0 μm and (d, h) z=0.84 μm. Scale bars = 1 μm; (i) Density profile along the dashed red line marked in (c) compared to the same profile, dashed blue line, in (g); Anisotropic quality index (AQI) comparison of slice pairs (b,f), (c,g) and (d,h). In all the cases the visibility of the slices is enhanced in the case when deconvolution is applied.

4. Conclusions

In this work, we have used experimental measures of the ATF at different defocus to calculate the 3D PAPSF. This distribution allows the estimation of the Rayleigh resolution and the depth of field of the Mistral microscope. We have also designed a Wiener filter which, once applied to experimental image projections, results in an increase of quality in the final reconstructed tomograms.

Our experimental estimation of the Mistral microscope DOF and resolution differ from the design specifications and, although the condenser manufacturing fits the design parameters, the effective illumination pattern provided by the capillary leads to a lower effective numerical aperture with respects to the theoretical one. Therefore, when ZP40 is used the microscope response matches the one of a partially coherent system instead of an incoherent one, while in the case of ZP25 the response corresponds to a more coherent system than design.

Biomedical Optics EXPRESS

Author contributions

JO, EP and JMC designed research; EP performed experiments; JO performed most data analysis with the support of EP, AJP, COSS, and RM; JO designed software tools for data analysis; We have used datasets from AJP and LM as examples of the effect of the deconvolution; JO, JMC, COSS and RM supervised the mathematics; data was acquired in the Mistral beamline at the ALBA synchrotron; JO, JMC and EP prepared the manuscript. All authors reviewed the manuscript.

Funding

Ministerio de Economía y Competitividad (MINECO) (AIC-A-2011-0638, BIO2013-44647-R, BFU2013-41249-P, BIO2016-76400-R, BFU2016-74868-P); Madrid regional government (S2010/BMD-2305); The European Union BioStruct-X Project (283570).

Acknowledgements

All the images in this work were acquired at Mistral beamline at ALBA Synchrotron. We thank ALBA staff, especially Marc Rosanes. We thank J.J. Conesa and F.J. Chichón for figure suggestions.

Annex II

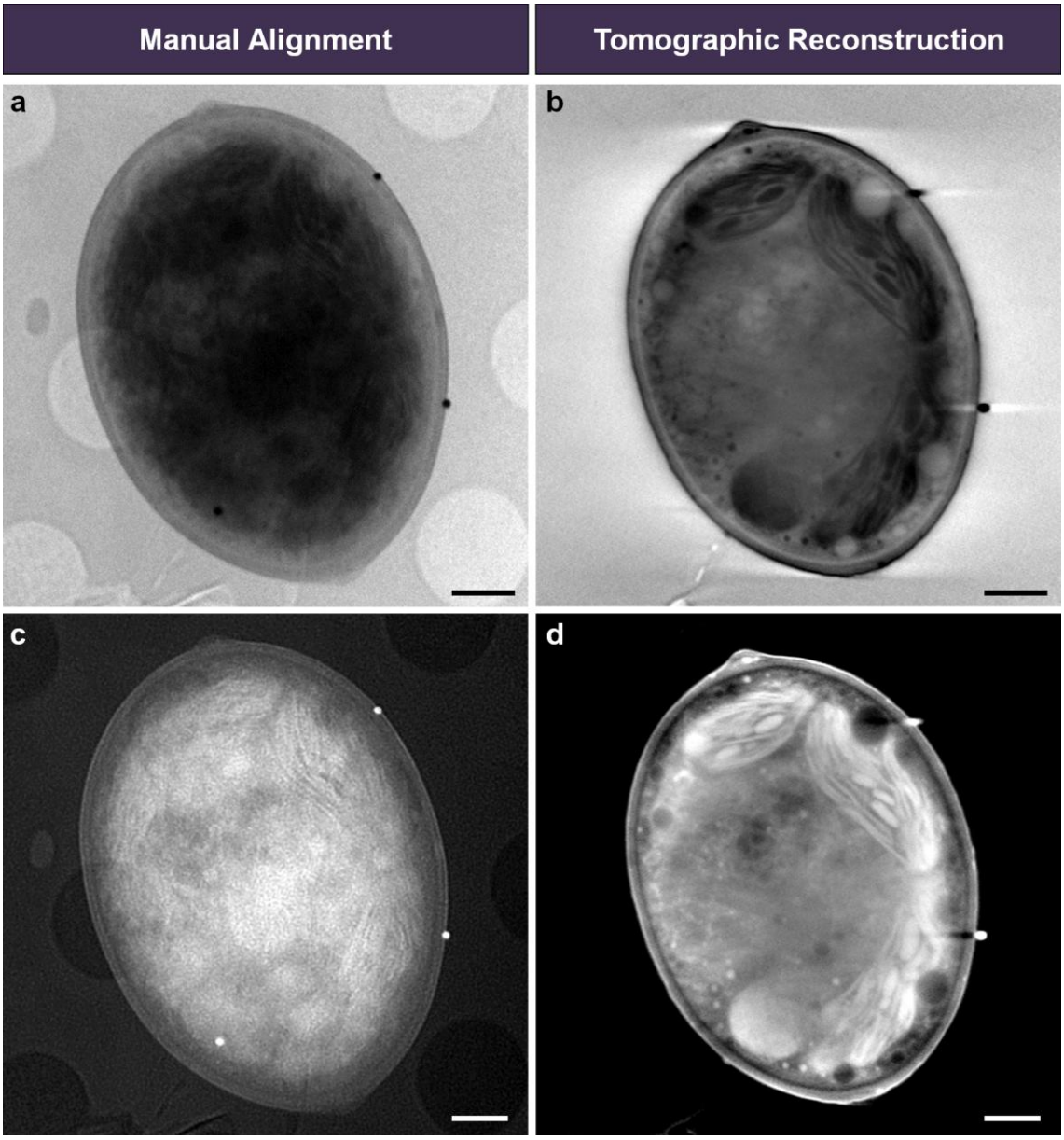

Fig. 1. TXM projection images of an non-polluted *Scenedesmus* sp. DE2009 cell. 2D soft X-ray cryo projections at tilt angle 0° **(a)** and with inverted contrast **(c)**; reconstructed soft X-ray cryo-tomogram in the *xy* plane and z=0 **(b)** and with inverted contrast **(d)**. Scale bars represent 1 μm.

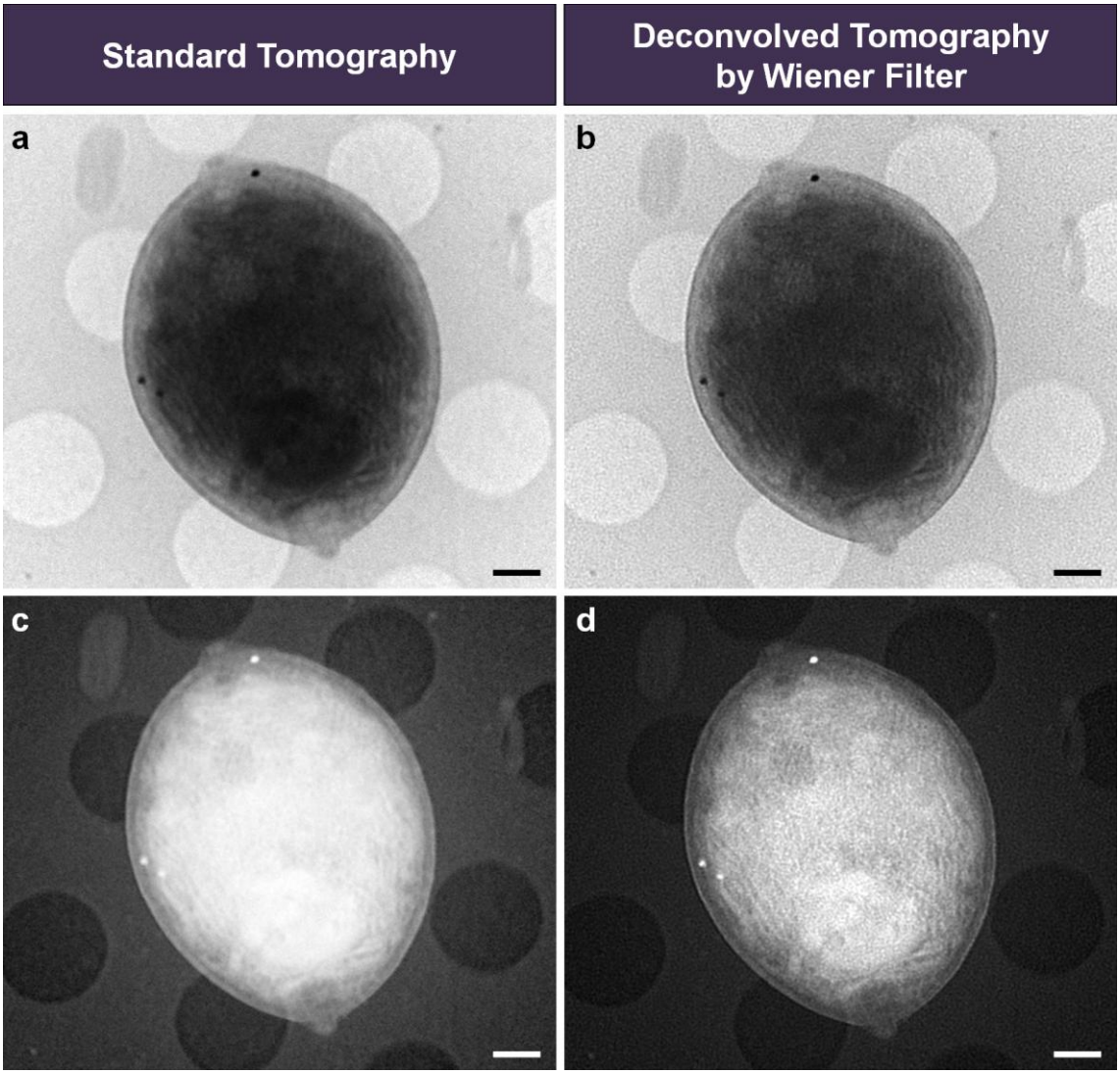

Fig. 2. Comparison of the 0° soft X-ray cryo-projections of non-polluted *Scenedesmus* sp. DE2009 cell. The left column shows standard alignment results (non-deconvolved) **(a)** and with inverted contrast **(c)**, while the right column presents the manual alignment from deconvolved tilt series tomograms using Wiener filter **(b)** and with inverted contrast **(d)**. Scale bars represent 1 μm. In all the cases the visibility of the slice is enhanced in the case when deconvolution is applied.

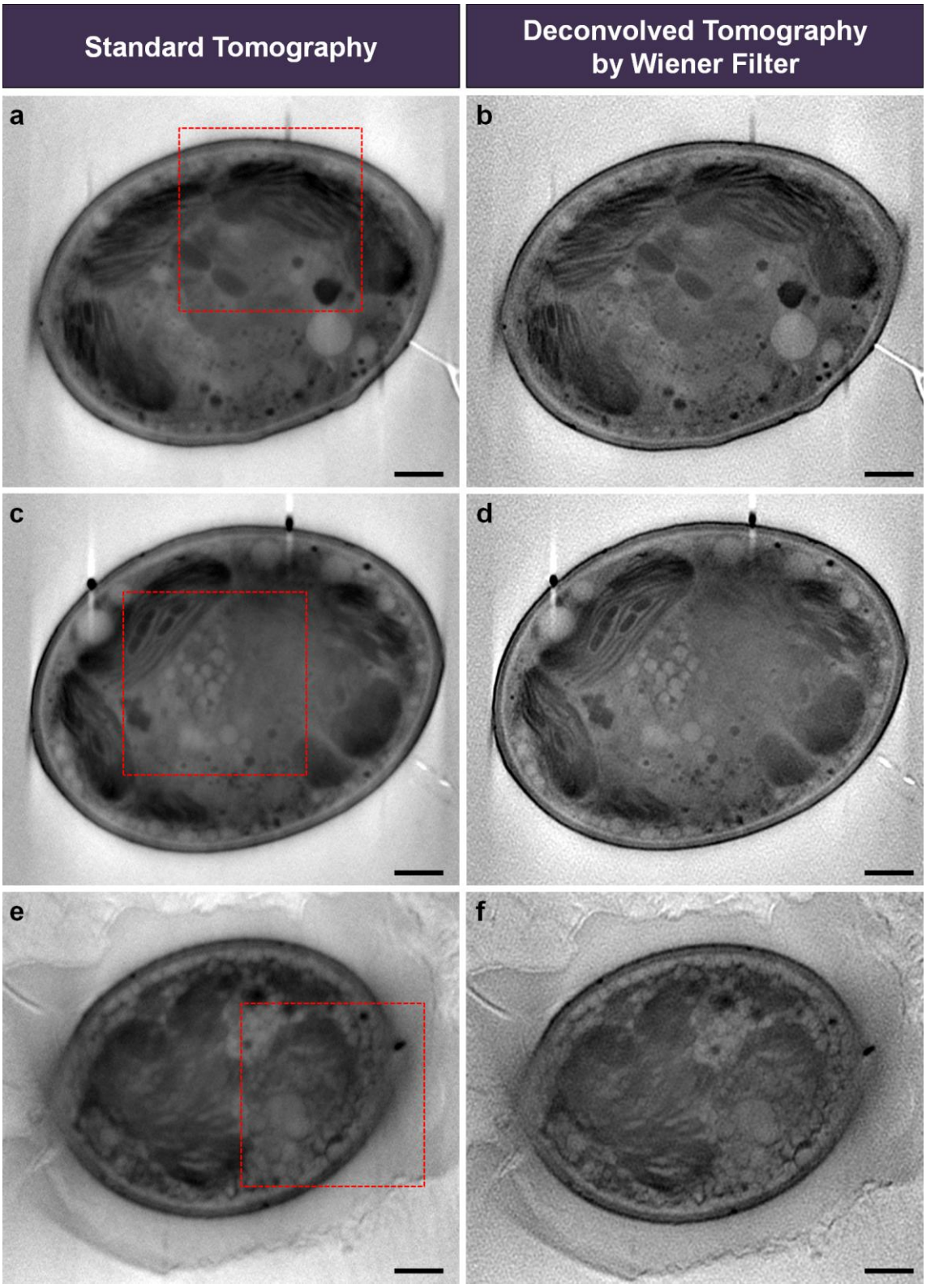

Fig. 3. Comparison of *Scenedesmus* sp. DE2009 cells tomograms. The left column shows standard tomographic results (non-deconvolved), while the right column presents the reconstruction from deconvolved tilt series tomograms using Wiener filter. Slices in *xy* plane at different distance in z, z=1.3 μm **(a, b)**, z=0.7 μm **(c, d)**; z=2 μm **(e, f)**. Scale bars represent 1 μm. In all the cases the visibility of the slice is enhanced in the case when deconvolution is applied. The red dashed squares correspond to the images showed in Otón et al., 2016.

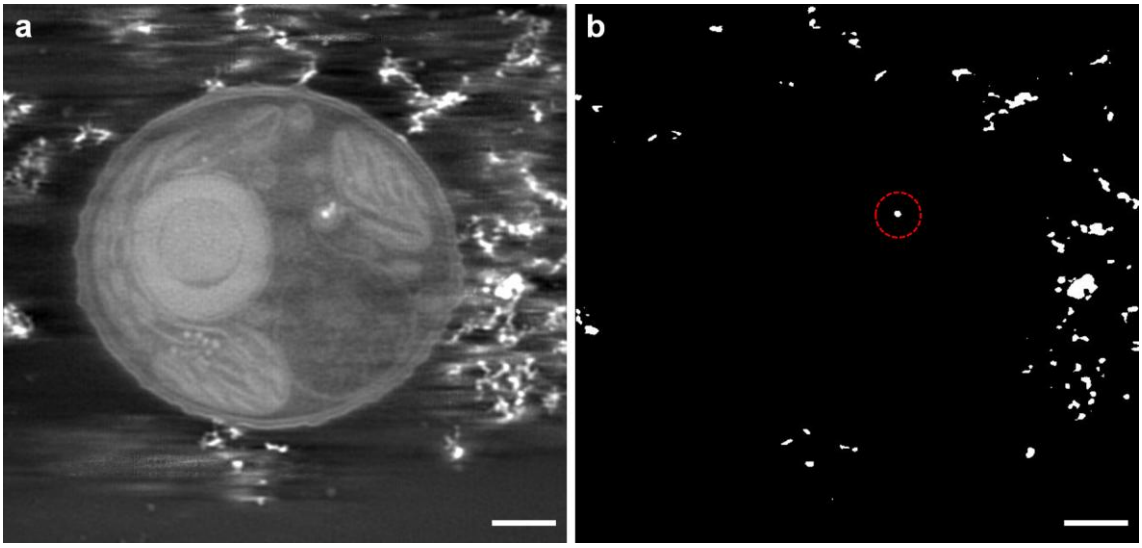

Fig. 4. ART reconstruction of *Scenedesmus* sp. DE2009 cell polluted with 2 mM Pb^{2+} (**a**) Threshold projection of Pb^{2+}, calibrating the signal using the external Pb^{2+}. Threshold parameters: 0.01-0.04, 0.86% of the total number of voxel. Gold beads are excluded with this choice. Scale bars represent 1 μm.
Pb^{2+} results localized inside spherical organelles, where it was expected to find in polyphosphate inclusions.